*Chapter – 1*

# INTRODUCTORY REMARKS

## 1.1. INTRODUCTION

Among all the natural calamities, earthquake has been the most major problem for mankind, killing thousands of people each year around the globe. Earthquake is manifold phenomenon causing tsunamis, landslide and conflagrations. Earthquake in all its forms causes massive destruction, human lives and economic loss. Earthquakes are not directly threat to human and economic loss. The loss occurs due to destruction of human made facilities like buildings, bridges and transportation system etc.

The significant earthquakes which hit in the last decade are Nepal (2015) with magnitude 7.8, Pakistan (2013) with 7.7, Japan (2011) with 9, Chile (2010) with 8.8, Haiti (2010) with 7, Indonesia (2009) with 7.5, China (2008) with 7.9, Peru (2007) with 8 and Pakistan (2005) with magnitude 7.6 hit the area leaving 80,000 people dead. In Indonesia (2004) an earthquake with magnitude 9.1 occurred with total death of 2, 30,000 people.

The destruction due to earthquake in developed countries is due to the existing stock of the building which pre dates to modern seismic codes. In developing countries inadequate detailing variation in material strength poor construction, poor beam column joints behavior cause the massive economic and human life loss. So it is necessary to have an idea of seismic vulnerability for the already constructed buildings to take measures to strengthen them and mitigating the losses. For the new buildings, research and industry both emphasis on the designing of safe structures which remains undamaged in frequent and a little damaged in case of rare events and are no threats to life in any situation. In the past decade performance based earthquake engineering is evolved which is powerful procedure to design buildings on the basis of probability of exceedance of certain earthquake in a particular time frame. Moreover it gives strong damage limits an damage

Though the performance based earthquake engineering has not gained attention in developing countries like Pakistan. But in countries alike many efforts are being done in developing the seismic codes and building the structures which are earthquake resilient. Moreover work has been done by the various researches in the field of risk and vulnerability assessment for the developing countries like Pakistan. Khan extended the techniques used for earthquake risk assessment which was developed by Kythreoti (2002). More recently Ahmad extended the methodology which was first established by Kyriakides (2007) for the analytical vulnerability assessment of Cyprus with sophisticated modeling. He derived the vulnerability curves for low rise and medium rise buildings taking Islamabad as case study. Earthquake data which was utilized was Kashmir Earthquake which hit Pakistan in 2005. Kamran (2011) used the same to develop vulnerability curves for the building designed using modern seismic codes. Arsalan (2015) drew vulnerability curves for existing building stock in Pakistan considering bar pull out and joint shear behavior in modeling. Usman (2015) considered number of stories and number of bays as variable and all the structures which are being constructed in Pakistan. He established the vulnerability curves using probabilistic applications for the buildings. For the present study one of the buildings from his research will be considered here. All of the above researchers used static methods for the derivation of vulnerability or fragility curves.

Whether it's about establishing the vulnerability assessment, fragility curves or defining the limit states for PBEE frame work, various methodologies exist. Among all incremental dynamic analysis is supposed to be the most promising tool. Ground motion records are scaled to various multiple intensities, to capture the full range of response of structure from elastic to global dynamic instability. The structure is modeled and subjected to scaled ground motion records the response (maximum drift ratio) is recorded against the intensity (spectral acceleration or PGA). Furthermore in this study, two different methods for selection of earthquake records for performing IDA will be compared. Choosing a set of random earthquake histories has been state of the art practice in past researches related to IDA.

## 1.2. AIMS AND OBJECTIVES

The main aim of this research study is to develop the IDA curves using the earthquake records which are selected based on two different methods and then drawing the fragility curves and defining limit states for performance based earthquake engineering frame work.

1. Selection and scaling of earthquake records according to the appropriate site specific design spectrum.
2. Structural sophisticated modeling in OpenSees of the subject reinforced deficient building.
3. Performing Incremental Dynamic Analysis.
4. Drawing fragility curve.

Organization of Thesis

**Chapter 1** consist of introduction of seismic fragility, building sock which are vulnerable in developing countries, structural deficiencies, and Incremental Dynamic analysis.

**Chapter 2** consist of detailed literature review of all the methods available for seismic vulnerability assessment their cons and pros. Different ways of indicating damage and intensity of ground shaking will be discussed and focus will be on selecting suitable indicators for IDA curves. A concise introduction to Incremental Dynamic Analysis will be included; definition of its basic parameters its pros and cons. Study of various factors which pose ambiguities to assess the true behavior of the structure.

**Chapter 3** includes a brief review of the methods for selection and scaling of earthquake records which previous researchers have used for nonlinear time history analysis. A discussion of all site and structure specific criteria for selection of earthquake records will be encompassed. A procedure of building of the target spectrum and selection of earthquake records according to the time period range and single time period. Ground motion database availability and discussion of all the parameters required to specify on which basis the ground motion records are chosen.

**Chapter 4** consists of detailed discussion modeling. A detailed literature review of joint shear failure and bar pull out failure in the model, analytical parameters and back bone curve for joint shear stress and strain. Verification of analytical tool with the joint model

which is being used with experimental results and explanation about selection of compatible nonlinear elements which can smoothly run incremental time histories will also be the part of this chapter.

**Chapter 5** comprises of results for an under reinforced and poorly detailed building subjected to incremental dynamic analysis and selection of suitable structural response and intensity measure. Effects of selection of earthquake from far field and near field region, comparison of method of selection and definition of limit states will also be included.

**Chapter 6** covers research summary and recommendations.

*Chapter – 2*

# LITERATURE REVIEW

## 2.1 INTRODUCTION

This chapter provides the review of literature about seismic vulnerability and its methods which are developed with the passage of time. A summary about how different researchers used diverse methodologies and parameter to present their vulnerability curves and functions. Moreover a concept of damage measure (DM) and intensity measure (IM). A broad view about Incremental Dynamic Analysis method is given. In addition its vital role in defining the limit states for newly born but comprehensive Performance Based Earthquake Engineering method. And the concept of introducing spectral ordinates as intensity measure rather than structural independent quantities with advantages and disadvantages. And finally a proposal to derive the fragility and vulnerability curves from IDA method.

## 2.2 BACKGROUND

The seismic vulnerability is susceptibility of damage for given earthquake to the element which is at risk(Tyagunov, 2004). Vulnerability assessment needs to be carried out for a typical ground motion records for a building or assembly of buildings to find the seismic capacity. Which is after that can be compared with seismic demand of the region to estimate the expected probability of exceeding various limit states and damage.

Vulnerability curve is a graphical correlation between damage measure and intensity measure, so unique parameters have been used for damage scale and intensity scale by different researchers according to the methodology adopted. The selection for method depends on scope, availability of data and technology.

## 2.3 METHODS FOR VULNERABILITY ASSESSMENT

There are four methods for vulnerability assessment;

i. Empirical (based on observational data)
ii. Judgmental (based on experts opinion)
iii. Analytical (based on analytical simulations)
iv. Hybrid (combination of above three)

### 2.3.1 Empirical method

In case of seismic event a post-earthquake survey is conducted and through the data obtained, vulnerability curves are drawn. Then it is assume that those vulnerability curves are valid for the similar type of future events for that region and also for the regions with the same building taxonomy.

In this method data source is most realistic because detailed survey is carried out. All the practical details are taken into account for the region and building stock for instance soil structure interaction, distance from fault, topography, stiffness and strength degradation, which all are difficult to model in analytical method.

One of the disadvantages of this method is damage data obtained is specific because a very few surveys are carried out for a region or earthquake event. Empirical vulnerability needs to be carried out from damage data of large number of earth quakes. But as seismic events of high intensity in larger populate cities happen rarely so damage data is clustered at the low damage and low ground motion range.

Generally no attention is given to incorporate varied characteristics of buildings e.g. building heights, seismic design provision and material in survey rather typology of the region is main feature. Consequently the given curve is limited and specific to that built environment (T. Rossetto, 2003). Errors in damage classification are introduced because surveys are carried out by the engineers of different experiences and using poor discrete damage scales. Moreover damage may be aggregated and accredited to other calamities (landslides, tsunamis and fire etc.) and not just specifically to earthquakes. In this case these uncertainties cannot be eliminated even from manipulation and cause data scatter (Orsini, 1999).

In empirical method macro seismic scale is set according to the damage data, so both ground motion and vulnerability are selected according to damage data.

Sub-standard construction and retrofitted structure cannot be modeled easily but building stock can be upgraded to higher or lower vulnerability class respectively.

Seismic hazard maps are now in form of PGA (peak ground acceleration) or spectral ordinates so uncertainty arises when intensity is converted.(Calvi et al., 2006)

There are two main types of empirical assessment method;

a) Damage probability matrices
b) Continuous Vulnerability function

**a) Damage probability matrices (DPM)**

Whitman et al (1973) proposed damage probability matrix for the first time for same typology buildings to undergo in given damage state for given intensity (Scawthorn & Chen, 2002) . The damage state format with respect to intensity is given in table 1. Whitman compiled damage probability matrices for 1600 buildings of various typologies for real earthquake (San Fernando).

Braga et al (1982), derived DPM for the first time in Europe with data from the Italian earthquake Irpinia (1980). He used binomial distribution for the damage which can be represented with only one parameter from 0-1. Buildings were divided into three vulnerability classes and damage probability matrix was derived for each class. There is a direct relationship between damage and typology of buildings and MSK scale was used. This method is still in use in Italy. Other researchers now have made an attempt to update DPMs in new scale.(Scawthorn & Chen, 2002)

**Table 2.1: Damage Probability Matrix**

| Damage State | Structural Damage | Non-Structural Damage | Damage ratio (%) | Intensity of Earthquake | | | | |
|---|---|---|---|---|---|---|---|---|
| | | | | V | VI | VII | VIII | IX |
| 0 | None | None | 0-0.05 | --- | --- | --- | --- | --- |
| 1 | None | Minor | 0.05-0.3 | --- | --- | --- | --- | --- |
| 2 | None | Localized | 0.3-1.25 | --- | --- | --- | --- | --- |
| 3 | Not noticeable | Widespread | 1.25-3.5 | --- | --- | --- | --- | --- |
| 4 | Minor | Substantial | 3.5-4.5 | --- | --- | --- | --- | --- |
| 5 | Substantial | Extensive | 7.5-20 | --- | --- | --- | --- | --- |
| 6 | Major | Nearly total | 20-65 | --- | --- | --- | --- | --- |
| 7 | Building condemned | | 100 | --- | --- | --- | --- | --- |
| 8 | Collapse | | 100 | --- | --- | --- | --- | --- |

**b) Continuous Vulnerability Function**

Continuous vulnerability curve were derived a short while after damage probability matrices, one of the problem in their derivation was that macro seismic intensity was not the continuous variable.

Spence et al (1992), used Parameter less Seismic Intensity (PSI) to develop the vulnerability curve using MSK (Medvedev-Sponheuer-Karnik) scale (Spence, Coburn, Pomonis, & Sakai, 1992).

Orisini also derived vulnerability curves based on PSI for apartment building in Italy from damage data obtained from Irpinia earthquake. Ultimate both studies converted to PSI to PGA using empirical correlation (Orsini, 1999).

Sabetta et al (1998), MSK macro seismic scale was used to draw the fragility curves with binomial damage distribution. Damage data was obtained from post-earthquake surveys of approximately 50,000 buildings divided into three structural classes and six damage levels (Sabetta, Gorretti, & Lucantoni, 1998)

Yamazaki and Murao (2000), also obtained empirical vulnerability curves from statistics attained from Kobe earthquake. Peak ground velocity was the ground motion parameters.

Rota et al (2006), conducted a survey from post-earthquake damage data of 90,000 buildings. Damage probability matrices were obtained first then fragility curves were drawn, which related the probability of exceeding any damage state to mean PGA at location of damaged buildings. PGA was derived from the attenuation equations given by Sabetta and Pugliese in 1987 (Rota, Penna, & Strobbia, 2006).

Rosetto and Elnashai (2003), Scawthorn et al (1981), Shinozuka et al (1997) derived vulnerability curves using spectral ordinates rather than PGA or macro seismic intensity using normal and lognormal distribution as shown in figure 1. These curves are supposed to be the enhanced curves as buildings' seismic characteristics were taken into account and showed a compatible relationship between ground motion and damage. This has been made possible because of the emergence of more and more equations based on spectral ordinates. So such kinds of vulnerability curves assess the analytical seismic capacity of buildings rather than typology of the region.

Miriam et al (2008), developed a methodology to obtain vulnerability curves which are based on 30 years of empirical data in Italy and then compare it with analytical or mechanical methods to highlight the shortcomings of both.

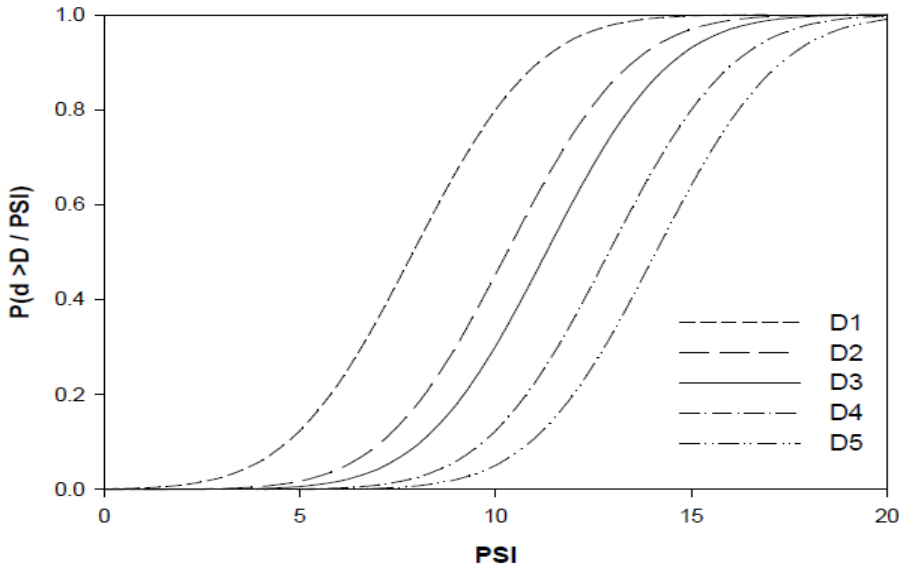


**Figure 2.1: Continous Vunerability Function with Parameter less Seismic Intensity and Probability of exceedance of Damage**

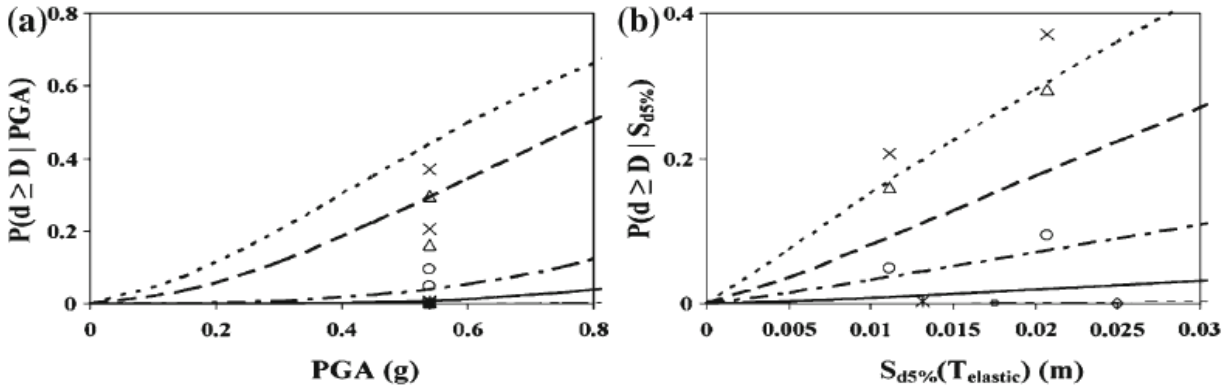


**Figure 2.2: Continous Vunerability Function, (a) Peak Ground Acceleration with Probability of certain Damage, (b) Spectral Acceleration with Probability of certain Damage**

### 2.3.2 Judgment based Method

In this method a panel of civil engineers expert in earth quake are asked to provide an estimate of damage distribution for different type of structure at given intensity level. The experts should provide appropriate predictions with respect to damage distribution functions so that damage states are plotted against ground motion intensity.

Experts take into account all the seismic characteristics of structures e.g. height, material, time period etc, which was a draw back in Empirical vulnerability assessment. Ultimately judgment based curves are used in most of the codes in United States of America for the generation of damage probability matrices and vulnerability curves (ATC-13 and ATC-40).

The disadvantage of this method is subjectivity and conservatism in the opinion of an expert. In addition to that local structure properties are taken into deliberations, so those vulnerability curves are not valid for structure which varies in structural properties.

Freeman (1932), was the first to offer his judgment to insurance companies for future losses for different type of structures and soil conditions for all the buildings in the region affected by large ground motion severity.

DPM based on expert judgment was introduced in ATC-13 for the first time (ATC-13, 1985). More than 50 researchers were asked to deliver their estimates for low, best and high damage for Modified Mercalli Intensity (MMI) for VI to XII for 36 different building. So from ATC-13, this approach was used in vulnerability and risk assessment for different cities.

Giovinazzi and Lagomarsino (2001,2004) proposed a method that leads to define the damage probability matrix based on European Macro seismic Scale EMS-98 (Grunthal, 1998). EMS describe qualitatively few, many and most for five damage grades for intensity range V to XII for six different classes A-F of vulnerability in damage matrix. A damage matrix is given in table 2 for vulnerability class C. (Yamazaki & Murao, 2000)Schnabel (1987), made an attempt to derive vulnerability curves from the damage data and expert opinion for Cyprus as shown in figure 3. Lower and upper bounds are shown for superior and substandard construction. This became reference point for Kyridies who made an effort to obtain vulnerability curves for Cyprus through mechanical method.

**Table 2.2: Judgment Based Vulnerability Function**

| Damage Level Intensity | Damage Grade | | | | |
|---|---|---|---|---|---|
| | 1 | 2 | 3 | 4 | 5 |
| V | | | | | |
| VI | Few | | | | |
| VII | | Few | | | |
| VIII | | Many | Few | | |
| IX | | | Many | Few | |
| X | | | | Many | Few |
| XI | | | | | Many |
| XII | | | | | Most |

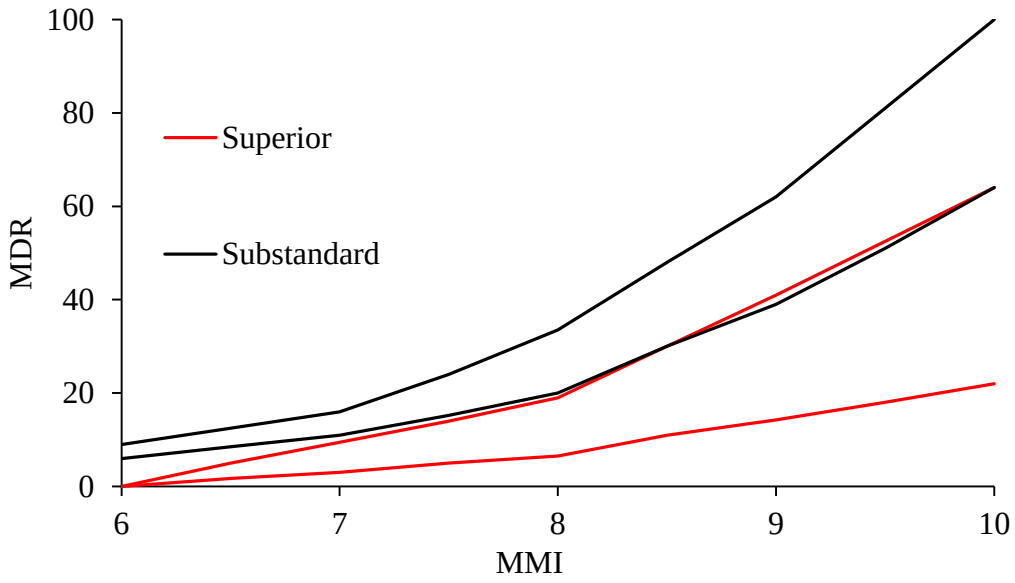


**Figure 2.3: Mean Damage Ratio with MMI**

### 2.3.3. Analytical assessment method

Analytical vulnerability curves are drawn by damage distribution data simulated from the structure model subjected to earthquake loading. Analytical approach is less biased and more reliable compared to empirical and judgmental assessment. This method covers a

wide range of procedures from 2D, elastic analysis of single degree of freedom structure (Mosalum et al) to 3D inelastic time history analysis (Singhal and Kiremidjian). Derivation of analytical vulnerability curves posed a difficult challenge about modeling of the structure regarding inclusion of details.

But with the development of this method the improvement in shortcomings occurred and finer models and better computational efforts are being practiced. Moreover with new analysis procedures, it is convenient to expedite damage data from extensive analysis efficiently.

Most of the analytical vulnerability curves are used in USA. The choice in input parameter like structure idealization, loss model and seismic hazard greatly influence the derived curves. A lot of contradictions had been found in vulnerability curves drawn by different authorities for same location, structure type and typology.

There are two main categories of analytical methods;

a) Simple analytical methods
b) Detailed analytical methods

**a) Simple analytical methods**

Following is the flow chart given for the derivation of probability matrices and vulnerability curves analytically; adapted from Dumova and Javanosk (2004).

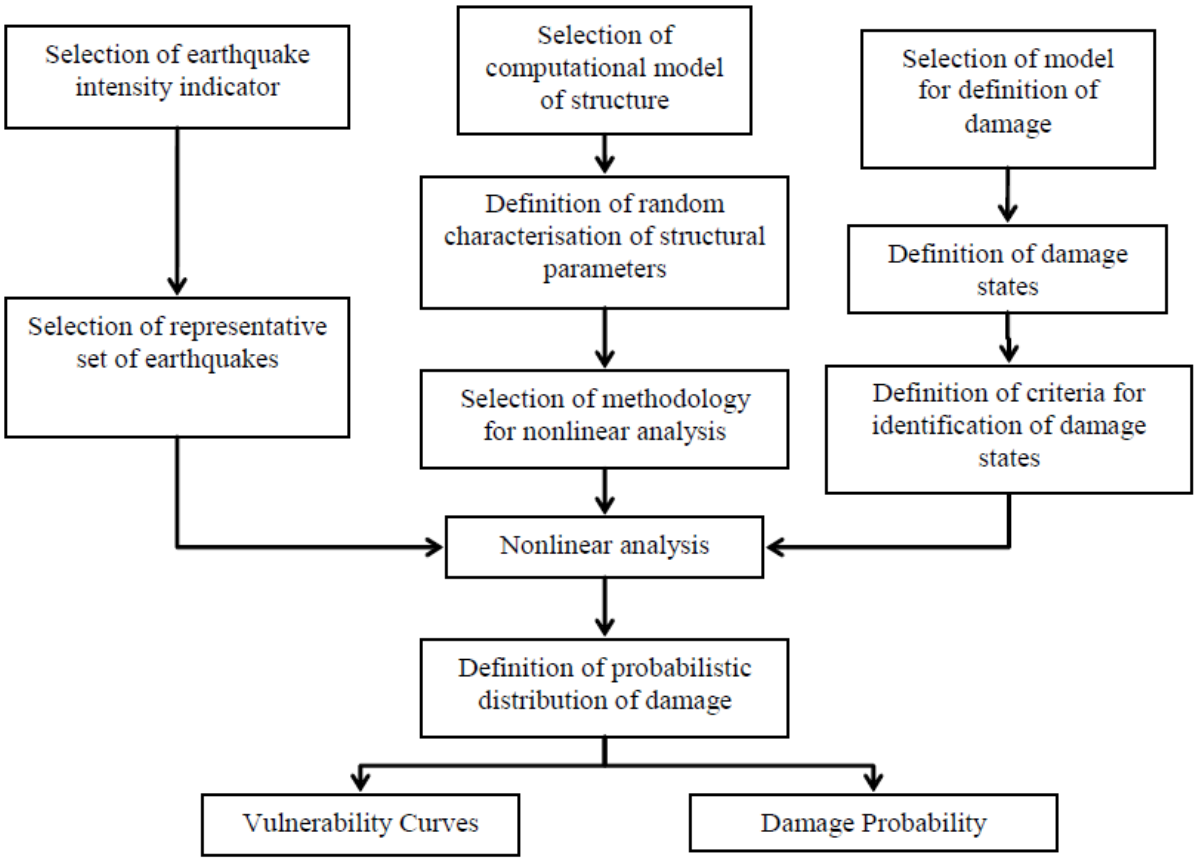


**Figure 2.4: Frame Work for Analytical Vulnerability**

Czarnechi's method (1973) is one of the earliest vulnerability assessment methods for estimation of loss using structural analysis. Loss model considered was weak pier-strong spandrel and only damage to columns is significant. The steps involved were;

- Stress strain curve for column was drawn and area "$A_T$" under that curve till stress reached its ultimate point was evaluated. ($A_T$ value is same for all columns).
- Peak inter-story drift was determined by structural analysis and bending strain was computed at quarter point of the column.
- Through bending strain, stress strain curve was developed for each column and $A_X$ was computed which was area under stress strain curve.
- Ratio $A_X/A_T$ was found for each column at each story. Estimated cost to repair the structure using relation given below;

$$D = \frac{1}{n}\sum_{i=1}^{n}\frac{1}{k}\sum_{j=1}^{k}\frac{A_{xi,j}}{A_{Ti,j}} \qquad (2.1)$$

Where “n” is number of stories and “k” is number of columns in every story.Total damage was estimated through vulnerability functions as a function of total cost calculated from above equation.

Kustu and Scholl (1981,1982) presented a methodology to estimate damage for high rise buildings. They enumerated numerous features of any analytical method and they emphasis that these method should satisfy the following requirements;

- It should be based on engineering principles.
- Easily adaptable.
- Uncertainty in ground motion, structure model and method assumptions should be taken into account.
- It should be easily automated.

A theoretical approach was developed by estimating damage for a hypothetical structure subjected to ground motion with known response spectrum. Inter-story drift “$\delta_{roof}$” was found at fundamental mode of vibration through following relationship in terms of modal participation factor “γ” and spectral displacement “$S_d$”.

$$\delta_{roof} = \gamma S_d \qquad (2.2)$$

The fundamental time period of the building is computed as;

$$T = 0.1\,N \qquad (2.3)$$

Lateral deformation “Δu” is calculated as given in the following equation;

$$\Delta u = {}^{\gamma S_d}/_{N} \qquad (2.4)$$

If lateral deformation can be known for various levels of damage then “$S_d$” verses “N” can be evaluated and tabulated in Table. Kustu et al (1982) gave empirical relationship for component damage with structure response.

Singhal and Kiremidjan (1996) developed fragility curves and DPM for three categories of reinforced concrete structures using Monte Carlo Simulations. The damage distribution was found using MMI and PGA but fragility curves were using spectral ordinates. The main components of this procedure are;

- Characterization of model when subjected to earthquake load.
- Depiction of ground motion.
- Quantification of change of response with respect to varying ground motion.

They used nonlinear time history analysis for various structures with different characteristics to estimate global damage index using relationships given by Park and Ang (1985); simple and calibrated using past earthquake damage data. Shinghal and Kinremidjan presented their fragility curves for low rise buildings which were subsequently updated using observational data obtained from a survey of 84 buildings damaged by 1994 Northridge Earthquake.

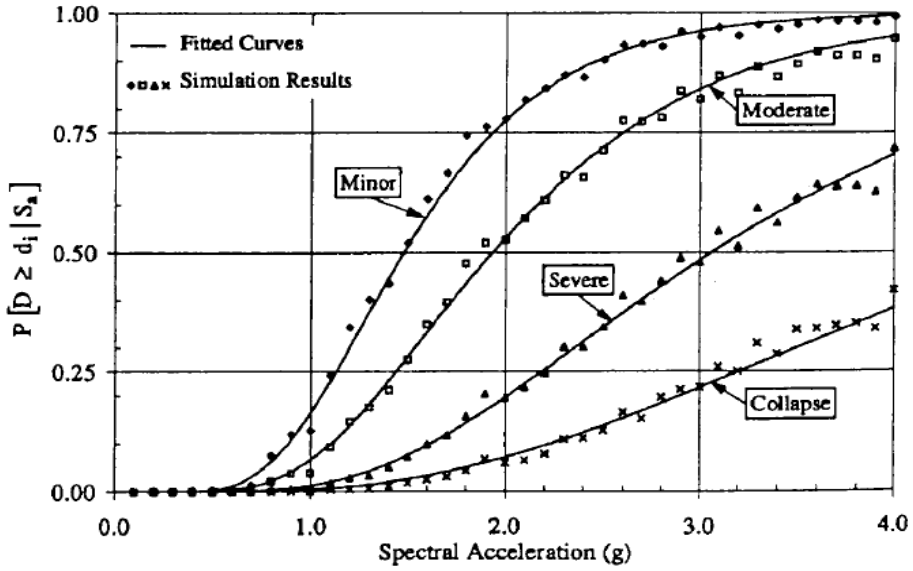


**Figure 2.5: . Shinghal and Kinremidjan Fragility Curve**

G.M Calvi (1999) proposed a method based on estimation of displacement and energy capacity of existing coterie of reinforced and masonry buildings. Damage distribution was represented in terms of probability of exceeding given limit states at given intensity using suitable spectra. Limit states were define by setting ranges of strains for structural damage and range of drift ratios for non-structural damage. The steps in procedure involved;

- Structures were converted to SDOF model, secant stiffness was chosen using displacement demand and damping with respect to energy dissipation.

- Minimum and maximum displacements and time period were found according to yielding of reinforcement using relationships based on drift ratios.
- These smallest and largest values of both quantities were marked on the response spectrum and a rectangle was plotted as show in figure.
- Displacement demand and capacity was estimated by finding the area of rectangle above and below the intersecting line of response spectrum. Then damage was computed according to capacity and demand.

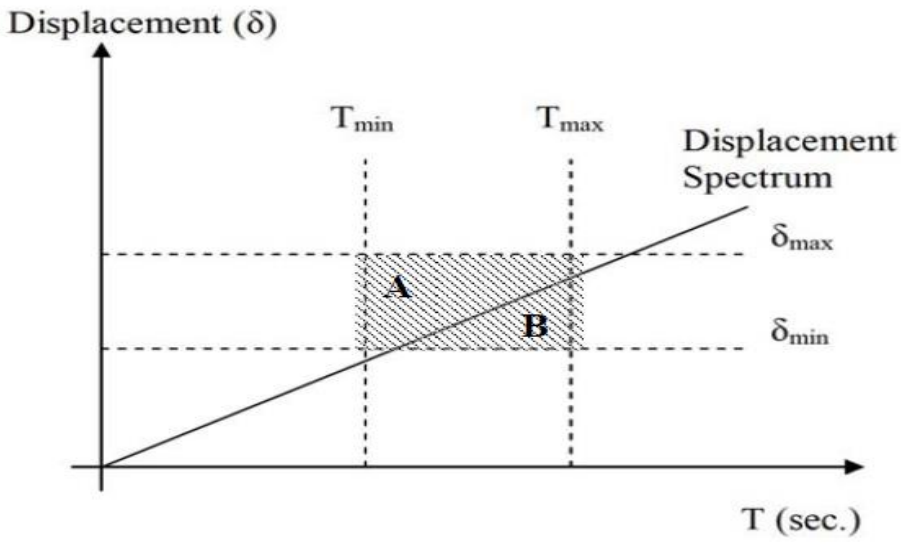


**Figure 2.6: Damage Distribution**

**b) Detailed analytical method**

Detailed analytical methods are thorough and demanding and require for important buildings or where there is no empirical data available. Accuracy of these methods relies on precise determination of hazard parameters, refined structure modeling and appropriate method analysis. Hazard involves selection of parameter for ground motion for instance response spectrum or time history etc. In modeling of structure intricate details should be kept in mind about failures and should be modeled. As if these issues are not addressed in these studies then choosing any sophisticated method for analysis becomes invaluable.

Details will be provided about hazard and structure modeling in subsequent chapter. There is four broad classification of analysis;

i. Linear static procedures
ii. Linear dynamic procedure
iii. Nonlinear static procedure
iv. Nonlinear dynamic procedure

### i) Linear static procedures (LSP)

This method is applicable to the symmetric buildings where there is no issue for seismic torsion and higher modes. Displacement computed using equivalent elastic stiffness is assumed to be equal to the displacement of the structure when undergoes design loads. This method cannot be used when demand to capacity ratio exceeds 2. Total lateral load applied can be calculated from the following formula;

$$V = C_1 C_2 C_3 C_m S_a W \qquad (2.5)$$

"V" is total base shear, $C_1$ is ratio of peak displacement of inelastic system to peak displacement of elastic system, $C_2$ accounts for pinching effect, $C_3$ is considered for P-Δ effects and $C_m$ is for higher mode effects. "$S_a$" is spectral acceleration and "W" weight of the structure comprises of 25% live load also. Fundamental time period of the structure can be calculated from;

$$T = C_T (H_n)^{\beta} \qquad (2.6)$$

*"$H_n$"* is the building height from base to roof, "$C_T$" and "$\boldsymbol{\beta}$*"* depends on structural system. Fundamental time period is an important parameter in assessment of procedure because it alters the force in static and change the displacement in dynamic analysis. The total base shear is distributes story wise by the following formula;

$$F_x = \frac{w_x h_x^k}{\sum w_i h_i^k} V \qquad (2.7)$$

"$w_x$" & "$w_i$" and "$h_x$" & "$h_i$" is weight and height at level "$x$" and "$i$" respectively. K=1 for T<0.5sec and k=2 for T>2.5sec. As there is no reduction factor applied so demand will be exceeded than strength for those components which are expected to reach their yield point. (FEMA 356)

### ii) Linear dynamic procedures (LDP)

These procedures involve analysis through response spectrum and time history analysis. Elastic stiffness and equivalent damping is use in analysis.

Linear response spectrum is used which is unmodified to account for nonlinear response. Response spectrum includes calculation of modal response from maximum number of modes to capture 90% of mass participation of the building in both principal orthogonal directions. Peak deformation and forces are measured through square root of sum of squares (SRSS) or complete quadratic combination (CQC).

The response of the structure is taken at discrete time steps subjecting structure to time history or synthetic ground motion. Damping associated shall reflect the damping at yield. The peak response will be taken if structure is subjected to three ground motions and average response is taken when seven or more than seven ground motions are taken.(Chen and Lui)

Though LSP and LDP have indirect relationship in developing vulnerability curves but all those new methods are developed based on these pioneer procedures.

### iii) Nonlinear Static procedures (NSP)

In these methods a mathematical model chosen should be capable of incorporating inelastic response and includes strength, stiffness degradation. Displacement Coefficient Method is nonlinear static procedure in which target displacement is assumed to be the maximum displacement which a structure will experience during design earthquake. The procedure involves in calculating displacement is by selecting a control node at the center of the mass which is considered to be at the floor level and subjecting a structure to increasing lateral loads until target displacement reached. For application of lateral load two modal patterns can be selected one from each of the following;

1. When 75% of the modal mass participates in fundamental mode then lateral load from above equation is calculated or vertical distribution of lateral force proportional shape of fundamental mode or lateral force proportional to story shear combining all the modal responses where 90% of the total mass participates.

2. Lateral force which is distributed according to the mass in each story or adaptive load pattern according to the displaced position of the structure.

The target displacement is given as;

$$\delta_t = C_0 C_1 C_2 C_3 S_a \left[\frac{T_e^2}{4\pi^2}\right] g \qquad (2.5)$$

$C_0$ is a factor which relates the spectral displacement of SDOF system to MDOF system. $C_1$, $C_2$ and $C_3$ are the factors which are already defined in linear static procedures. $S_a$ is spectral acceleration. "$T_e$" is effective time period, can be calculated from the following formula;

$$T = T_i \sqrt{\frac{K_i}{K_e}} \qquad (2.6)$$

"Ki" and "Ke" are initial and effective stiffness and can be observed in idealized force displacement relationship. Ke" is effective lateral stiffness considered at 60% of yield strength. There is also a post yield stiffness is a slope calculated at line which passes through the target displacement (FEMA 356).

Nonlinear static procedure consider peak demand without considering an explicit account of cumulative damage but in ***Capacity Spectrum Method*** the backbone curve of pushover hysteresis implicitly take account of aggregated response. Capacity spectrum is an altered form of pushover curve or capacity curve which is in form force displacement relationship. Then this pushover curve is converted to ADRS (acceleration – displacement response spectrum) format. The capacity of the building is determined by applying static load incrementally until the capacity of the building is reached. Pushover curve is obtained by applying the load until the target displacement is achieved. Capacity curve essentially has to be pushover curve. If inelasticity of every component is modeled clearly in the analysis then resulting force displacement relationship is required capacity curve. But ATC 40 has provided a linear and simplified procedure to approximate nonlinear behavior of the building. In this procedure lateral load is applied to the structure till most of the members reached its 90% capacity then analysis is stopped. In next step stiffness is reduced and the again analysis is run. A pushover curve is drawn at the end of the analysis.

Following formulae are used to convert pushover curve to ADRS format;

$$S_{d,n} = \alpha_n \left( {}^{V_n}/_{W} \right) \quad (2.7)$$

$$S_{a,n} = \frac{\Delta_{c,n}}{\beta_n \phi_{c,n}} \quad (2.8)$$

$$\alpha_n = \frac{\sum_{i=1}^{N} w_i \phi_{i,n}^2}{\left(\sum_{i=1}^{N} w_i \phi_{i,n}\right)^2} \quad (2.9)$$

$$\beta_n = \frac{\sum_{i=1}^{N} w_i \phi_{i,n}}{\sum_{i=1}^{N} w_i \phi_{i,n}} \quad (2.10)$$

$S_{d,n}$ and $S_{a,n}$, is spectral displacement and spectral acceleration at mode "n", $V_n$ is base shear, W is seismic weight of the building, $w_i$ is weight of the building at level "i", $\phi_{i,n}$ is modal amplitude at level "i" for mode "n", $\Delta_{c,n}$, $\phi_{c,n}$ is displacement and modal amplitude of control node at mode "n".

Now the next step is to covert the response spectrum; which shows demand side is converted to ADRS format, so that the comparison between capacity and demand can be done. Design response spectrum is in terms of period and spectral acceleration and results by analyzing SDOF system.

The following relationship between pseudo acceleration and displacement is used for the alteration into required format;

$$S_d = \frac{PS_a T^2}{(2\pi)^2} \quad (2.11)$$

$$\frac{PS_a}{S_d} = \lambda = \left(\frac{2\pi}{T}\right)^2 \quad (2.12)$$

Radial lines emanating representing each λ value c-orresponding to $T_i$. Now both demand and capacity curves are overlapped to find the performance point, as demand curve is obtained by elastic design spectrum so is valid if structure response remains elastic. If structure doesn't remain elastic, then comparison of capacity curve is made with reduced design spectrum. (ATC 40)

***Development of Capacity Spectrum Method***

Freeman et al (1975) used this method for the first time to measure the deformation of SDOF system. Then Kircher et al (1997) established a methodology of deriving

vulnerability curves for NIBS and FEMA by using this method. Since then evolution of this method is done by various researchers. ***Fajfar (1999)*** pointed out some flaws and highly damped spectrum is used in ATC-40 conventional method such as highly damped spectrum is used. There is no stable relationship between hysteresis energy and equivalent viscous damping. Time period which is related to highly damped spectrum may not be applicable to inelastic spectrum. Fajfar proposed that inelastic spectrum can be used obtained from time history analysis of inelastic SDOF and performance evaluation method N2 was also found in CSM (Fajfar 1999). ***A.K Chopra*** found out conventional CSM method underestimate the deformations for wide range of period when type "A" damping model is chosen and is deficient to relative elastic spectrum in displacement and velocity regions. So he introduced a constant ductility demand diagram by dividing demand diagram with appropriate ductility dependent reduction factor. The performance point is selected where demand diagram intersect the capacity diagram at that value of ductility calculated from capacity diagram. ***Yu-Yuan Lin (2003)*** suggested that in lieu of using pseudo acceleration for the generation of elastic demand spectrum, real acceleration should be used without using inelastic demand spectrum. It was shown in his studies that when equivalent viscous damping is more than 10% and time period is greater than 0.15sec then pseudo acceleration is not an appropriate choice. Because iterative results were more accurate when real acceleration "$S_a$" was used.

### iv) Nonlinear Dynamic Procedures (NDP)

Non-linear dynamic procedures include non-linear time histories. The evolution of IDA is based on NDP;

***Incremental Dynamic Analysis*** is extensive and comprehensive method which has recently evolved to have thorough and complete response of the structure under seismic loads. In this method structure model is subjected to one or more scaled ground motions to produce one or more response verses intensity curves. Cornell and Krawinker used drift ratio as peak response and first mode spectral acceleration "$S_a(T_1)$" as ground motion intensity. Elnashai used peak displacement instead of story drift. "$S_a(T_1)$" was plotted on ordinate and peak response on abscissa. IDA, when done for large number of ground motion intensity depicts full range of response for a structure. With the increase

in intensity measure drift ratio increases dramatically, such increase suggest that there structure has reached to its capacity and further increase in intensity measure will lead to instability. IDA covers a wide range of response from elastic to yielding and finally dynamic collapse.

***Fundamentals of IDA;***

***Scale factor***

Scale factor "λ" for IDA is non-negative scalar which is multiplied to a time history to scale up or scale down the original accelerogram. Scaling of an accelerogram is one to one mapping to its scaled images.

***Monotonic Scalable Ground Motion Intensity Measure (IM);***

The intensity measure is non-negative scalar that consist a function that has unscaled accelrogram which is scaled with respect to scale factor "λ".

There are many quantities which can be proposed to represent intensity measure of the ground motion but it should be scalable and monotonic. Moment magnitude, Duration or Modified Mercalli Intensity are not non-scalable. One the other hand Peak Ground Acceleration (PGA), Peak Ground Velocity (PGV), and 5% damped spectral acceleration at first mode period ($S_a(T_1,5\%)$).

But for the sake of seismic vulnerability calculations it is necessary to use structure dependent quantities like ($S_a(T_1,5\%)$ for the better damage distribution) rather than independent ones such as PGA (T. Rossetto, 2003). Moreover PGA is not a good descriptor of damage potential of structure for higher magnitudes because its correlation with observed damage data is inadequate (Wald, Quitoriano, Heaton, & Kanamori, 1999). Also structure is sensitive to the strength of frequency content near it first mode frequency, which can be well represented by $S_a(T_1,5\%)$ rather than PGA (Vamvatsikos & Cornell, 2002). The choice of $S_a(T_1,5\%)$ as IM is efficient and sufficient as there is minimum scatter in the result and least number of earthquakes records are required for the best estimates of capacity and demand of the structure.

***Damage Measure (DM);***

The representation of response of the structure model due to prescribed loading is damage measure.

Choices for damage measures are peak story ductilities, node rotations, maximum base shear or cumulative hysteresis energy or maximum interstory drift, floor interstory drift etc. Selection of damage measure depends on structure itself, assessment of different characteristics of response, defining limit states in performance based design etc. In IDA maximum interstory drift is best option for damage measure because it relates joint rotations well with global and story collapse.

***Single Record IDA;***

"It is study of response of a structure model when subjected to single seismic time history which is scaled up to various levels."

IDA also known as dynamic pushover; consist of many non-linear analysis to be performed on structure model to cover a range of behavior from elastic to non-linear and finally dynamic collapse.

***IDA curve and its characteristics;***

IDA curve is plot of damage measure recorded is verses one or more intensity of ground motion as continuous curve.

In IDA studies Vamvatsikos and Cornell studied various SDOF and MDOF models. Particularly MDOF model, a 20 story steel moment resisting frame and 5 story chevron braced frames with ductile member and connections with fundamental period 4s and 1.8 sec respectively, incorporating P-Δ effects. A nine story with T1=2.2 sec and 3 story with 1.3 sec with ductile members and fracture connections including P-Δ effects. And found the limit states on IDA curves.

John B. Mander et al (2007) found financial risk assessment of bridges using IDA. A prototype bridge pier was considered which was designed for an event of earthquake with probability of exceedance 10% in 50 years with PGA 0.4g according to the three codes of different countries i-e New Zealand, Caltrans and Japan. A general set of earthquake records were selected for performing IDA. Instead of using performance based limit states; damage states which are specified for bridges were selected. Among all the

damage cost for the bridge pier designed on basis of Japan guidelines was coming out to be the lowest because of the conservative design recommendation.

Karbassi and Nollet (2013) carried out IDA on a 6 story industrial unreinforced masonry building situated in Canada. The building is located in the region where less data of earthquake damage is available so a set of real and synthetic ground motion were developed. The ground motion records which were selected were based on site specific spectrum. Applied element modeling was used to model the building and promising results were developed for defining limit states and mean annual frequency of exceedance for each limit state was found for the performance based design.

These above are the main and significant researches carried out on IDA. There is other many present but can't be presented here. There can be some draw backs in IDA which can lead to over or under estimation of structural response. These concerns in IDA are;

- Uniform scaling of ground motion.
- Uncertainty in accuracy of structure model.
- Ambiguity in defining capacity because investigators use different parameters.
- Selection of reliable parameter for collapse.

There are issues in modeling limitations;

- Estimation of initial strength and stiffness.
- Uncertainty in difference of material properties, strength and dimension of designed and as built structure.
- Behavior complexity.
- Limitations in application and modeling complex loading to the structural model.

## 2.4 STRUCTURAL MODELING

Structural modeling in OpenSEES includes incorporating all the possible failures in beam column joints. And non-linear beam column elements are chosen for

### 2.4.1. Beam Column Joint Element

#### 2.4.1.1. Types of joint in RC Structures

There are three types of joints in the structures depending on their end conditions and behavior i-e Edge, Corner and Interior joint as shown in Figure 4.1,

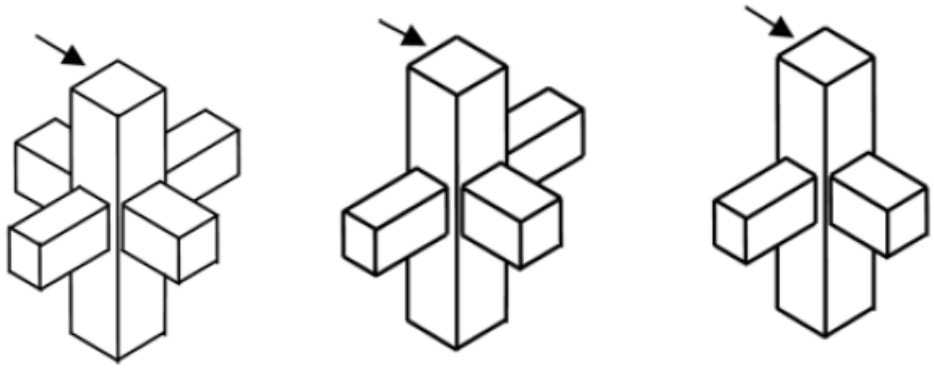

(a) (b) (c)

**Figure 2.6: Interior, Exterior and Corner Joint**

During the seismic loadings each joint behaves differently depending upon the degree of confinement, longitudinal reinforcement and embedment length of the longitudinal reinforcement.

#### 2.4.1.2. Joint behavior under Seismic Forces

Figure 4.2 shows beam column sub assemblage under the moderate to severe earthquake. The moments develop during the ground shaking are supposed to be transferred to joint through tension and compression forces. Tension stresses will be transferred through longitudinal reinforcement (white arrows) and compression forces will be carried by concrete. Shear force will be carried out through flexure compression zone of beam and column as shown in figure 4.3. Figure 4.4 idealized loading of joint core which show that compression and shear is assumed to be transferred through concrete and tension force through bond between concrete and reinforcement.

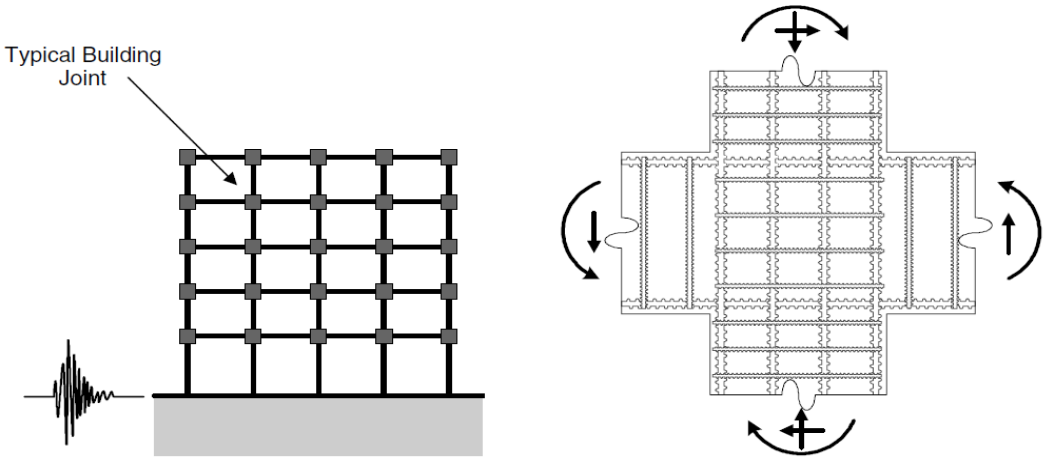


**Figure 1: Building Joint in OpenSEES**

Figure 4.4 shows load distribution mechanism of joint element. There can be various factors which can determine the joint response. Firstly the bond strength partly contributes to joint capacity. Bonnaci and Pantazopoulou (1993) tested 86 joint sub assemblages for reversed cyclic loading and found that 19 specimens were failed due to anchorage failure. Paulay et al (1978) suggested that distribution of bond stresses also effect beam column joint response.

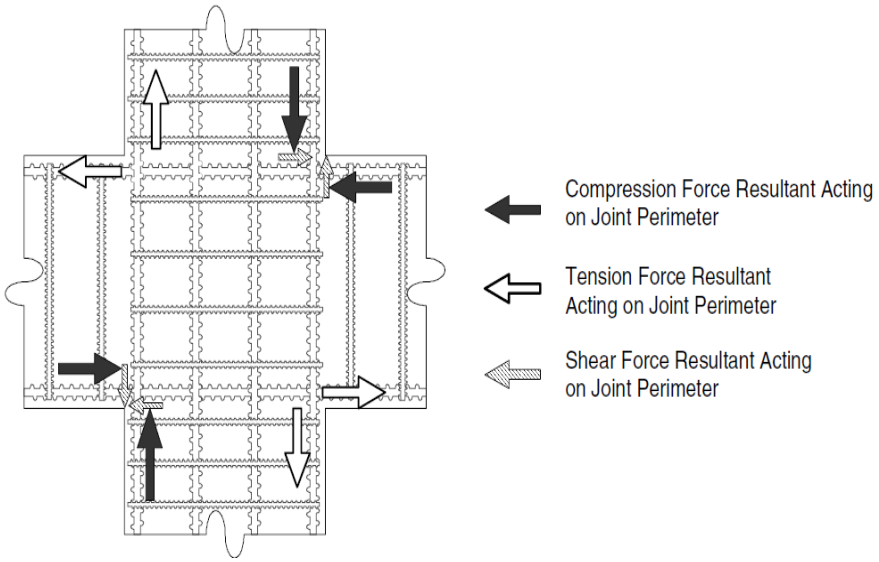


**Figure 2.7: Internal Forces in Joint Perimeter due to Cyclic Loading**

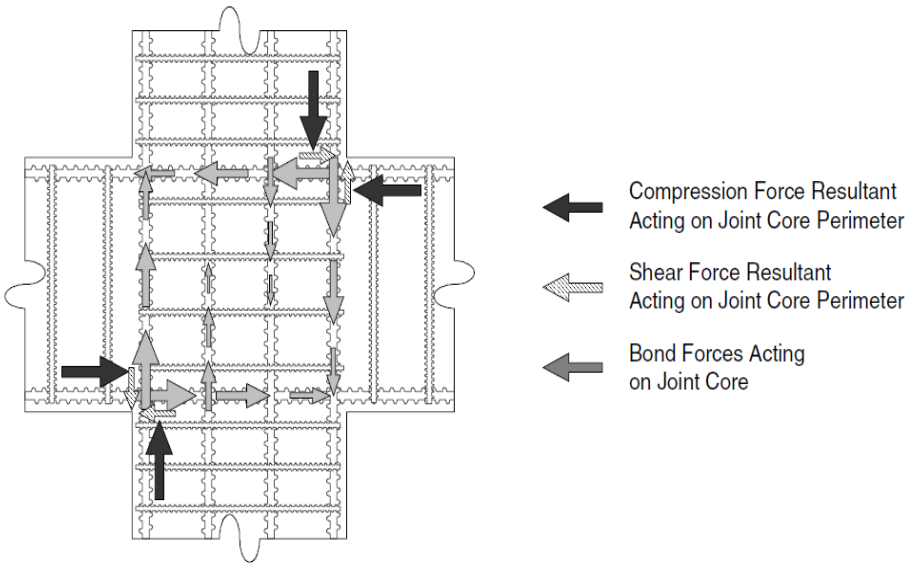


**Figure 2.8: Internal Forces acting on Joint Core due to Cyclic Loading**

Joint shear failure is the most significant factor for the joint failure; shear is applied through grey arrows as in above figure. Compression stress also contributes to joint shear stress. Bonnaci and Pantazopoulou (1953) found 51 out of 86 joint specimens failed due to shear failure of joint. Paulay et al (1953) identified two different load distributions for the joint failure due to shear stress which is uniform and well distributed. Secondly load distribution follows that load transfer primarily through the compression of the joint core concrete, damage occurs due to dilation of compression core.

In addition to the bond failure and joint shear failure another component includes which is due to increased sliding shear failure and decreased interface shear strength. Experimental testing shows that under severe reversed cyclic loading cracks which opens don't get closed when loading cycle reversed [Ma et al 1976] which leads to decrease in strength and stiffness at interface mechanism. Figure 4.5 shows typical joint failure due to bond failure, joint shear degradation and bar pullout.

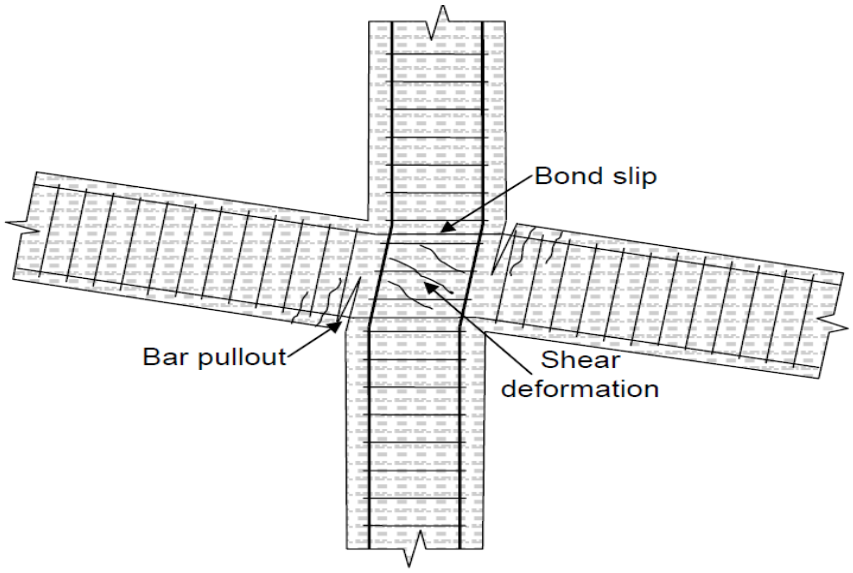


**Figure 2.9: Typical Failure due Bond slip, Bar pullout and Shear Deformation**

### 2.4.1.3. Background and Literature Review

One of the previously used beam column joint is rotational hinge model [El Metwally and Chen 1988; Alath and Kunnath 1995] used by the researchers; represent shear distortion of beam column joint. Moment rotation data from beam and column is used for such model. To cater for the anchorage failure which was not modeled, two assumptions were made. First was that longitudinal reinforcement which is embedded in joint will control the anchorage failure. Secondly total energy dissipation was assumed to be constant. Though this model provides the inelastic behavior of joint action with little increase in computational effort but this model does not facilitate the refined modeling. It needs experimental data of moment rotation from beam column sub assemblages.

Continuum Model is also being used by other researchers, two elements are used; transition element or transition zone to formulate the compatibility of beam column line element which represent the structure outside the joint and continuum element represent structure inside the joint. This model has high resolution and accuracy. Draw backs are additional computational effort, not valid for wide range of joint design and model parameters, many constitutive material parameters needs to be introduced which is not functional for designers.

### 2.4.1.4. Laura Lowes Joint Element

The model which is proposed for this study was developed by Laura N.Lowes and is in built in OpenSEES. As shown in figure 4.6 it consists of eight bar slip spring, which is intended to simulate the strength and stiffness degradation which is associated with bond strength deterioration due to cyclic loading. One component for shear panel which is associated with strength and stiffness degradation for joint core shear failure. Four components to simulate interface shear degradation during seismic loading.

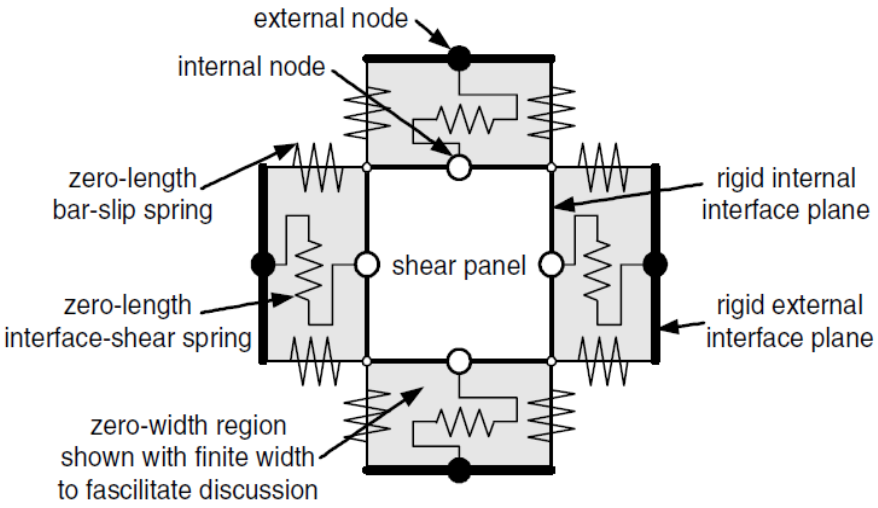


**Figure 2.10: Laura Lowes Joint Element**

### 2.4.1.5. Modeling Joint shear panel

***Pinching4 material*** is used to model joint shear panel, this material exhibits the pinched load deformation response and degradation under cyclic loading. It accounts degradation in three ways, unloading stiffness degradation, reloading stiffness degradation and strength degradation. Following figures show load deformation history for unloading, reloading stiffness and strength degradation.

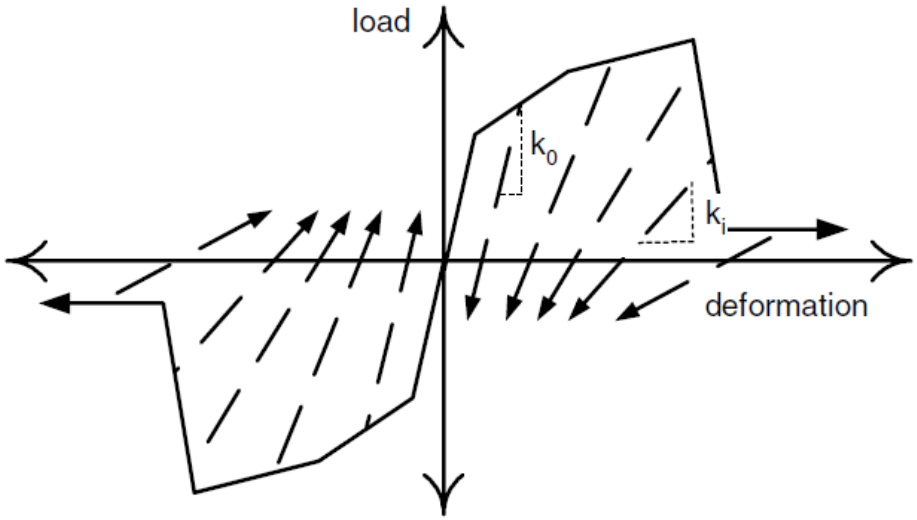


**Figure 2.11: Load deformation curve for Loading and re-loading**

The form of each damage rule is same for strength and stiffness deterioration. This form is proposed from the damage index given by Park and Ang [1985];

$$\delta_i = (\alpha_1 (d_{max})^{\alpha 3}) + \alpha 2 \left(\frac{E_i}{E_{monotonic}}\right)^{\alpha 4} \quad (2.13)$$

Where,

$$d_{max} = \max\left[\frac{d_{\max i}}{def_{max}}, \frac{d_{\min i}}{def_{min}}\right] \quad (2.14)$$

$$E_i = \int_{load\ history} dE \quad (2.15)$$

"*i*" = current displacement

$\delta i$ = Damage index (0 in case of no damage, 1 in case of maximum damage)

α's = parameters used to fit the damage rule to experimental data

$E_{monotonic}$ = Energy required to achieve under monotonic loading

$def_{max}$ and $def_{min}$ = Positive and negative deformation that define failure

$d_{max}$ and $d_{min}$ = max historic and minimum historic deformation

For the case of stiffness degradation

$$k_i = k_0(1 - \delta k_i) \quad (2.16)$$

Where

$k_i$ = current unloading stiffness

$k_0$ = initial unloading stiffness for the case of no damage

$\delta k_i$ = Current value of stiffness damage index

Same form of damage will be applicable for envelope strength degradation

$$(f_{max})_i = (f_{max})_0 \ (1 - \delta f_i) \quad (2.17)$$

Where;

$(f_{max})_i$ = Current envelope maximum strength

$(f_{max})_o$ = Initial envelope maximum strength for the case of no damage

$\delta f_i$ = Current value of the strength damage index

The reduction in strength due to reloading can be simulated by applying the same form to deformation damage.

$$(d_{max})_i = (d_{max})_0 \ (1 - \delta d_i) \quad (2.18)$$

Where;

$(d_{max})_i$ = Current deformation that defines the end of reload cycle for increasing deformation demand

$(d_{max})_o$ = Maximum historic deformation demand

$\delta d_i$ = Current value of the reloading stiffness

**2.4.1.6. Modeling bar slip response**

The bond slip relationship with bar stress is developed on the basis of several simplified assumptions. Bond stress along the anchored length of the bar is assumed to be uniform when reinforcement to be elastic and is piece wise continuous when if more than the yield strength. Slip of bar is function of steel strain distribution. Bar has zero slip at the point of zero bar stress. Bond strength is function of material state of embedded bar, concrete and transverse reinforcement in the vicinity of the bar [Lowes 1990]. Bond strength is high in the compression zone region and is low in tension zone. Following are the equations show bar stress and slip relationship.

For $f_s<f_y$

$$slip = \int_0^{l_{ts}} \tau_E \frac{\pi d_b}{A_b} \frac{1}{E} x dx = 2\frac{\tau_E}{E}\frac{l_{fs}^2}{d_b} = \frac{1}{8}\frac{f_s^2}{\tau_E E} d_b \quad (2.19)$$

For $f_s > f_y$

$$slip = \int_0^{l_e} \frac{4}{d_b}\frac{\tau_E}{E} x dx + \int_{l_e}^{l_y+l_e} \frac{f_y}{E} + \tau_y \frac{4}{d_b}\frac{1}{E_h}(x - l_e)dx$$

$$= 2\frac{\tau_E}{E}\frac{(l_e)^2}{d_b} + \frac{f_y}{E} I_y + 2\frac{\tau_y}{E_h}\frac{(l_y)^2}{d_b}$$

$$= \frac{1}{8}\frac{f_y}{\tau_E}\frac{f_y}{E} d_b + \frac{1}{4}\frac{f_s - f_y}{\tau_y}\frac{f_y}{E} d_b + \frac{1}{8}\frac{(f_s - f_y)^2}{\tau_y E_h} d_b$$

$$l_{fs} = \frac{f_s}{\tau_{ET}}\frac{A_b}{\pi d_b}$$

$$l_e = \frac{f_y}{\tau_{ET}}\frac{A_b}{\pi d_b} \quad (2.20)$$

$$l_y = \frac{f_s - f_y}{\tau_{YT}}\frac{A_b}{\pi d_b} \quad (2.21)$$

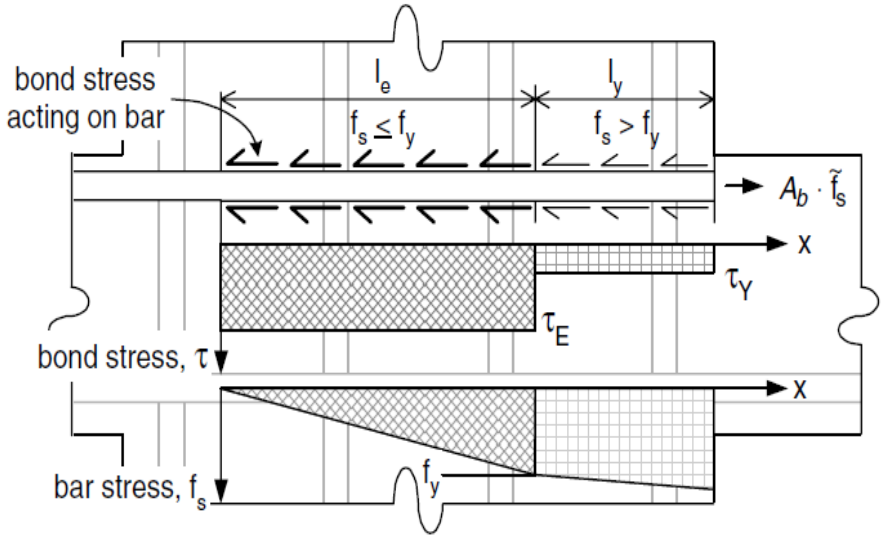


**Figure 2.12: Bar Slip Stress**

To extend the bar slip response from monotonic loading to cyclic loading some parameters need to specify. First is unloading stiffness; which in this model assumed to be equal to elastic stiffness. Residual bar stress which is assumed to be uniform bond stress provided by the study done by Eligenhausen et al [1983]. Slip and force at the time of reloading is assumed to be 0.25 of the maximum historic slip [Eligenhausen and Hawkins].

#### 2.4.1.7. Interface shear modeling

When structure is subjected to severe earthquake loading, the cracks which appear in the vicinity of beam column joint don't get close upon load reversal. Shear transfer occurs in three ways; compression strut mechanism, aggregate interlock and dowel action of longitudinal reinforcement. When the cracks don't appear the shear transfer occurs through strut mechanism, in the presence of crack the purpose is served through aggregate interlocking. Dowel action doesn't play significant role.

The result of study by Walvaren [1981, 1994] is used as a basis for calibrating interface response. He developed a model defining that that normal and shear stress get transferred as a function of bond slip and concrete cracks. It was assumed that shear strength as a function of slip doesn't deteriorate at larger slip. For the closed crack Walvaren used crack width 0.1mm. For cyclic loading following parameters are assumed;

- Unloading stiffness is extremely large and does not deteriorate as a function of loading history.
- Reloading stiffness is almost equal to initial stiffness.
- Displacement is required to develop shear strength.
- Deterioration in strength and stiffness doesn't include in this model.

### 2.4.2. Model Evaluation and Verification

The model proposed by Laura N Lowes was evaluated through the comparison of response tested by Park and Ruitong [1988] for different joint assemblies. Those joint assemblies were tested to achieve different level of ductility under cyclic loading. Four units were tested; one of them was ductile and was designed according to the NZS 3101:1982, others were brittle either with short embedment length or decreased joint shear capacity. Joint shear capacity is function of amount of hoops in beam column joint

and longitudinal reinforcement of column. Schematic diagram of the beam column joint which is caliberated, shown in following figure;

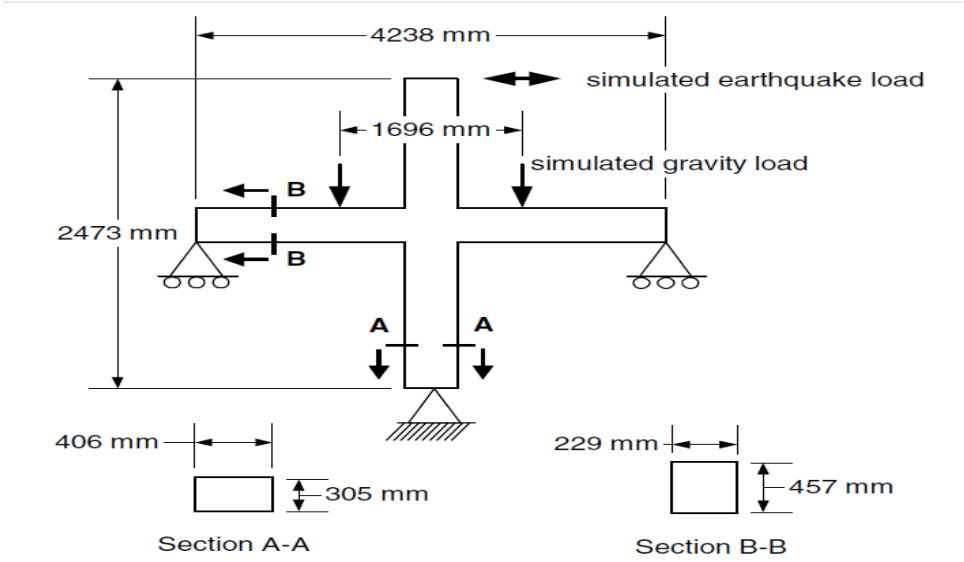


**Figure 2.13: Experimental Model for Beam Column Joint**

A lumped plasticity numerical beam column model was developed to simulate the Park and Ruitong experimentally tested sub assemblages of joints. The model was calibrated on the basis of following assumptions;

- Crack sections are used.
- A plastic hinge equal to depth of beam column is assumed which moment rotation response is taken as beam and column curvature response.

Following figures show the simulated and observed response of ductile and limited ductility specimen;

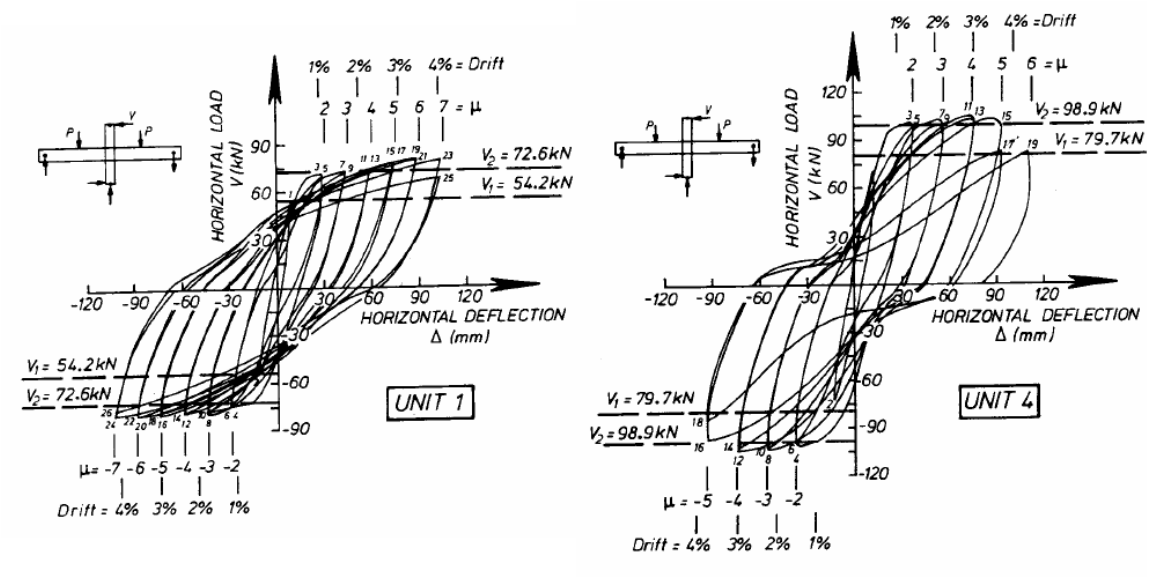


(a) Unit 1 — ductile specimen (b) Unit 4 — limited ductility specimen

**Figure 2.14: Experimental Results of Beam Column Joint; (a) Ductile Specimen, (b) Limited Ductility Specimen**

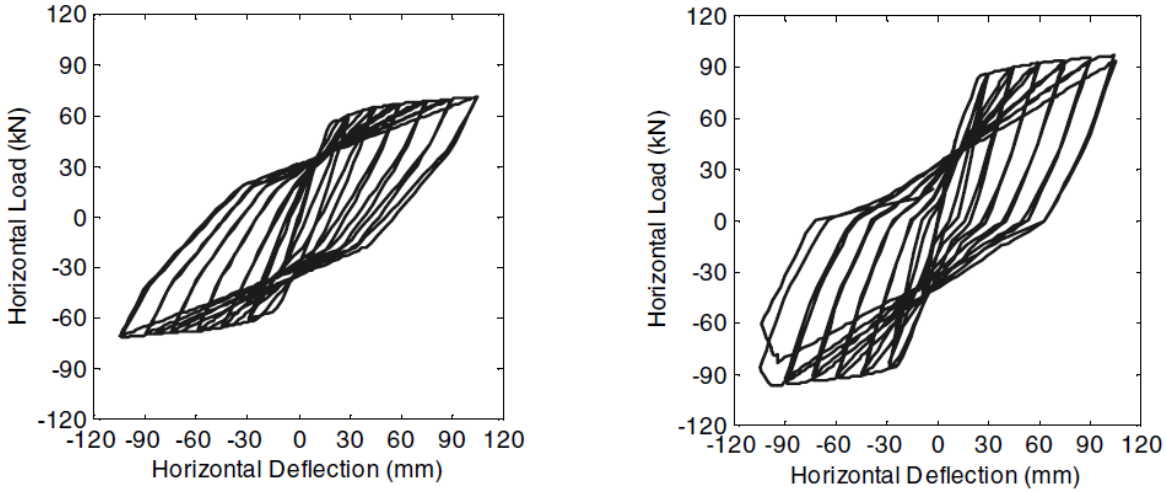


(a) Unit 1 — ductile specimen (b) Unit 4 — limited ductility specimen

**Figure 2.15: Analytical Results; (a) Ductile Specimen, (b) Limited Ductility Specimen**

Comparing the observed and simulated response of experimentally tested specimen, this can be concluded that the present model is appropriate for using in building frames which

are supposed to be tested against cyclic or seismic loading. Simulated response shows this model best fit for the present case where structure is subjected incremental ground motion, as it fulfills well the fundamental characteristic of failure of joint and energy dissipation within joint.

*Chapter – 3*

# GROUND MOTION SELECTION AND SCALING

## 3.1 INTRODUCTION

Using general earthquake ground motion records for conducting fragility analysis through incremental dynamic analysis is current state of practice. Ground motion selection for the said purpose has significant effects on the response of the structure. The other component is scaling which also plays vital role. Frequently, bias in structure response occurs due to consideration of inappropriate parameters for selection and scaling of acceleration records.

In this chapter various methods for selection and scaling will be discussed along with methodology. Moreover, selected earthquake records will be presented for the buildings which are being considered in the present study.

## 3.2 BACKGROUND

Selection and scaling of ground motion records has been a debatable subject almost over a decade for carrying nonlinear dynamic analysis. Because inappropriate methods used for this purpose lead to, over or underestimation of structural response (Luco and Bazzurro, 2007). But bias in structural response can be alleviated by using well selected parameters and by applying more constraint in selection and scaling (Hancock et al 2008).

According to the code requirements (ASCE 2005), the scaling of ground motion should be carried out in such that for 2D analysis, average spectrum of time histories of records to be selected should not be less than design spectrum at $0.2T_o$ to $1.5T_o$ where "$T_o$" is natural time period of structure at its fundamental mode. This period range is considered significant because inelastic behavior leads towards elongation in periods than fundamental period and shorter periods than fundamental take care of higher mode effects. Instead of matching the spectrum for a range of period, modification can also be done by scaling the ground motion to single spectral acceleration say at fundamental mode (Kunneth et al). Baker and Cornell described that selection and modification of ground motions based on spectral shape can decrease the bias and variance in structure

response, which is comparable to reduction when advanced vector valued intensity of ground motion is considered as criterion of selection. On the other hand if scaling is done to target peak ground acceleration then large scatter in structure response occurs (Nau and Hall 1984, Vidic et al 1994, Shome and Cornell 1998). Furthermore, inelastic behavior of the structure is not taken into account while scaling the ground motion, so the method considering the elastic response spectrum will not be applicable for near fault region, so an inelastic deformation spectrum is more suitable for such sites while scaling is done or time history is scaled unless global dynamic instability reaches. Modification of ground motion can be done over selected period bands, to effective peak acceleration, Arias intensity based parameter, effective peak velocity and maximum incremental velocity reported by Kuram and Farrow (2003). It is also reported that most of the scaling methods are most suited for stiff soil and far field region but lose their efficacy with loose soil and near field sites. Heo and Kunnath (2010), compared the two method of scaling, first amplitude scaling to spectrum ordinate at fundamental period of structure and other is spectrum matching for 4 storey and 12 storey building. A regression model was developed to predict the response of structure which is considered to be the so called true response. It was found out that ground motion modification done by spectrum matching were closer to the true median response than scaling carried out to match the ordinate at fundamental period of the structure, the method given by FEMA 695. For selection purpose FEMA 695(2009) classified two groups of ground motion as near fault (site located less than 10km from the rupture line) and far fault ground motion (site located equals to or more than 10km from rupture line). For ground motion modification there are two steps involve, firstly ground motions are normalized to maximum peak ground velocity (PGV) to alleviate the inherent variances due to the difference in fault distance, magnitude, and source type and site conditions. Then normalized ground motions are scaled to specific intensity say median spectral acceleration at fundamental period in order carry out nonlinear dynamic analysis. Recommendations from FEMA 695 for selection of both the set include that records should be independent of structure and hazard site for which IDA should be conducted. Thus those records are appropriate for wide variety of structural system and regions. Referring to FEMA 695 record sets, Christovasilis et al (2011) conducted study on a hypothetical wood frame building in

Tuscany, Italy for developing the fragility curves. He used conditional mean spectra (CMS) for spectral matching because uniform hazard spectrum (UHS) would be more conservative (BAKER 2011). And the results of IDA curves obtained from FEMA 695 pre-defined record set found out to be more conservative than the procedure adopted.

## 3.3 GROUND MOTION DATABASE

Source of ground motion records for this study is PEER NGA West 2 database which is extension of previously used PEER strong motion database which was made publically available in 1999. There are 3551 ground motion records from 173 earthquakes obtained from 1456 different recording stations. There are two horizontal components of every record and vertical component is also available for some of the records. For this study PEER version NGA West 2 is used.

PEER NGA database well quantified and evaluate ground motion parameters. It includes earthquake source information, depth to top of the fault rupture, source to recording path, recording station location, local site condition at recording station and average shear wave velocity $V_{S30}$ in upper 30m.

### 3.3.1 Introduction

Its graphic user interface makes the search and processing user friendly. Numerous facilities like check boxes, popup menus and buttons make this tool promising. It can retrieve previous data and load sample values. Whichever kind of spectrum is being used it can plot interactively. Flexible to find any type of earthquake i-e fault parallel, fault normal, scaled and un scaled records, with pulse or without it. This robust tool has easy output in form of tables, time histories of displacement, velocity and acceleration and excel spread sheet providing all the data of ground motion record for which the search has been done.

## 3.4 CRITERIA FOR SELECTION OF GROUND MOTIONS

Following factors should be considered to meet the above mentioned objectives for selection of ground motion;

### 3.4.1 Source Magnitude

It is understood that earthquake with larger magnitudes pose great threat to buildings because of longer duration, strong shaking and more energy release. But in this study records with moderate intensity (M=5) will also be included because the buildings considered were designed prior to seismic codes. Moderate intensity earthquake with larger shaking can cause the equal damage to old structure even if its duration is smaller.

### 3.4.2 Site conditions

Record sets which are available in database are recorded on soft rock (soil class C) or stiff soil (soil class D). Ground shaking recorded on the sites which are susceptible to ground failure like on very soft soil not included in data base. For this study Stiff soil (site class $S_D$) is chosen for the selection of records.

### 3.4.3 Site-Source

In the present case earthquake ground motions will be divided into two groups near field (having source to site distance < 15km) and far field (having source to site distance > 15km).

### 3.4.4 Number of Records per Event

As recording instruments are not evenly placed in the region with high seismicity so an earthquake with large magnitude may produce more records than others with smaller magnitude. In order to not produce event based biased only single record will be chosen from one earthquake.

### 3.4.5 Strong Ground motion

In the present study the buildings which are considered, are non-seismic old buildings and records with even moderate magnitude may cause damage. So range of ground motion from moderate to high magnitude is used in order to cover the full and record to record variability of response.

### 3.4.6 Strong Ground motion Instrument Capability

Strong ground motion recording instruments may have inherent incapability and are unable to record motions with larger period. For the dynamic analysis of tall buildings records which are up to 4 second are considered. Others are excluded.

### 3.4.7 Instrument Location

Instruments placed in the basement of the building which is if large can influence recorded ground motion because of soil-structure-foundation interaction. So the records should be taken from the devices installed on free field location of smaller building.

## 3.5 GROUND MOTION SELECTION PROCEDURE

Following are the three components of selection procedure;

Construction of target spectrum

1. Specifying criteria and limits
2. Selection and evaluation

### 3.5.1 Design Spectrum

PEER NGA West 2 ground motion data base offers three types of spectra. Code spectrum, user defined spectrum and scenario based spectrum. For the present case UBC 97 spectrum is being used for the selection purpose of ground motion records. As probabilistic seismic hazard studies has not been conducted for most of the Asian developing countries which would allow to use capacity mean spectrum or uniform hazard spectrum which serve the purpose of being more site specific. Moreover as studies is being conducted for no seismic buildings so zone 2B is chosen no to produce bias in structures instability.

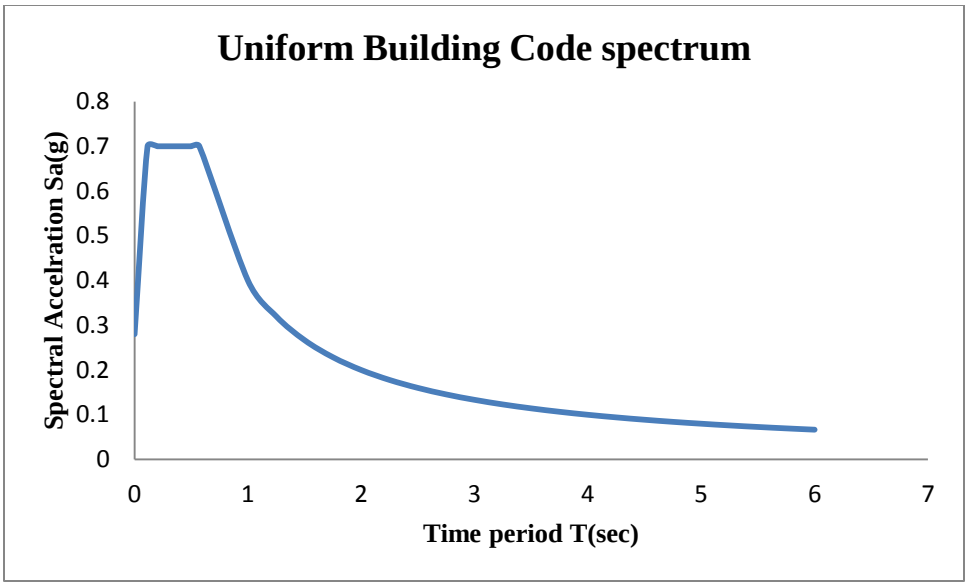


**Figure 3.1: Design Spectrum**

### 3.5.2 Specifying Criterion

For the present study building with four bays and three story is considered with time period 0.4935s. For this building there will be two sets of 40 ground motion records, each set contains 20 accelerograms naming "Near Distance" and "Far Distance". "Near Distance" comprises magnitude 5.5-6.75 and $R_{rup}$ 0-15km and "Far Distance" contains magnitude 6.75-8 with $R_{rup}$ 15-90km. While shear wave velocity lies in 180-360m/s range for soil profile type $S_D$.

The selection of records will be done according to selected range of time period. Then the records will be sorted out with respect to mean square error (MSE) between the response spectrums of individual record and target spectrum.

$$MSE = \frac{\sum w(T)\{\ln\left[S_a^{target}(T_i)\right] - \ln[f\,(S_a^{recorded})(T_i)]\}^2}{\sum w(T_i)} \qquad (3.1)$$

Where $w(T_i)$ is weight function which can be seen in next equation 3.2. It is simplest way to assign equal weight to one value or period range. In above expression "f" is scaling factor. One option is to apply the scale factor to the record to minimize MSE for user defined period range which provide best match to target spectrum. (DGML)

$$\ln f = \frac{\sum_i w(T_i) ln\left( {S_a^{target}(T_i)}/{S_a^{record}(T_i)} \right)}{\sum_i w(T_i)} \quad (3.2)$$

The second option is to scale the record to match the single value of spectral acceleration to target acceleration at fundamental period of building. In this case scale factor is given by:

$$f = \frac{S_a^{target}(T_0)}{S_a^{record}(T_0)} \quad (3.3)$$

For the present case both the methods for selection and scaling will be chosen for carrying out Incremental Dynamic Analysis.

## 3.6 SPECTRUM MATCHING FOR THE SELECTION OF EARTHQUAKE RECORDS

For the sake of selection of earthquake records two methods will be adopted for matching the spectrum,

i. Spectrum matching for the range of periods
ii. Spectrum matching for single period

### 3.6.1 Spectrum matching for range of period

For the 4 story building which is being considered in the present study, its fundamental time period is coming out to be 0.4935sec. The arithmetic mean of the entire spectrum for the period range 0.0986-0.7402sec lies above the target spectrum both for far field and near field motion.

### 3.6.1.1 Far Field Ground Motion

Following figure shows far field and near field ground motion spectrums matching the target spectrum.

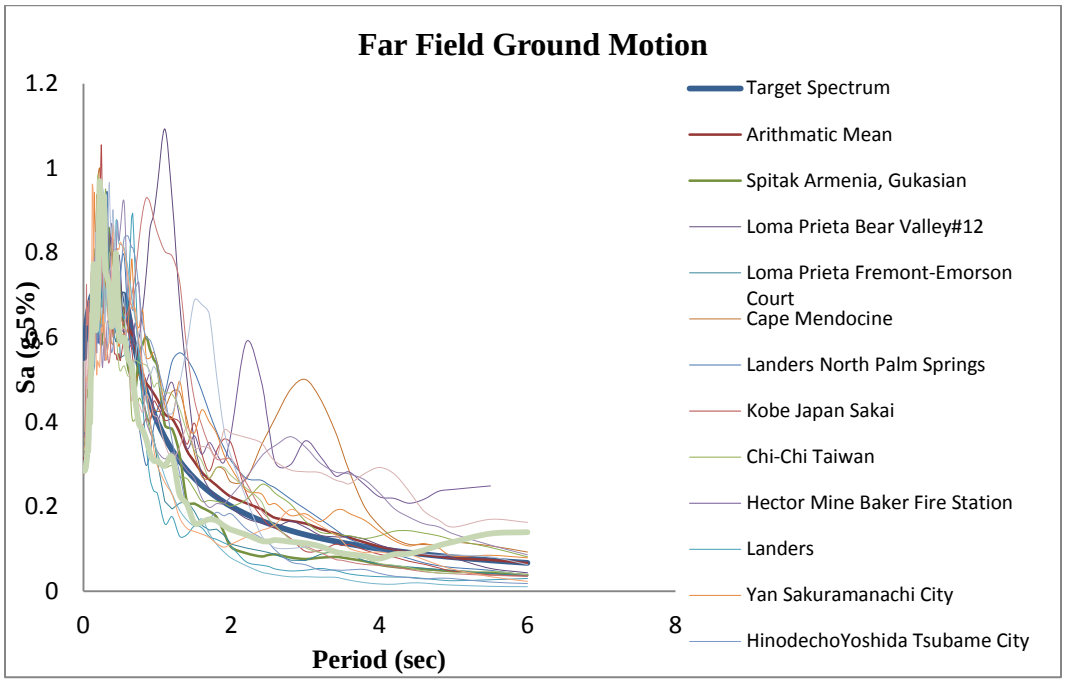


**Figure 3.2: Far Field Ground Motions**

**Table 3.1: Far Field Ground Motions**

| Event | Station Name | Year | Magnitude | $Vs_{30}$ (m/sec) | $R_{rup}$ (km) | Sa(g) |
|---|---|---|---|---|---|---|
| "Spitak Armenia" | "Gukasian" | 1988 | 6.77 | 343.53 | 23.99 | 0.742278 |
| "Loma Prieta" | "APEEL 2E Hayward Muir Sch" | 1989 | 6.93 | 271.06 | 52.68 | 0.593983 |
| "Loma Prieta" | "Bear Valley #12 | 1989 | 6.93 | 331.21 | 50.99 | 0.794969 |
| "Loma Prieta" | "Fremont - Emerson Court" | 1989 | 6.93 | 284.79 | 39.85 | 0.627027 |
| "Loma Prieta" | "Sunnyvale - Colton Ave." | 1989 | 6.93 | 267.71 | 24.23 | 0.641425 |
| "Cape Mendocino" | "Eureka - Myrtle & West" | 1992 | 7.01 | 337.46 | 41.97 | 0.685441 |
| "Landers" | "North Palm Springs" | 1992 | 7.28 | 344.67 | 26.84 | 0.561692 |
| "Kobe Japan" | "Sakai" | 1995 | 6.9 | 256 | 28.08 | 0.59518 |
| "Chi-Chi Taiwan" | "TCU098" | 1999 | 7.62 | 346.56 | 47.67 | 0.64394 |
| "Hector Mine" | "Baker Fire Station" | 1999 | 7.13 | 324.62 | 64.79 | 0.624964 |
| "Landers" | "Thousand Palms Post Office" | 1992 | 7.28 | 333.89 | 36.93 | 0.578757 |
| "Chuetsu-oki Japan" | "Yahiko Village Yahagi" | 2007 | 6.8 | 223.12 | 23.16 | 0.677987 |
| "Chuetsu-oki Japan" | "Yan Sakuramachi City watershed" | 2007 | 6.8 | 265.82 | 18.97 | 0.661353 |
| "Chuetsu-oki Japan" | "Hinodecho Yoshida Tsubame City" | 2007 | 6.8 | 261.55 | 24.42 | 0.532152 |
| "Iwate Japan" | "Nakashinden Town" | 2008 | 6.9 | 276.3 | 29.38 | 0.82924 |
| "Iwate Japan" | "Wakabayashi-ku Sendai Tomizuka" | 2008 | 6.9 | 295.35 | 66.18 | 0.82076 |
| "Iwate Japan" | "Oomagari Hanazono-cho | 2008 | 6.9 | 262.25 | 47.93 | 0.808068 |
| "Iwate Japan" | "Shinmachi Wakayu" | 2008 | 6.9 | 359.13 | 42.02 | 0.615668 |
| "El Mayor-Cucapah Mexico" | "EJIDO SALTILLO" | 2010 | 7.2 | 242.05 | 17.32 | 0.632611 |
| "El Mayor-Cucapah Mexico" | "Holtville Post Office" | 2010 | 7.2 | 202.89 | 36.52 | 0.612551 |

Following figures shows far field ground motion spectrums with target spectrum divided into groups for the sake of understanding.

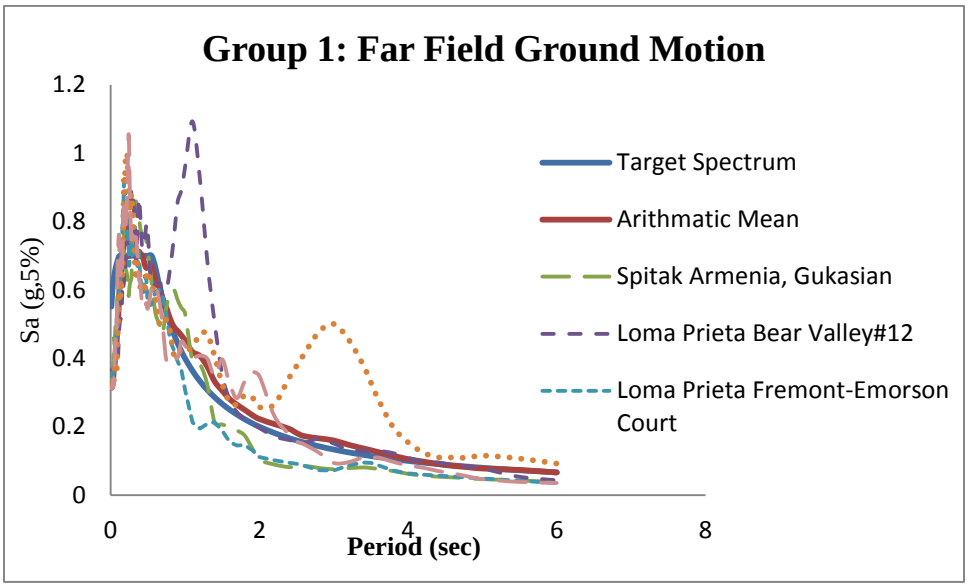


**Figure 3.3: Group 1 Far Field Ground Motions**

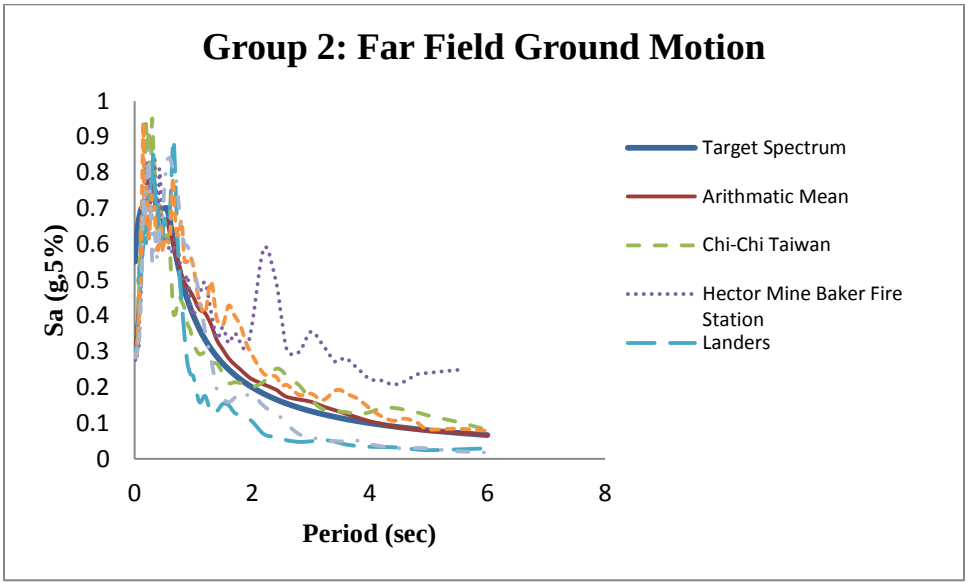


**Figure 3.4: Group 2 Far field Ground Motions**

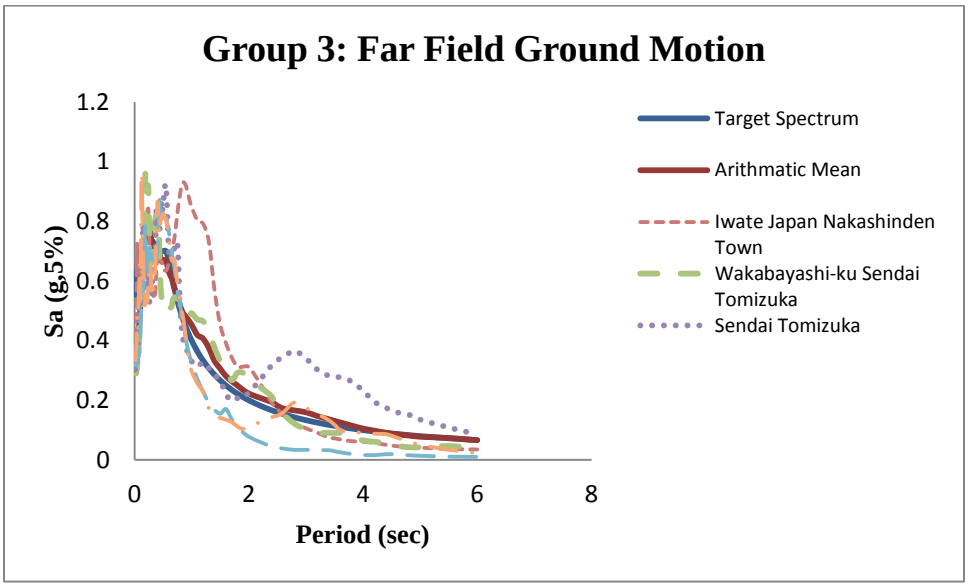


**Figure 3.5: Group 3 Far Field Ground Motions**

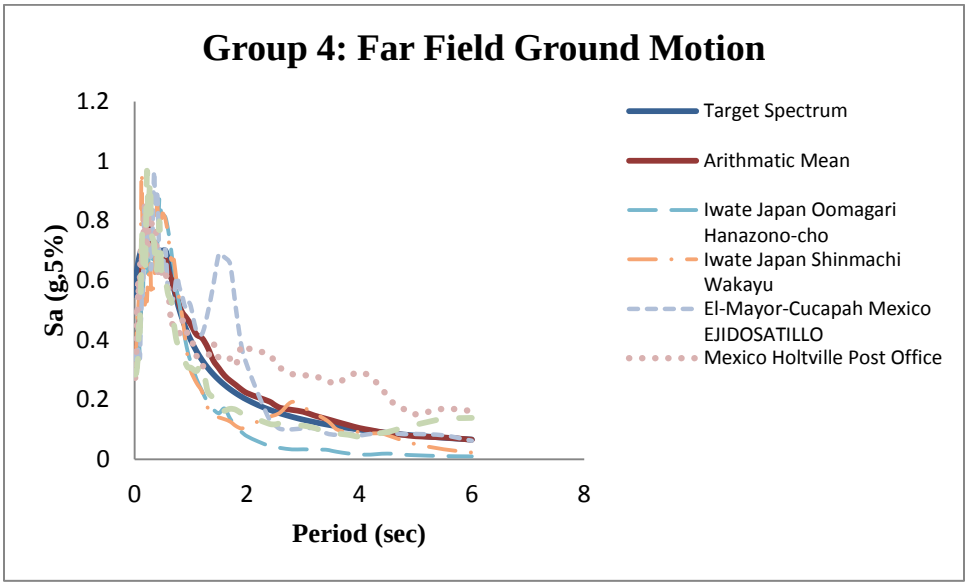


**Figure 3.6: Group 4 Far Field Ground Motion**

### 3.6.1.2 Near field Ground Motions

Following are the records of near field motions;

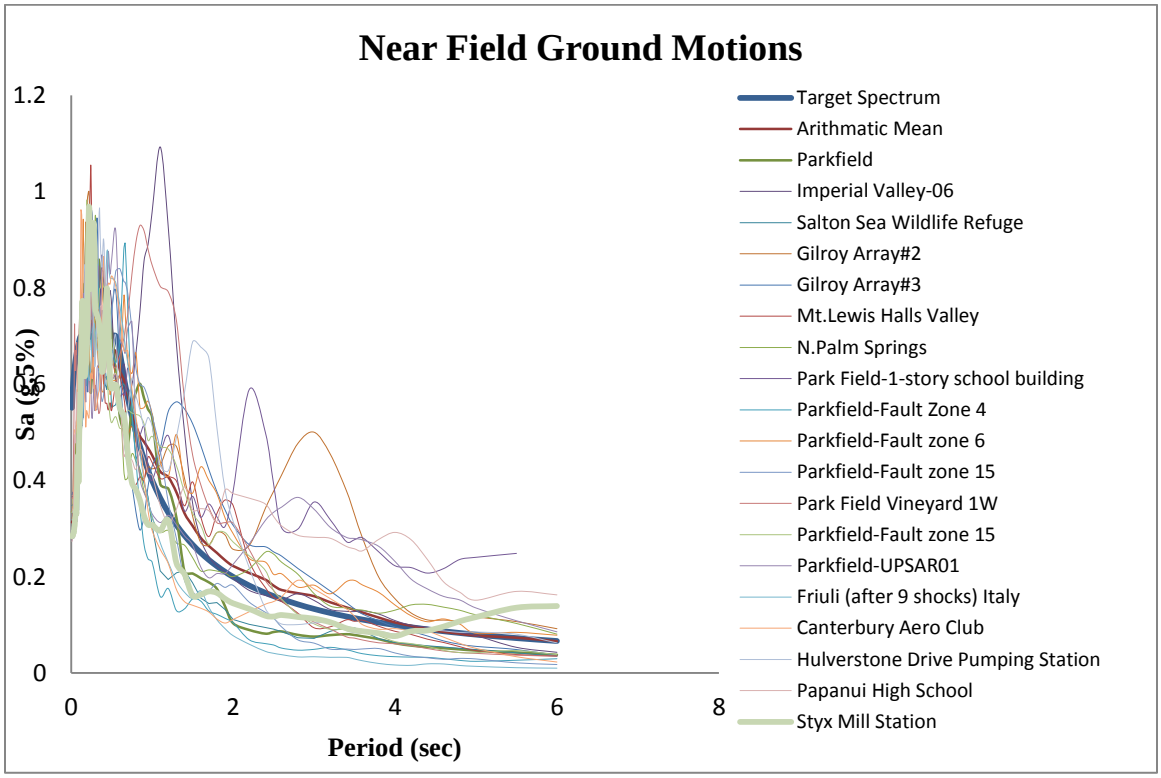


**Figure 3.7: Near Field Ground Motions**

**Table 3.2: Near Field Ground Motions**

| Event | Station Name | Year | Magnitude | $Vs_{30}$ (m/sec) | $R_{rup}$ (km) | Sa(g) |
|---|---|---|---|---|---|---|
| "Parkfield" | "Cholame - Shandon Array #8" | 1966 | 6.19 | 256.82 | 12.9 | 0.560307 |
| "Imperial Valley-06" | "Parachute Test Site" | 1979 | 6.53 | 348.69 | 12.69 | 0.676743 |
| "Westmorland" | "Salton Sea Wildlife Refuge" | 1981 | 5.9 | 191.14 | 7.83 | 0.438849 |
| "Morgan Hill" | "Gilroy Array #2" | 1984 | 6.19 | 270.84 | 13.69 | 0.433204 |
| "Morgan Hill" | "Gilroy Array #3" | 1984 | 6.19 | 349.85 | 13.02 | 0.525459 |
| "Mt. Lewis" | "Halls Valley" | 1986 | 5.6 | 281.61 | 13.54 | 0.766429 |
| "N. Palm Springs" | "Palm Springs Airport" | 1986 | 6.06 | 312.47 | 10.84 | 0.4013 |
| "Parkfield-02 CA | "Parkfield-1-story School Bldg" | 2004 | 6 | 269.55 | 2.68 | 0.821017 |
| "Parkfield-02 CA | "Parkfield - Fault Zone 4" | 2004 | 6 | 220.75 | 2.65 | 0.783544 |
| "Parkfield-02 CA | "Parkfield - Fault Zone 6" | 2004 | 6 | 266.65 | 2.7 | 0.37731 |
| "Parkfield-02 CA | "Parkfield - Fault Zone 15" | 2004 | 6 | 307.59 | 2.67 | 0.670073 |
| "Parkfield-02 CA | "Parkfield - Vineyard Cany 1W" | 2004 | 6 | 284.21 | 2.75 | 0.421235 |
| "Parkfield-02 CA | "Parkfield - Vineyard Cany 5W" | 2004 | 6 | 320.39 | 9.67 | 0.433442 |
| "Parkfield-02 CA | "PARKFIELD - UPSAR 01" | 2004 | 6 | 357.79 | 10.08 | 0.531286 |
| "Friuli (aftershock 9) Italy | "Buia" | 1976 | 5.5 | 310.68 | 12.39 | 0.910111 |
| "Umbria Marche Italy | "Colfiorito" | 1997 | 6 | 317 | 6.92 | 0.38754 |
| "Christchurch New Zealand | "Canterbury Aero Club" | 2011 | 6.2 | 280.26 | 14.41 | 0.458083 |
| "Christchurch New Zealand | "Hulverstone Drive Pumping Station" | 2011 | 6.2 | 206 | 4.35 | 0.831636 |
| "Christchurch New Zealand | "Papanui High School " | 2011 | 6.2 | 263.2 | 9.06 | 0.842003 |
| "Christchurch New Zealand | "Styx Mill Transfer Station " | 2011 | 6.2 | 247.5 | 11.25 | 0.796476 |

Above ground motions are divided into groups for the sake of understanding;

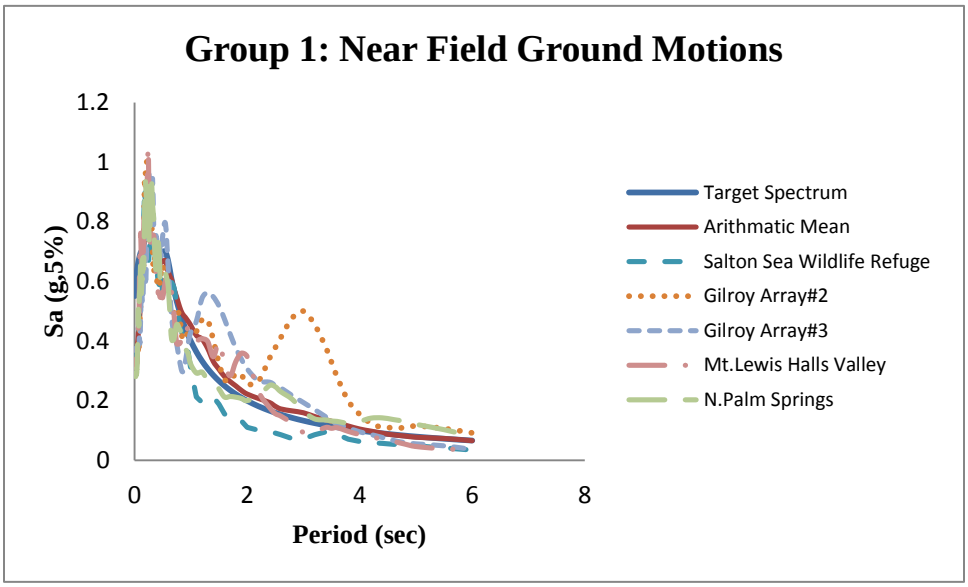


**Figure 3.8: Group 1 Near Field Ground Motions**

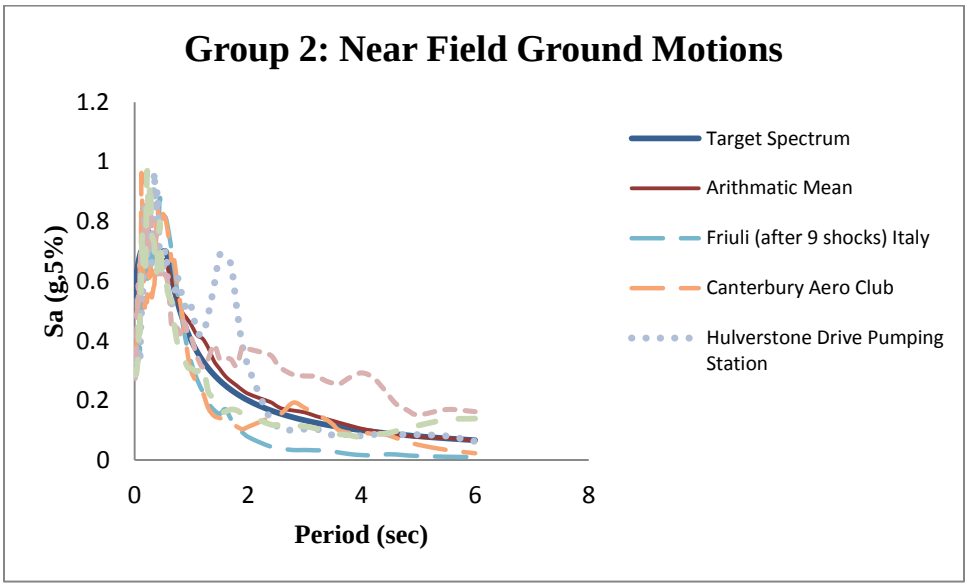


**Figure 3.9: Group 2 Near Field Ground Motions**

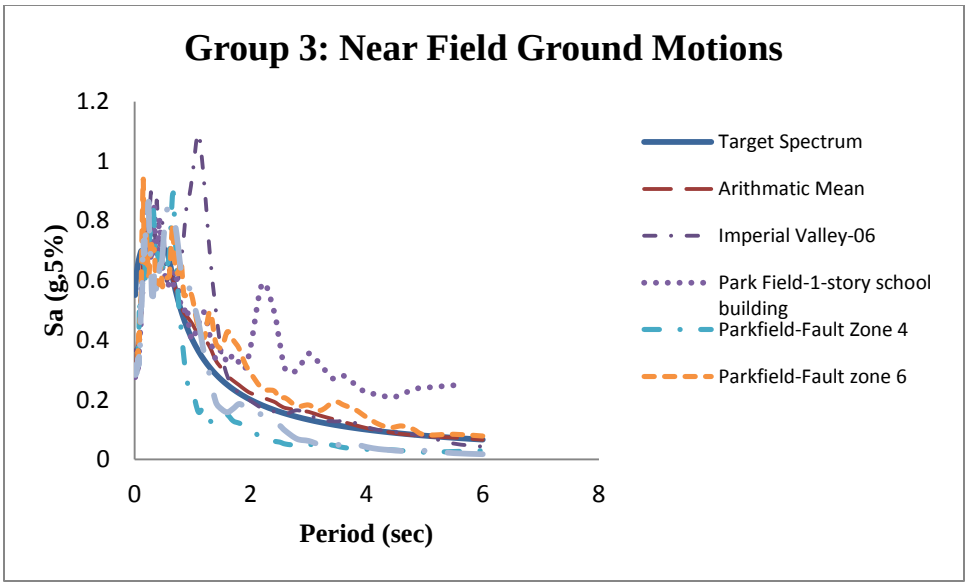


**Figure 3.10: Group 3 Near Field Ground Motions**

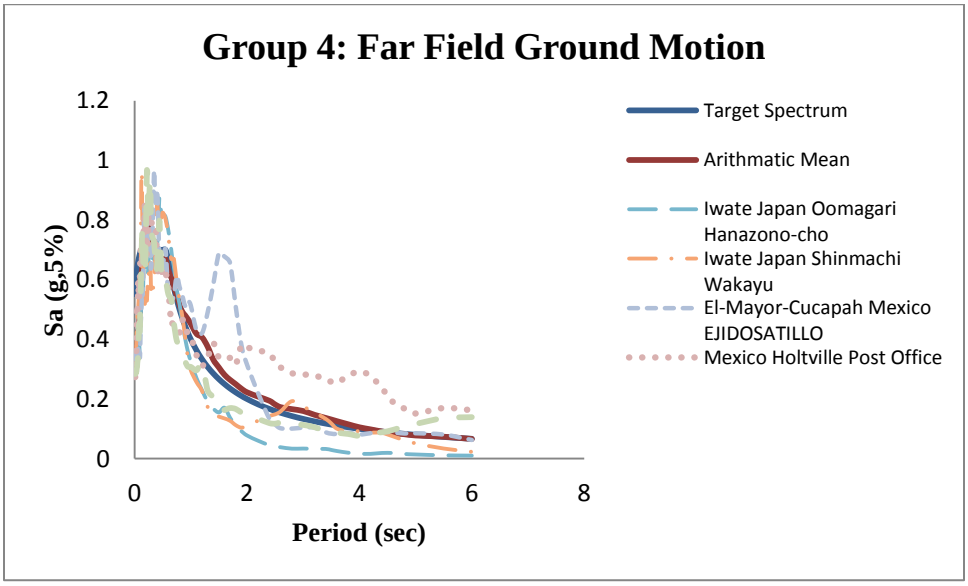


**Figure 3.11: Group 4 Far Field Ground Motions**

### 3.1.2. Spectrum matching for single period

In this case, the spectrums for the selected ground motions only match for the single point which is the natural time period. Following figure shows far field and near field ground motion spectrums matching the target spectrum.

#### 3.1.2.1. Far field Ground Motions

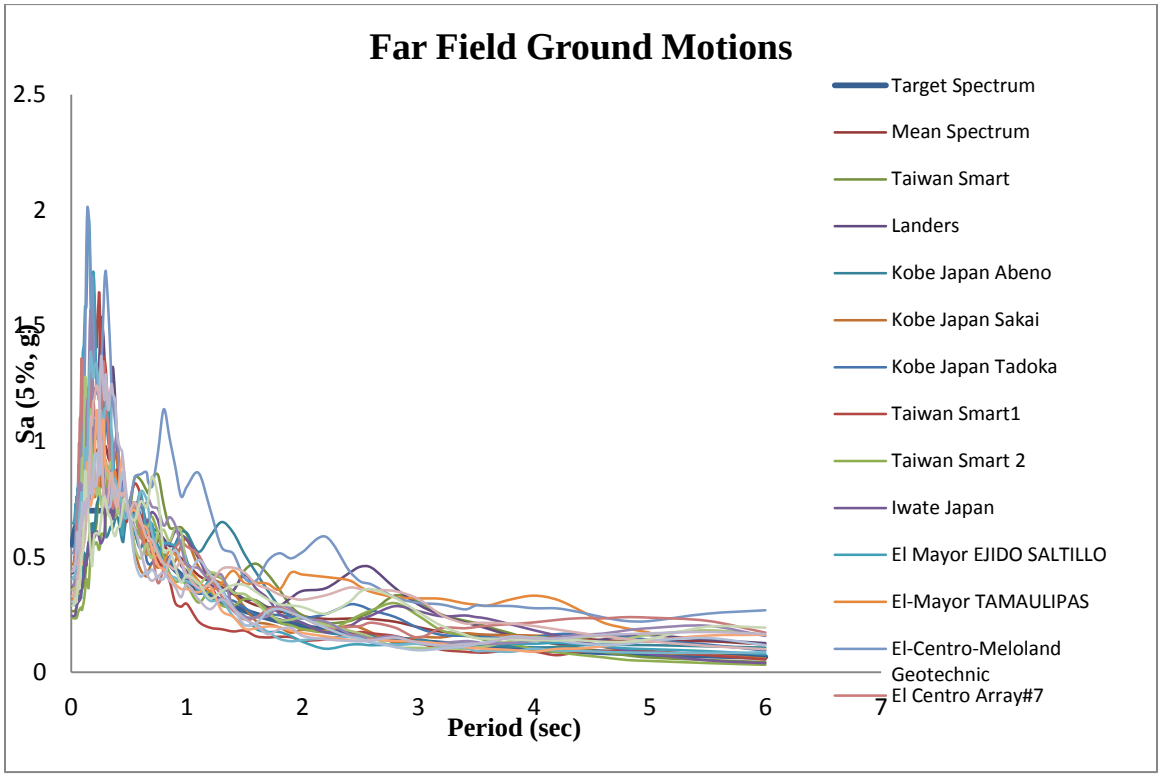


**Figure 3.12: Far Field Ground Motions**

**Table 3.3: Far Field Ground Motions for Single Period Scaling**

| Event | Station Name | Year | Magnitude | $Vs_{30}$ (m/sec) | $R_{rup}$ (km) | Sa(g) |
|---|---|---|---|---|---|---|
| "Taiwan SMART" | "SMART1 I01" | 7.3 | 1986 | 275.82 | 56.18 | 0.748065 |
| "Loma Prieta" | "Agnews State Hospital" | 6.93 | 1989 | 239.69 | 24.57 | 0.683039 |
| "Landers" | "Yermo Fire Station" | 7.28 | 1992 | 353.63 | 23.62 | 0.679529 |
| "Kobe_ Japan" | "Abeno" | 6.9 | 1995 | 256 | 24.85 | 0.658917 |
| "Kobe_ Japan" | "Sakai" | 6.9 | 1995 | 256 | 28.08 | 0.69437 |
| "Kobe_ Japan" | "Tadoka" | 6.9 | 1995 | 312 | 31.69 | 0.652149 |
| "Taiwan SMART1(45)" | "SMART1 M04" | 7.3 | 1986 | 306.38 | 55.55 | 0.725621 |
| "Taiwan SMART1(45)" | "SMART1 O03" | 7.3 | 1986 | 278.32 | 56.16 | 0.683433 |
| "Iwate_ Japan" | "Misato_ Miyagi Kitaura - A" | 6.9 | 2008 | 278.35 | 38.04 | 0.751105 |
| "El Mayor-Cucapah_ Mexico" | "EJIDO SALTILLO" | 7.2 | 2010 | 242.05 | 17.32 | 0.718655 |
| "El Mayor-Cucapah_ Mexico" | "TAMAULIPAS" | 7.2 | 2010 | 242.05 | 26.55 | 0.679205 |
| "El Mayor-Cucapah_ Mexico" | "El Centro - Meloland Geotechnic" | 7.2 | 2010 | 186.21 | 29 | 0.722355 |
| "El Mayor-Cucapah_ Mexico" | "Westmorland Fire Sta" | 7.2 | 2010 | 193.67 | 42.61 | 0.686995 |
| "El Mayor-Cucapah_ Mexico" | "Meloland_ E Holton Rd." | 7.2 | 2010 | 196 | 30.63 | 0.686172 |
| "El Mayor-Cucapah_ Mexico" | "El Centro Array #7" | 7.2 | 2010 | 210.51 | 27.91 | 0.669026 |
| "El Mayor-Cucapah_ Mexico" | "Holtville Post Office" | 7.2 | 2010 | 202.89 | 36.52 | 0.717262 |
| "El Mayor-Cucapah_ Mexico" | "El Centro - Meadows Union School" | 7.2 | 2010 | 276.25 | 28.3 | 0.736492 |
| "Darfield_ New Zealand" | "Pages Road Pumping Station" | 7 | 2010 | 206 | 24.55 | 0.732739 |
| "Darfield_ New Zealand" | "Styx Mill Transfer Station " | 7 | 2010 | 247.5 | 20.86 | 0.733074 |
| "El Mayor-Cucapah_ Mexico" | "El Centro Array #4" | 7.2 | 2010 | 208.91 | 35.46 | 0.76104 |

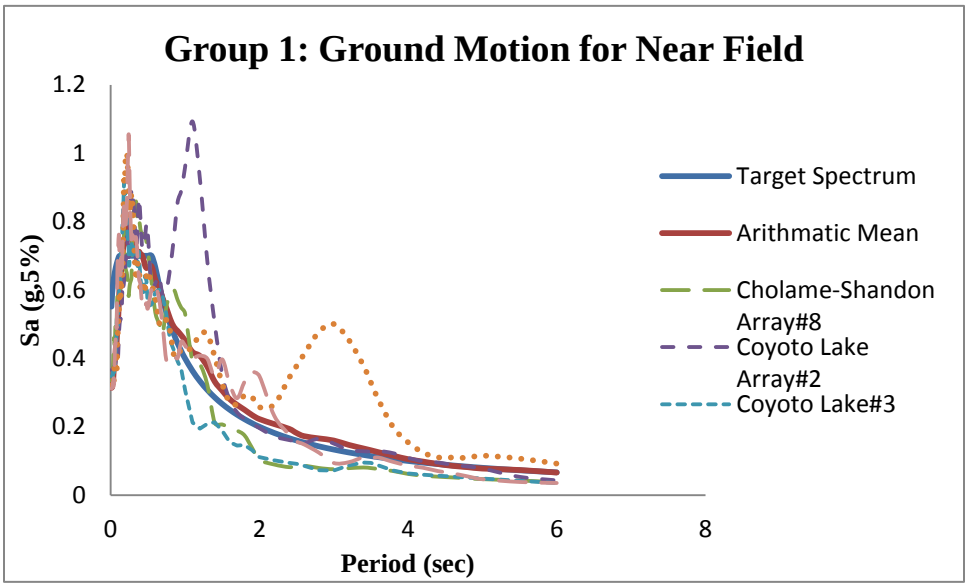


**Figure 3.13: Group 1 Ground Motion for Near Field**

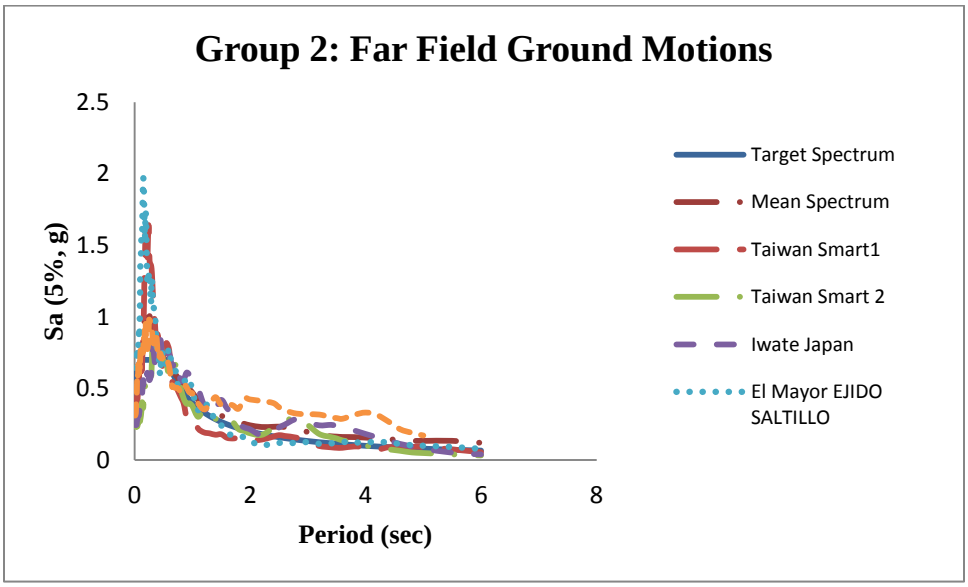


**Figure 3.14: Group 2 Far Field Ground Motions**

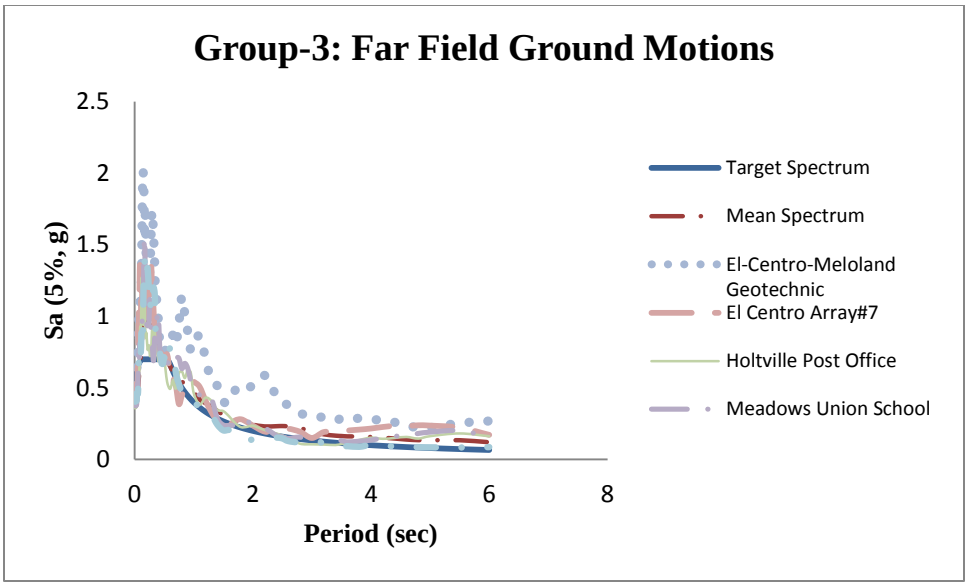


**Figure 3.15: Group 3 Far Field Ground Motions**

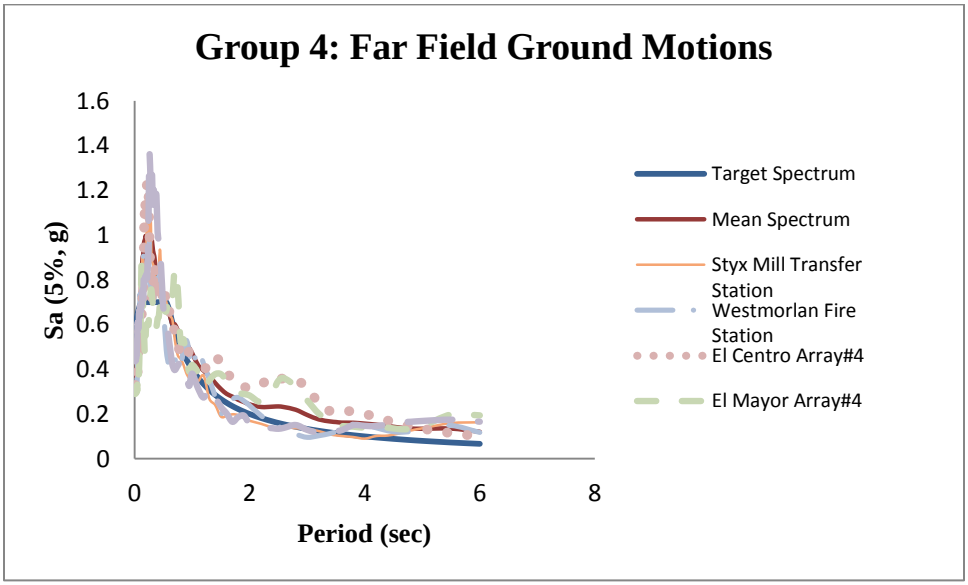


**Figure 3.16: Group 4 Far Field Ground Motions**

### 3.1.2.2. Near field Ground Motions

Following is the spectrum for twenty ground motions matching the design spectrum;

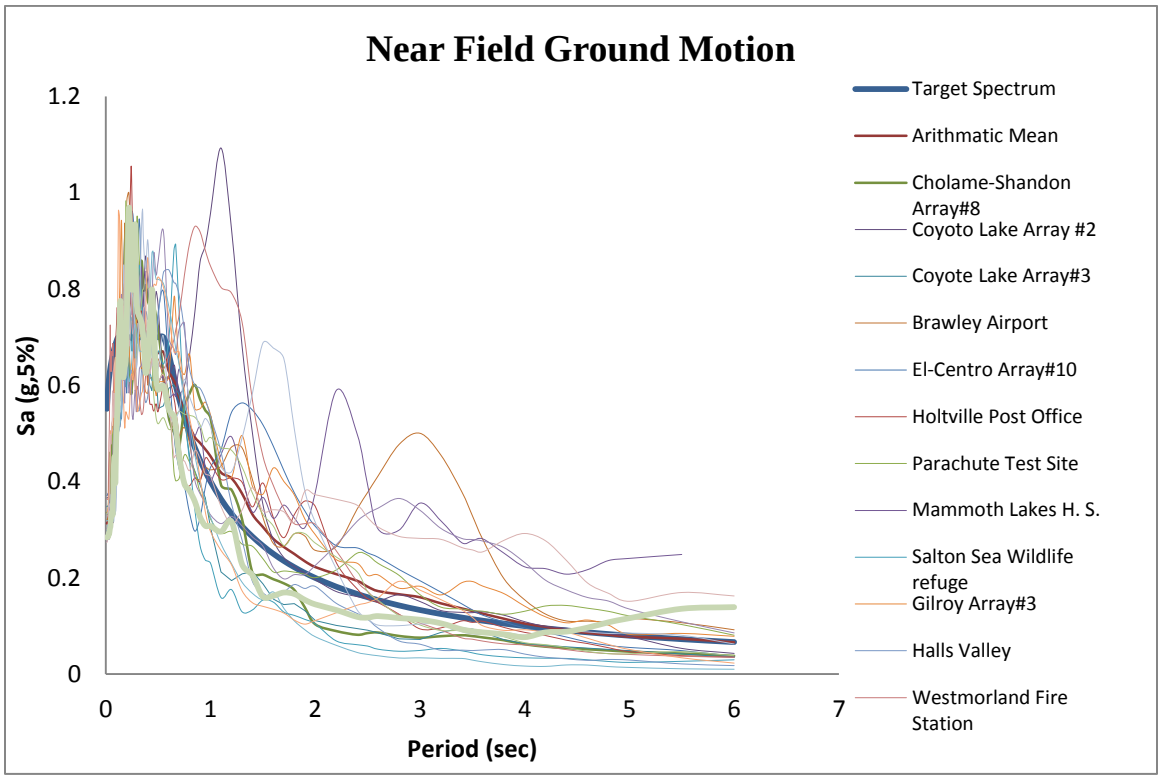


**Figure 3.17: Near Field Ground Motions**

**Table 3.4: Near Field Ground Motions for Single Point Scaling**

| Event | Station Name | Year | Magnitude | Vs30 (m/sec) | Rrup (km) | Sa(g) |
|---|---|---|---|---|---|---|
| "Parkfield" | "Cholame - Shandon Array #8" | 1966 | 6.19 | 256.82 | 12.9 | 0.689653 |
| "Coyote Lake" | "Gilroy Array #2" | 1979 | 5.74 | 270.84 | 9.02 | 0.74754 |
| "Coyote Lake" | "Gilroy Array #3" | 1979 | 5.74 | 349.85 | 7.42 | 0.749081 |
| "Imperial Valley-06" | "Brawley Airport" | 1979 | 6.53 | 208.71 | 10.42 | 0.7213 |
| "Imperial Valley-06" | "El Centro Array #10" | 1979 | 6.53 | 202.85 | 8.6 | 0.717141 |
| "Imperial Valley-06" | "Holtville Post Office" | 1979 | 6.53 | 202.89 | 7.5 | 0.686995 |
| "Imperial Valley-06" | "Parachute Test Site" | 1979 | 6.53 | 348.69 | 12.69 | 0.693575 |
| "Mammoth Lakes-01" | "Mammoth Lakes H. S." | 1980 | 6.06 | 346.82 | 4.67 | 0.65501 |
| "Westmorland" | "Salton Sea Wildlife Refuge" | 1981 | 5.9 | 191.14 | 7.83 | 0.727009 |
| "Morgan Hill" | "Gilroy Array #3" | 1984 | 6.19 | 349.85 | 13.02 | 0.692977 |
| "Mt. Lewis" | "Halls Valley" | 1986 | 5.6 | 281.61 | 13.54 | 0.675204 |
| "Superstition Hills-02" | "Westmorland Fire Sta" | 1987 | 6.54 | 193.67 | 13.03 | 0.733986 |
| "Northridge-01" | "N Hollywood - Coldwater Can" | 1994 | 6.69 | 326.47 | 12.51 | 0.710129 |
| "Tottori_ Japan" | "SMN001" | 2000 | 6.61 | 331 | 14.42 | 0.734024 |
| "Parkfield-02_ CA" | "Parkfield - Fault Zone 15" | 2004 | 6 | 307.59 | 2.67 | 0.719693 |
| "Parkfield-02_ CA" | "Parkfield - Vineyard Cany 3W" | 2004 | 6 | 308.87 | 5.21 | 0.745493 |
| "Umbria Marche (foreshock)_ Italy" | "Colfiorito" | 1997 | 5.7 | 317 | 4.02 | 0.699132 |
| "Christchurch_ New Zealand" | "Canterbury Aero Club" | 2011 | 6.2 | 280.26 | 14.41 | 0.74503 |
| "Christchurch_ New Zealand" | "Hulverstone Drive Pumping Station" | 2011 | 6.2 | 206 | 4.35 | 0.691243 |
| "Christchurch_ New Zealand" | "Styx Mill Transfer Station " | 2011 | 6.2 | 247.5 | 11.25 | 0.742349 |

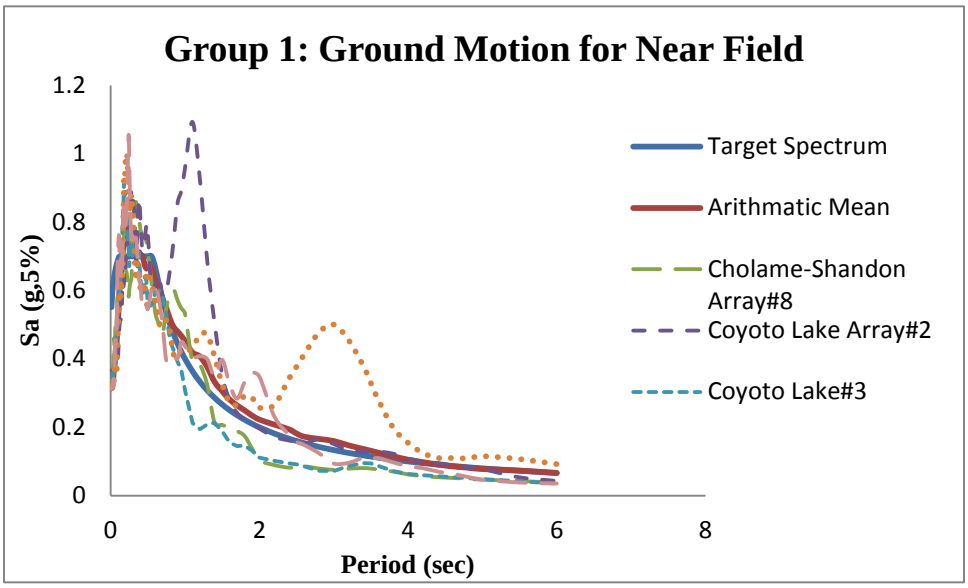


**Figure 3.18: Group 1 Ground Motion for Near Field**

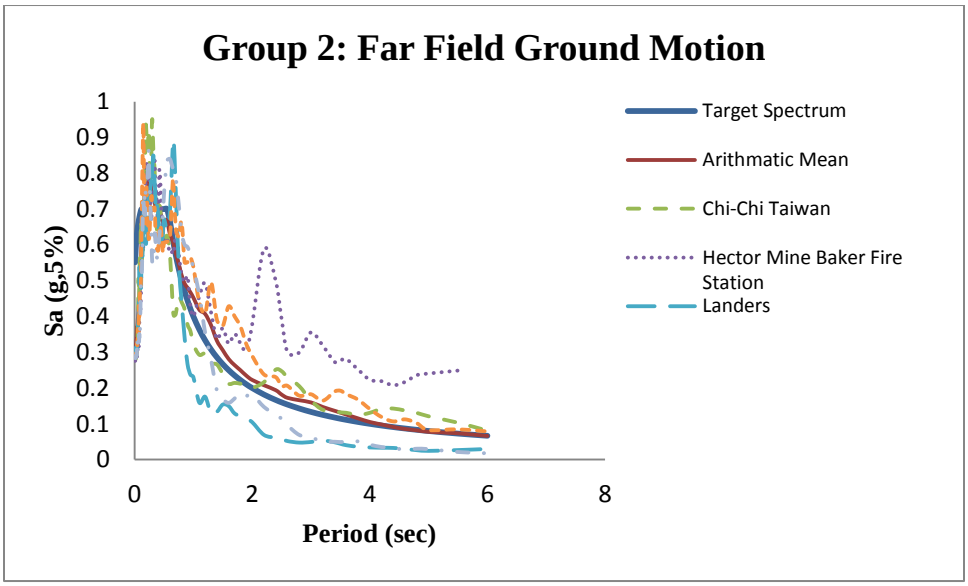


**Figure 3.19: Group 2 Far Field Ground Motion**

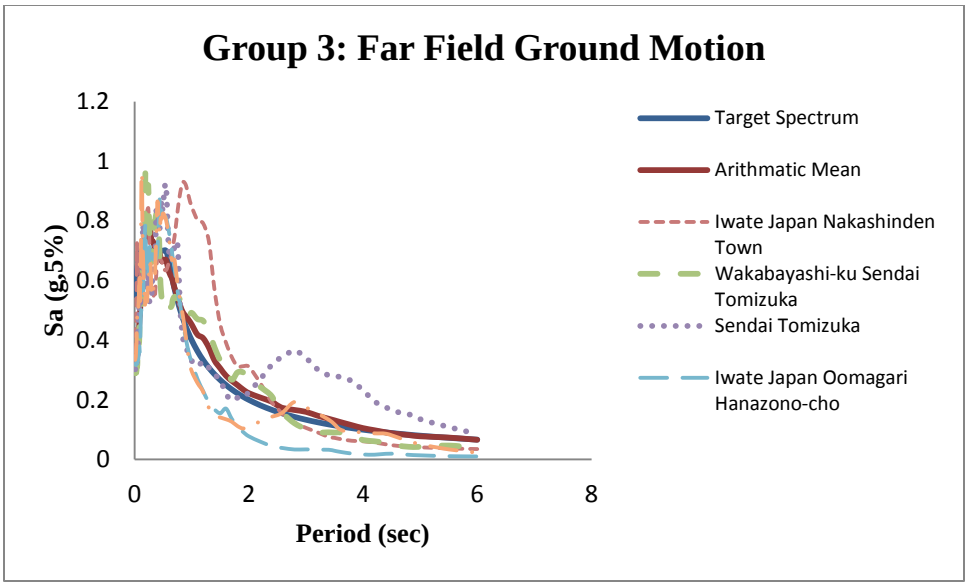


**Figure 3.20: Group 3 Far Field Ground Motion**

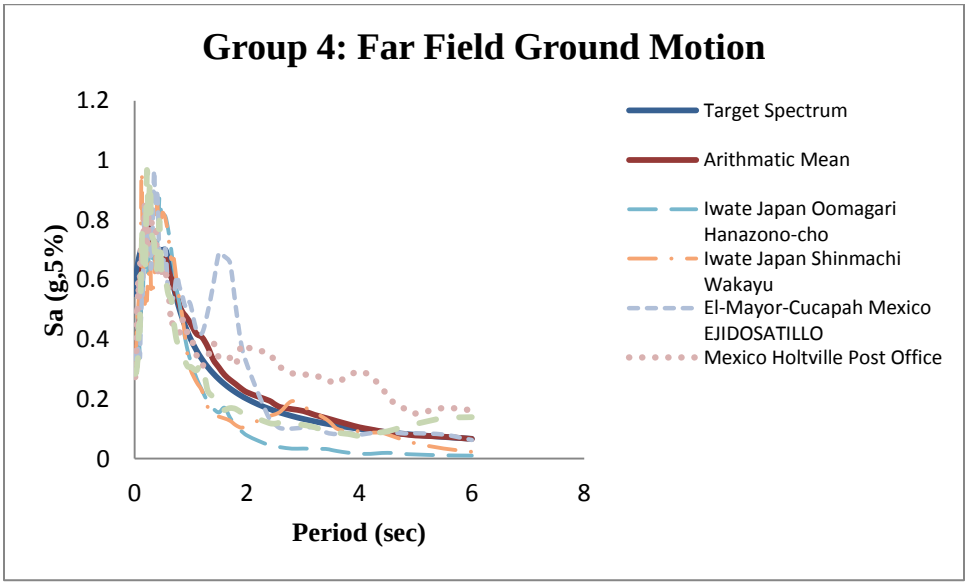


**Figure 3.21: Group 4 Far Field Ground Motion**

*Chapter – 4*

# STRUCTURAL MODELING

## 4.1. INTRODUCTION

For analytical research to be carried out for IDA the choice of analytical tool is very important; which can simulate all the possible failure modes when structure is subjected to severe ground motion with increasing intensity. It should incorporate the material failure such as crushing of concrete, strength and stiffness degradation and yielding of steel, joint shear failure, bar pullout, bond failure, column shear and axial failure and development of the plastic hinges.

## 4.2. INTRODUCTION TO OPENSEES

OpenSEES is full form of Open System for Earthquake Engineering and Simulations, a powerful program written in object oriented language C++. Frank McKenna is developer of OpenSees. OpenSees is not a code, it's a robust tool which can perform nonlinear incremental dynamic analysis and performance based design with less effort and time because of the coding loops that can be made.

## 4.3. WHY OPENSEES

It consists of wide variety of material models and one can also customized one's own material, and its ever growing library. It has numerous options to define the element from elastic to non-linear, from lumped plasticity to concentrated plasticity and from force based to displacement based. Intricate linear or nonlinear structural and geotechnical modeling can be done. It is very robust tool for simulations capable of performing static pushover, static reversed cyclic, dynamic time history analysis, and uniform support excitation, multi support excitation and incremental dynamic analysis.

## 4.5. CALIBRATION OF ANALYTICAL TOOL

Although, this saclay frame has already been used to validate Drain 3D, by many researchers. But for this study OpenSees is being used and need to get validated. So a sophisticated model in OpenSees for saclay frame is developed and its results are

compared with the experimental results, when this full scale model was tested on five increasing intensity of PGAs.

### 4.5.1. Introduction to Saclay frame

A full scale two story model with single bay was tested in France in Saclay laboratory in 2004. The structure which was tested was part of a European program called (Ecoleader no 2). The design was carried using old non-seismic European code with low strength concrete and reinforcement detailing so as to simulate the behavior and vulnerability of the building stock which pre dates to the evolution of seismic codes. Construction and testing of frame was carried out at shake table where PGAs with increased intensities (0.05g, 0.1g, 0.2g, 0.3g, 0.4g) were applied. The natural frequencies were determined using white noise test and result showed the values of 1.9Hz and 5.6Hz.This project was conducted to evaluate how the retrofitting strategies are effective. Initially a bare frame was tested with the above mentioned PGA's then test was repeated after retrofitting the frame. Full scale model is shown in figure below.

**Figure 4.1: Two Storey Full Model of Saclay Frame**

#### 4.5.1.1. Characteristics of model

| | |
|---|---|
| Total frame height: | 6.87 m |
| 4 x square Columns: | 260 cm |

2 x square slabs: 42 cm side and 12 cm thick

4 x beams per slab: 40 cm x 26 cm section

The beam and column sections remain constant throughout. Total self-weight of the structure is 20 tons. Two steel plates (43m x 3m) relatively stiffer than the RC slabs having mass 4.5 tons each were also installed on each slab (Chuadat et al., 2005).

Summary of the provided reinforcement is as follows.

- Column longitudinal reinforcement
    - 3Φ14+2Φ14+3Φ14 for columns on first floor
    - 2Φ14+2Φ14 for columns on 2nd floor
- Longitudinal reinforcement for beams
    - 4Φ14 for top and bottom in each beam
- Column transverse reinforcement
    - Φ6@200
- transverse reinforcement for beams
    - Φ8@200
- Slab reinforcement
    - 2 steel nets with mesh size 100mm x 100mm
    - Clear cover of slab reinforcement is 30mm

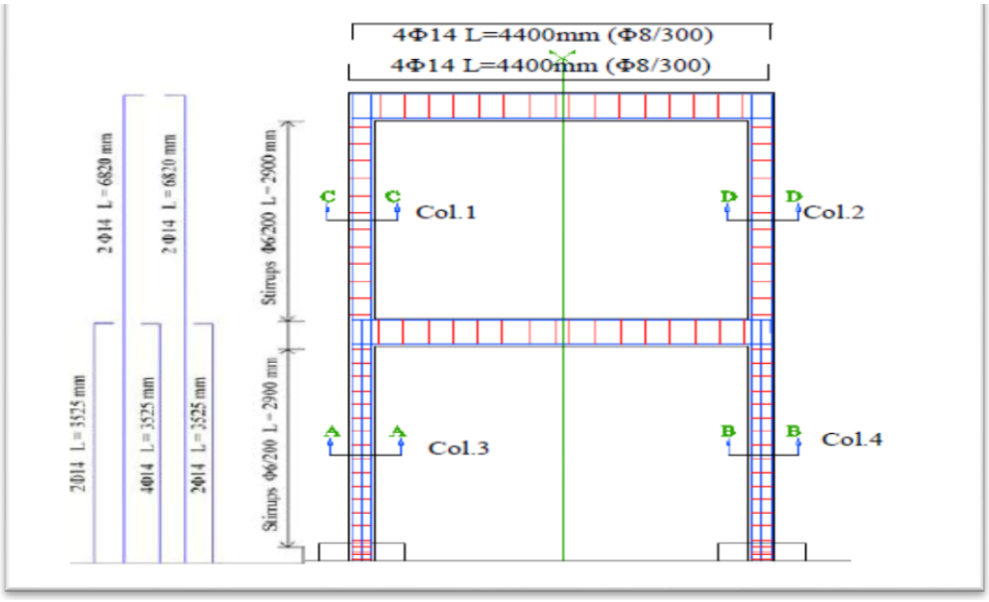


**Figure 4.2: Details of Frame Reinforcement ( Chaudat et al., 2005)**

#### 4.5.1.2. Material properties

Steel reinforcement with ultimate strength of $F_u$500-3 has been used in the frame after performing Tests on 8mm and 14 mm bars to determine the mechanical properties. Results obtained from the tests are summarized in table 4.1. Elongation (A %) represents the mid-point elongation which is the actual point of necking. In addition, concrete strength with 20MPa was used. Its properties were determined by conducting 12 cylindrical tests specimens. Concrete test results are shown in table 4.2.

**Table 4.1: Mechanical properties of steel**

| Diameter (mm) | $R_e$ (MPa) | $R_m$ (MPa) | A % |
|---|---|---|---|
| 8 | 582 | 644 | 25 |
| 14 | 551 | 656 | 23.6 |

**Table 4.2: Mechanical properties of concrete**

| Flow | $R_c$ (MPa) | $R_f$ (MPa) | $E_m$ (MPa) |
|---|---|---|---|
| Flow 1 | 22.1 | 2.1 | 25590 |
| Flow 2 | 19.6 | 2.07 | 23500 |

#### 4.5.1.3. Observed damages

This model was tested on increasing PGAs, after each test its crack pattern and natural vibration period was determined by low level white noise excitation. The results are also shown in the table 4.4. The cracks patterns are marked with markers after each test. In this way, the formation of cracks and their progress with increasing shaking level can be assessed.

After performing tests the different type of damages were observed. Tests were performed at PGA of 0.05g and 0.1g, there was no significant damage and structure behaved elastically with very minor cracks. While at 0.2g shaking intensities some cracks appeared at first floor joint and some horizontal cracks on the top interface of first floor

and bottom interface of second floor. Figure  the distance between the cracks is approximately equal to the shear link spacing.

At 0.3g level, the cracks which appeared tend to be more widened and concrete spalling occurs at the base of the column. In the final test where intensity was increased to 0.4g, at the first floor level those vertical and horizontal cracks were deeper thus indicated the formation of plastic hinges and second floor level almost hit the collapse point.

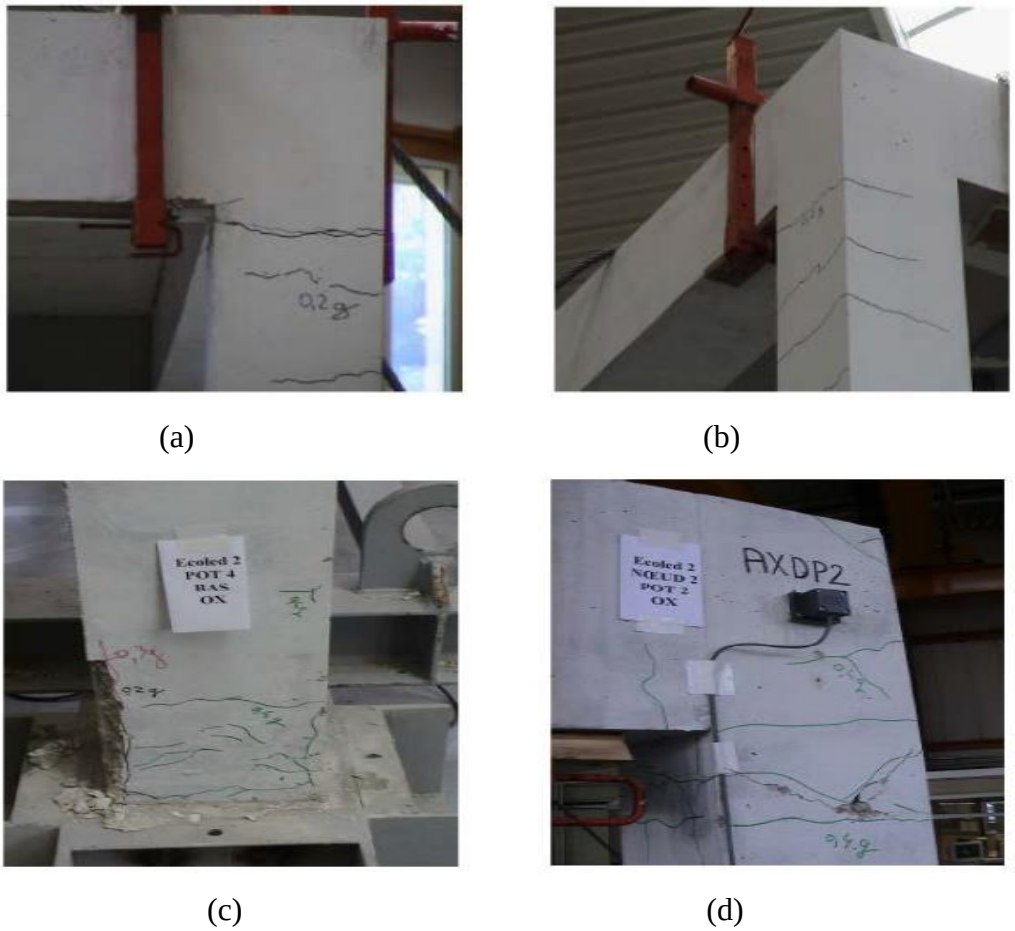


(a) (b)

(c) (d)

**Figure 4.3 Observed damage during testing; (a) and (b) development of horizontal cracks at 0.2g, (c) Concrete spalling at 0.3g, (d) Development of deep cracks at 0.4g (Chuadat et al., 2005).**

### 4.5.2. Modeling in OpenSees

A 2D model was developed in OpenSees using non-linear beam column element for beams and columns and beam column joint element to model joints.

#### 4.5.2.1 . Geometric modeling

The model is started by defining the coordinates of nodes in the Tcl language. Nodes are defined with respect to joint width and height. Because, joint element is defined as 4 noded element, connecting beams and columns.

#### 4.5.2.2. Section modeling

In OpenSees sections are divided into patches i-e concrete cover patch and concrete core patch. Those patches are further divided into sections which are necessary to represent nonlinear action of the members of structure. Steel will be represented by straight layer command. This represents the nonlinearity with in the section. To depict inelasticity within the member there are two options and three types of member available force based and displacement based elements. Force based elements are further sub divided into two elements “Beam with Hinges” and “Nonlinear beam column”; in the former inelasticity is considered to be concentrated near the joints and supports, in the latter it is considered to be distributed throughout the section. In displacement based elements nonlinearity is distributed along the total length of the member but section is with linear moment of curvature.

#### 4.5.2.3. Section modeling

Concrete and steel material models are derived from EC-2. The material which resembles to this material from OpenSees is Concrete02 Material with tension softening. This material can be defined with some points on the material curve, the points needed are compressive strength and strain at compressive strength, crushing strength and strain at crushing strength, ration between unloading slope and initial slope and tension softening stiffness. For reinforcement Steel02 material is the material with isotropic strain hardening with points which controls the transition from elastic to plastic region.

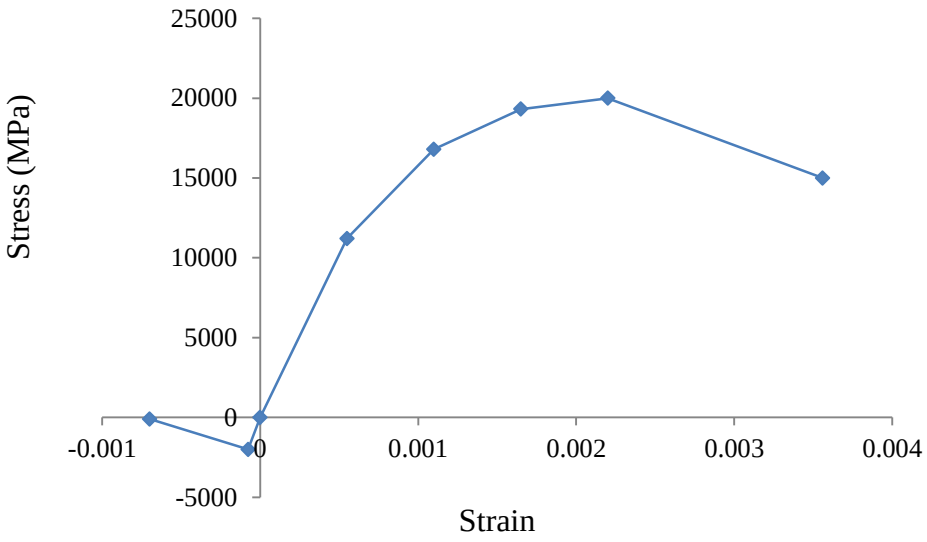


**Figure 4.4: Stress Strain Model for Concrete**

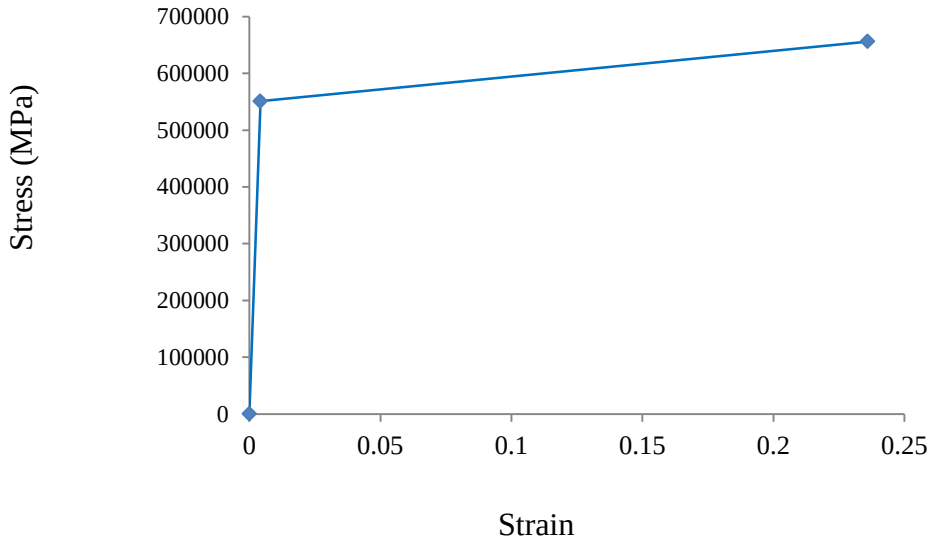


**Figure 4.5: Stress Strain Model for Steel**

#### 4.5.2.4. Frame masses

As structure had the symmetry so instead of modeling 3D structure a two dimensional model was developed in OpenSees. So, only half of the masses of Structure is model as a 2D model due to symmetry which represents half structure. Thus, only half of the masses of the structure are calculated shows the lumped masses on nodes.

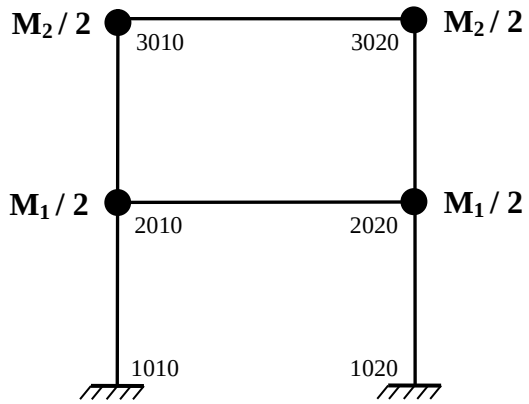


**Figure 4.6: Distribution of Masses on Nodes**

Mass of the each individual structural element is calculated as follows

- The slab: $M_{slab} = (4m \times 4m \times 0.12m) \times (24\ kN/m^3)/g = 4.7$ ton
- The beam: $M_{beam} = \left((4\text{-}0.26)m \times 0.4\ m \times 0.26m\right) \times (24\ kN/m^3)/g = 0.95$ ton
- The column: $M_{column} = (3.3m \times 0.26m \times 0.26m) \times (24\ kN/m^3)/g = 0.55$ ton
- Additional Masses: $M_{plate} = 9$ ton

Mass calculations are completed for the first level by adding the weight of half slab, two beams and half of the column height above and below this level. For second level the calculated mass consists of weight of two beams, half slab and column height only below the second level. All discussion can be summarized as follows:

$$m_1 = \left(\frac{1}{2}\ M_{slab}\right) + 2(\ M_{Beam}) + 4\left(\frac{1}{2}\ M_{Column}\right) + \left(\frac{1}{2}\ M_{Plate}\right) = 9.85 \text{ ton}$$

$$m_2 = \left(\frac{1}{2}\ M_{slab}\right) + 2(\ M_{Beam}) + 2\left(\frac{1}{2}\ M_{Column}\right) + \left(\frac{1}{2}\ M_{Plate}\right) = 9.30 \text{ ton}$$

**Table 4.3: Distribution of Masses at Different Nodes**

| Node | 2010 | 2020 | 3010 | 3020 |
|---|---|---|---|---|
| Mass (ton) | 4.925 | 4.925 | 4.65 | 4.65 |

#### 4.5.2.5. Frame damping

In OpenSees Rayleigh command is used to assign the damping to previously defined members and nodes. The procedure for calculation of "α" coefficient and "**β**" coefficient is given below;

$$\eta = \alpha m + \boldsymbol{\beta} k \qquad (4.9)$$

In this equation "α" represents coefficient of mass while "**β**" is the coefficient of element stiffness. This equation calls for a direct relationship between mass and stiffness to the Rayleigh Damping (Chopra, 2001)

Following relation can be used for calculation of nth mode damping ratio based on the equation (4.9) above.

$$\xi_n = \frac{\alpha_0}{2}\frac{1}{\omega_n} + \frac{\alpha_1}{2}\omega_n \qquad (4.10)$$

Where;

$\xi_n$ is the nth mode damping ratio

$\omega_n$ = nth mode natural angular frequency ($\omega = 2pf$ ).

Following matrix produced by a set of equations can be used to calculate "α" and "**β**" for corresponding ith and jth mode damping ratios $\xi_i$ and $\xi_j$.

$$\frac{1}{2}\cdot\begin{bmatrix}\frac{1}{\omega_i} & \omega_i \\ \frac{1}{\omega_j} & \omega_j\end{bmatrix}\cdot\begin{Bmatrix}\alpha \\ \beta\end{Bmatrix} = \begin{Bmatrix}\xi_i \\ \xi_j\end{Bmatrix} \qquad (4.11)$$

The second mode should have a damping ratio lower than the first mode according to the Anil. K Chopra's recommendations. Therefore, damping ratios ($\zeta_1$ and $\zeta_2$) 3% and 2% for the first two modes and the natural frequencies measured during the test (shown in table 4.4) are used to calculate the coefficients "α" and "**β**".

**Table 4.4: Damping Coefficient**

| Mode | f (Hz) | ξ % | A | **β** |
|---|---|---|---|---|
| **1** | 1.9 | 3 | 0.62647 | 0.00063 |
| **2** | 5.6 | 2 | | |

### 4.6. Structural Response

For Saclay test El Centro earthquake was used using 5 records with increasing intensity (0.05g, 0.1g, 0.2g, 0.3g and 0.4g), so for the simulation purpose same input parameters are used.

After modeling the Sacaly frame in OpenSEES time history analysis is performed. Analytical and experimental results are compared. The results which are given below are for top node number.

#### 4.6.1. Response at 0.05g PGA

After incorporating bar slip, column shear and panel zone failure for joint and distributed plasticity elements for beam and columns, the Saclay 2D model was subjected to time history of 0.05g scaled record. By comparing the analytical results with experimental in the figure below it is seen that both have a perfect match with each other. At some points peak displacement differs and then matches perfectly.

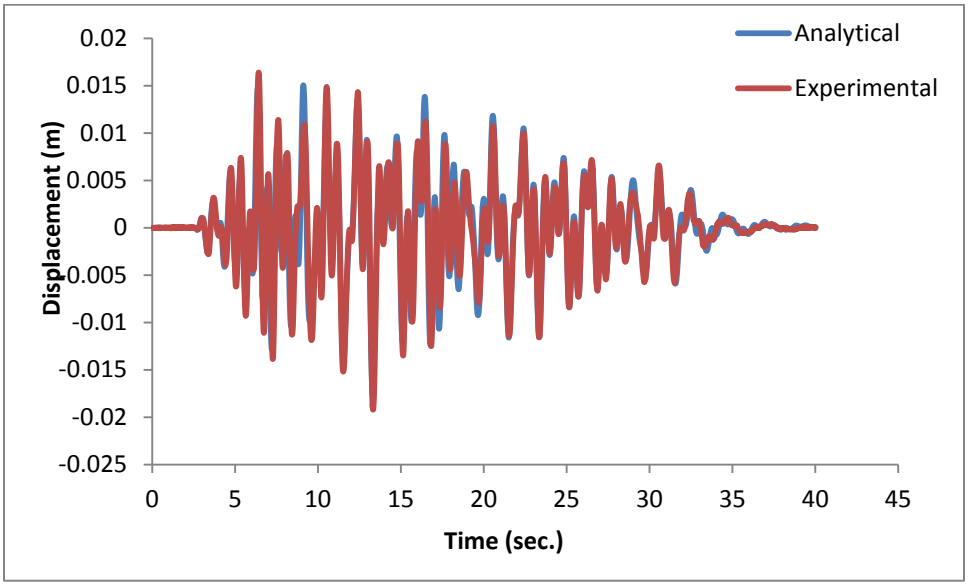


**Figure 4.6: Response of Seclay Frame at 0.05g PGA**

### 4.6.2. Response at 0.1g PGA

Now after increasing intensity from 0.05g to 0.1g, it is evident from the figure below that except some points there is a perfect coordination between analytical and experimental results. So the analytical model is indicating the quite accurate response.

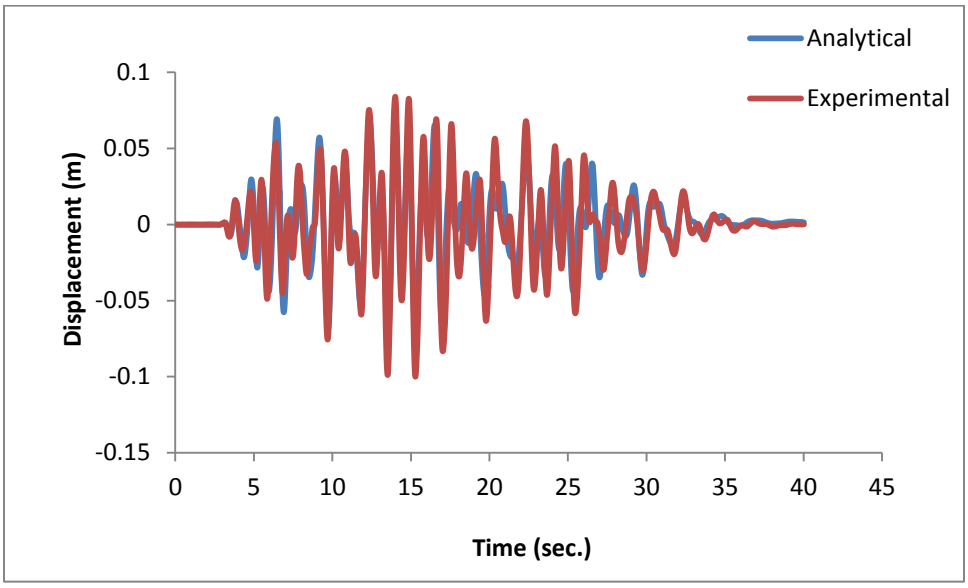


**Figure 4.7: Response of Seclay Frame at 0.1g PGA**

### 4.6.3. Response at 0.2g PGA

After increasing the intensity to 0.2g again the analysis was run in OpenSEES and comparison is presented in the figure below. Analytical results are matching with the experimental one even at the 0.2g intensity thus representing that analytical model is true depiction of experimental structure.

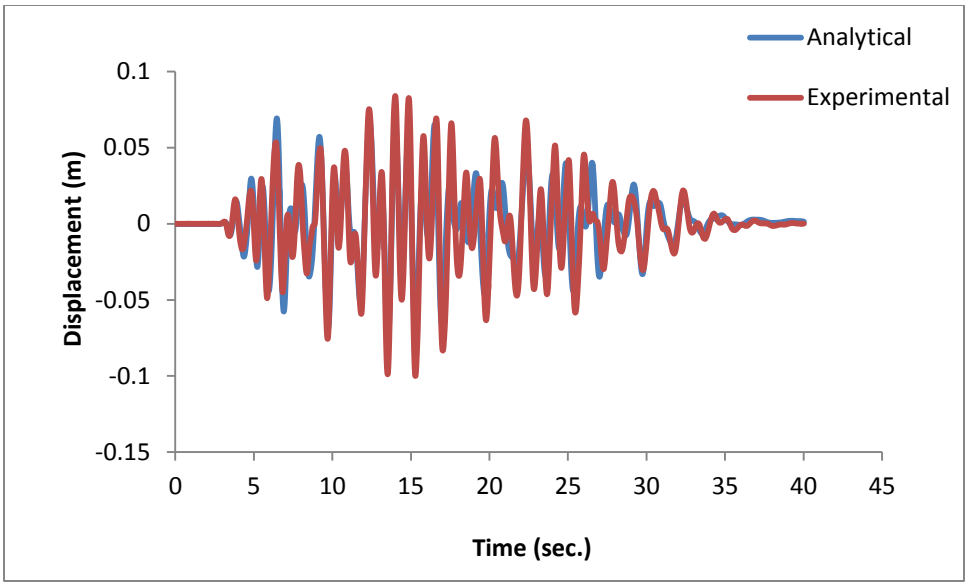


**Figure 4.8: Response of Seclay Frame at 0.2g PGA**

### 4.6.4. Response at 0.3g PGA

Visual comparison of analytical and experimental results show that the numerical model is in numerical model is in good agreement with experimental results.

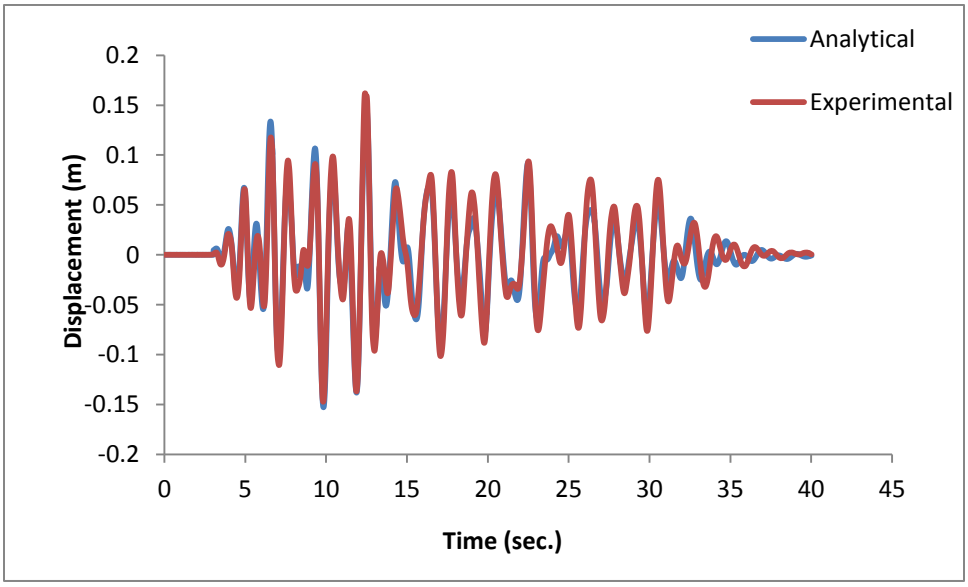


**Figure 4.9: Response of Seclay Frame at 0.3g PGA**

### 4.6.5. Response at 0.4g PGA

When 0.4g PGA record was applied, even at the higher intensity numerical model shows very good results. Until 27 seconds both the results were matching then there was a failure of strain gauge and experimental results stopped being recorded.

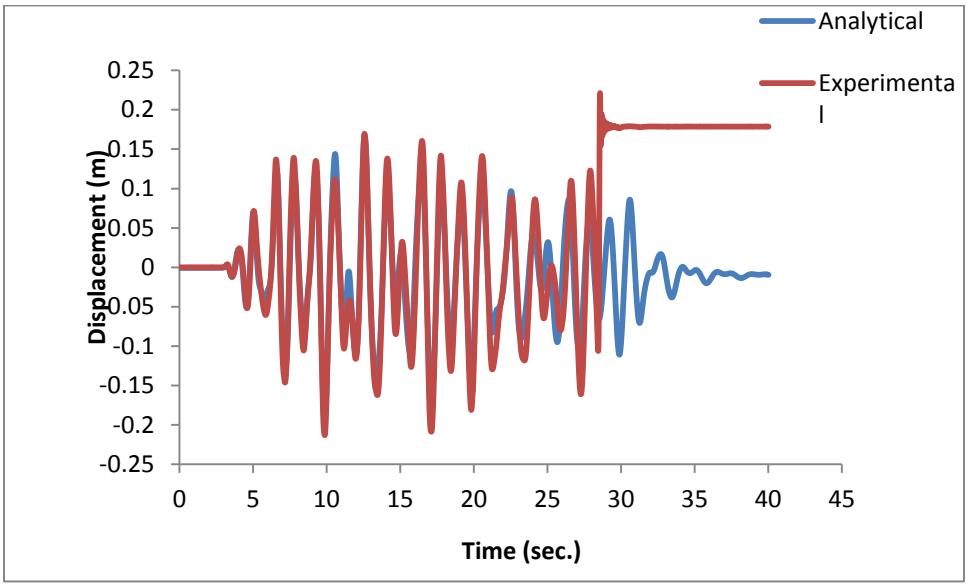


**Figure 4.10: Response of Seclay Frame at 0.4g PGA**

As from the above results it can be seen that OpenSEES is comprehensive tool to perform incremental dynamic analysis for the present case study. Though main comparison for this research focus on the method of selection and scaling of earthquake records, but the building which is chosen, its reinforcement is designed according to the non-seismic codes.

## 1.7. BRIEF INTRODUCTION TO THE SUBJECT BUILDING

This is four story, three bay building which is designed according to the non-seismic code, only the forces which are considered are gravity loads. As this building is a representative of the past construction which is the main stock in Pakistan and other developing countries. Beam and columns are modeled using displacement beam column elements in OpenSEES with distributed plasticity. And the paramount entity to be modeled is joint. Because non-seismically designed buildings tend to exhibit brittle failure due to opening of joints in severe earthquakes.

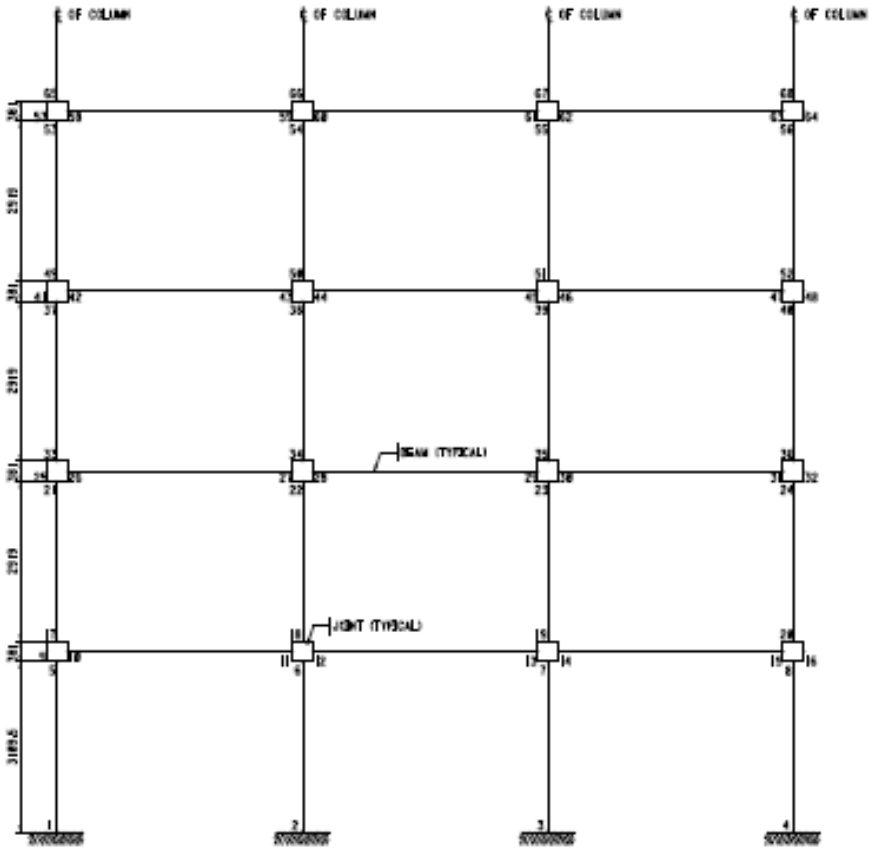

**Figure 4.11: Elevation of Subject Portal Frame**

## 1.8. METHODS OF PERFORMING IDA

1. As it has been discussed in introduction the current practice for IDA is using a set of earthquake records from FEMA 356, but for this study earthquake records are chosen which are site specific.
2. A design spectrum was chosen.
3. Earthquake records are chosen with respect to two methods which are already discussed before.
4. Ground motion spectrum were constructed and first mode spectral acceleration "Sa" is found with respect to the time period of the building.
5. Scaling of earthquake ground motion is done with respect to "Sa".

6. For one earthquake record maximum interstory drift "$\theta$max" is recorded for each scale factor.
7. For each value of spectral acceleration the maximum recorded interstory drift is plotted, called IDA curve.

*Chapter – 5*

# DERIVATION OF FRAGILITY CURVES

## 5.1. INTRODUCTION

For the sake of present case study a four story, 3 bay frame is selected which is deficient reinforced with poor detailing thus representing the usual construction trend in Pakistan. But the main focus will be deriving the result differences due to the site difference parameter for choosing the earthquake records to perform the IDA. Then the fractile curves will be deducted and various performance based limits are going to be marked on those curves according to the different criteria available.

## 5.2. INTRODUCTION TO THE STRUCTURE

The subject building is four story building which is designed according to the pre seismic codes with gravity forces. The reinforcement detailing is also very poor as to represent the true practice of construction conducted in Pakistan and developing countries in the past. Beam column joints are modeled with inappropriate development length. Beam column joint is modeled using "Joint 2D" command in OpenSEES which incorporates every failure i-e bar pull out, panel zone failure, column shear failure. The structure is subjected to total of 40 earthquake records, among which 20 are far field and 20 near field. The details of those ground motions are given in chapter 3 along with the criteria of selection.

## 5.4. NEAR FIELD GROUND MOTIONS FOR RANGE OF PERIOD

The criteria of selection and scaling of earthquake for the above building is discussed in details. The results which are obtained by subjecting the building for first bucket of ground shaking which are scaled according to the first mode of spectral acceleration $S_a$.

The results which are given in figure 5.1, shows DM increases with the increase in IM which is evident. From the IDA curves at first when the structure is in elastic regime, DM and IM increases linearly, and then even with the slight increase in intensity there tend to be more damage until curves get flatten as the dynamic instability reaches. The weaving behavior in some of the cases explains the reverse cycle of the earthquake with greater

magnitude tends accumulate the damage and then reversing the damage in other direction with the change of cycle.

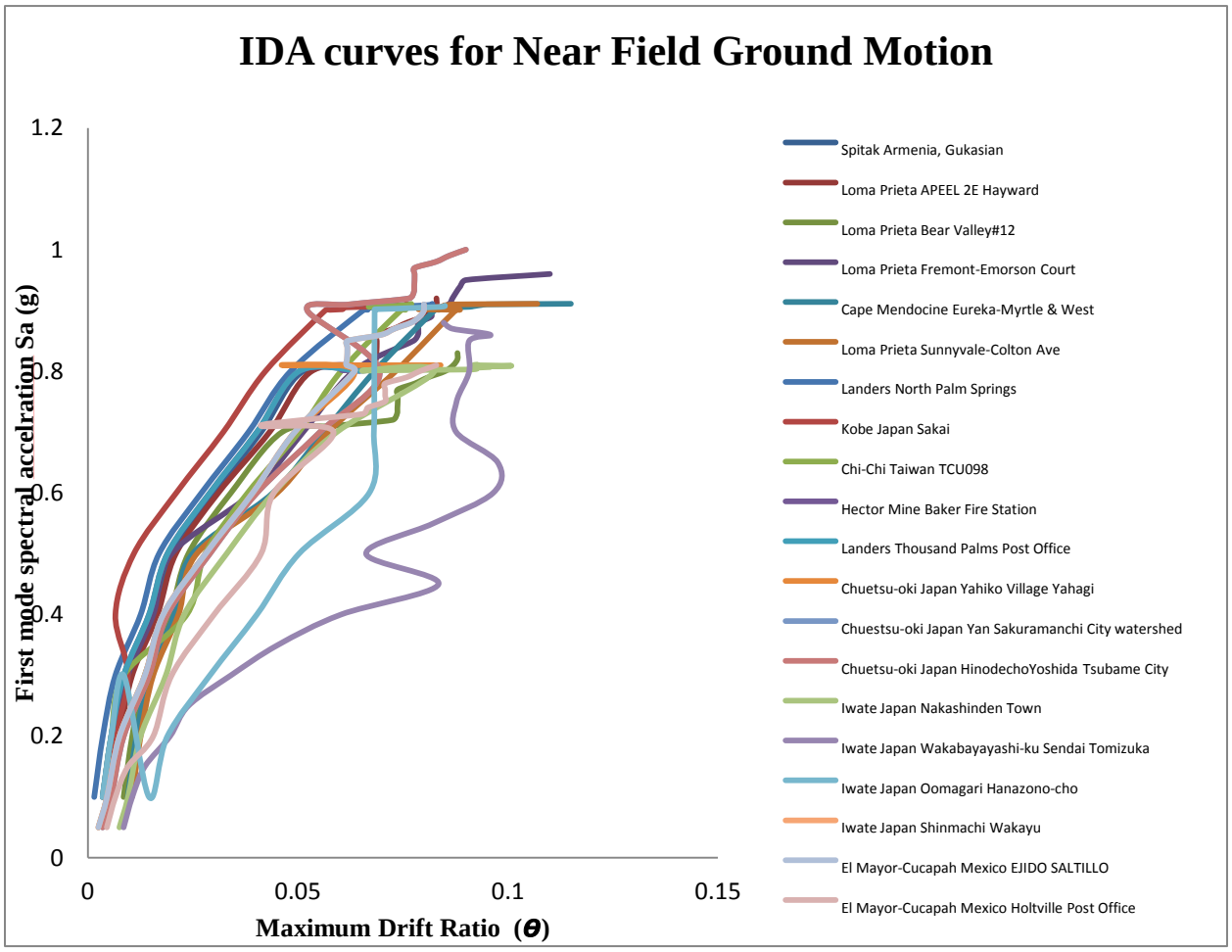


**Figure 5.1: IDA Curves for Near Fields Ground Motion**

Another way to describe the IDA curves is to find the fractiles for 16%, 50% and 84% to confine the confidence bound within a defined limit. If the near field ground motions are to be selected according to the criteria which are defined earlier, 16% of the ground motions will cause the building to cross the collapse prevention performance level at 0.91g spectral acceleration and exceeding the interstorey drift at 0.14%. Collapse prevention performance level is defined where IDA curve tend to get flat. Given in the following

**Table 4.1: Performance Based Limits for Near Field Ground Motions**

| | $S_a$(g) | | | $\theta_{max}$(%) | | |
|---|---|---|---|---|---|---|
| | CP | LS | IO | CP | LS | IO |
| 84% | 0.91 | 0.69 | 0.3 | 0.14 | 0.09 | 0.06 |
| 50% | 0.9 | 0.6 | 0.3 | 0.08 | 0.06 | 0.02 |
| 16% | 0.7 | 0.5 | 0.2 | 0.06 | 0.045 | 0.02 |

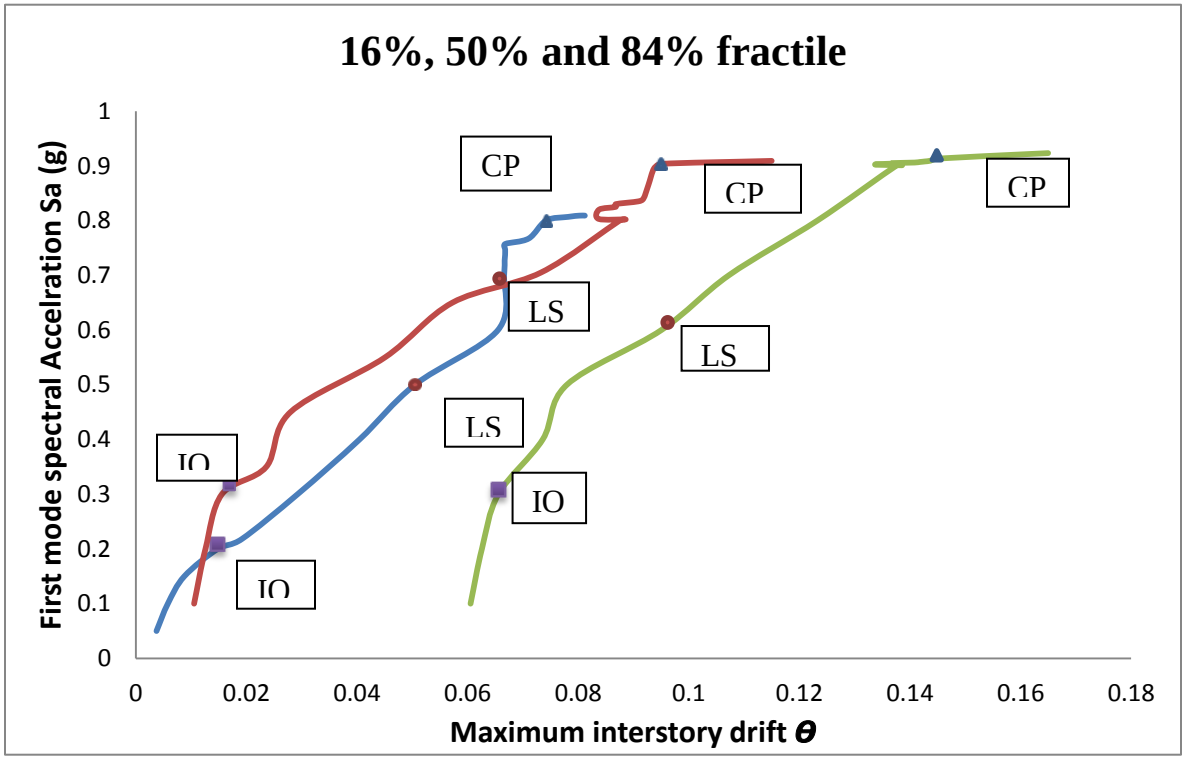


**Figure 5.2: 16%, 50% and 84% Fractiles for IDA**

## 5.5. FAR FIELD GROUND MOTIONS FOR RANGE OF PERIOD

The ground motions for this bin were mostly from the same event but different station and of somewhat same nature, that's why with only minor all the IDA curves tend to have the same nature. As these ground motions are recorded far from site where building is situated. So there is a more linear slope. Higher tangent at the initial represents the less

damage measure at the more intensity than the damage which caused by the near field ground motion records.

IDA curves in the following figure tend follow the same pattern except for two three records which show an immense increase in damage measure with the sudden shift in intensity because of the nature of the raw earthquake record. "El Mayor-Cucapah Mexico" was recorded for the two stations with intensity of 7.2 tend to have higher peaks at the beginning which is supposed to be the major cause for this kind of drastic change. Then as the cycle of the time history changes and thus reversing the damage caused and then following the same trend.

In the next portion of where structure is no more in the elastic range the slope tends to flatten, causing more damage with the smaller increase in intensity. Then all those IDA curves get straight line depicting that now with no increase in intensity damage measure is infinite showing the dynamic instability.

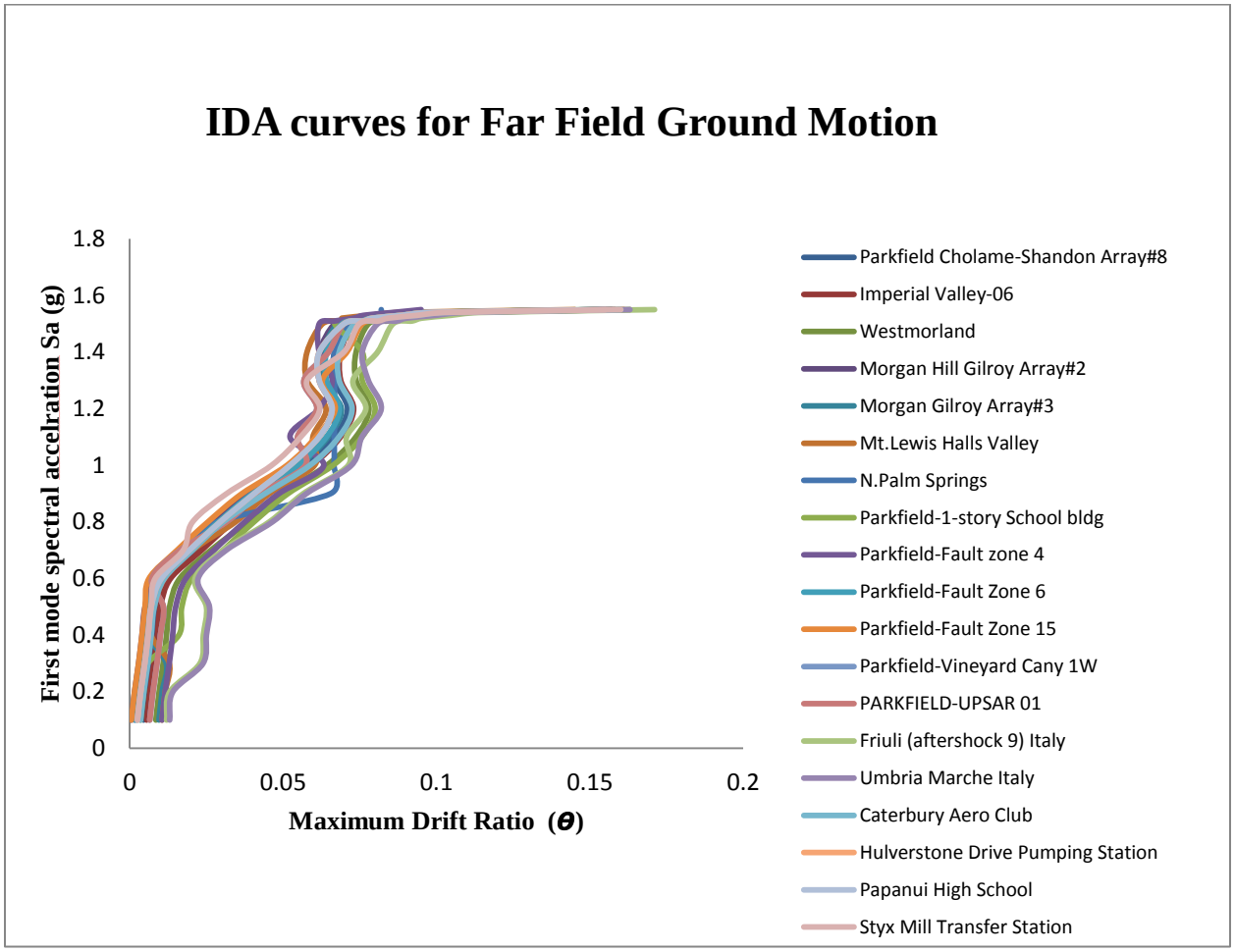


**Figure 5.3: IDA Curves for Far Field Ground Motion**

The performance limits are marked according the FEMA guidelines, collapse prevention is limit marked where global dynamic stability starts to occur. Life safety (LS) is considered to be three fourth of collapse prevention. And immediate occupancy is marked where structure tend to be in elastic range.

**Table 4.2: Performance Based Limits for Far Field Ground Motions**

| | $S_a$(g) | | | $\theta_{max}$(%) | | |
|---|---|---|---|---|---|---|
| | CP | LS | IO | CP | LS | IO |
| 84% | 1.5 | 1.05 | 0.5 | 0.07 | 0.065 | 0.02 |
| 50% | 1.5 | 1.05 | 0.5 | 0.065 | 0.06 | 0.01 |
| 16% | 1.5 | 1.05 | 0.52 | 0.06 | 0.059 | 0.01 |

In this group of earthquake records intensity measure is same but accordingly damage measure varies to the little extent. If whole is considered 84% of the total earthquakes will cross the collapse prevention level for spectral acceleration of 1.5g at ISD of 0.07%. On the other hand if the ground intensity chosen for the near field criteria for the same 84% of the records will cause the prevention level limit to cross at 0.91g spectral acceleration at 0.14 ISD.

As these two bins are selected on the basis of near field and far field locations for the range of time period, in which so as not to have a structural bias for failure magnitude is chosen more for far field than near field. After deriving the performance limits for both the cases it can be concluded that that near field motions tend to cause more damage than far field motion even if the intensity of far field motion is more than near field.

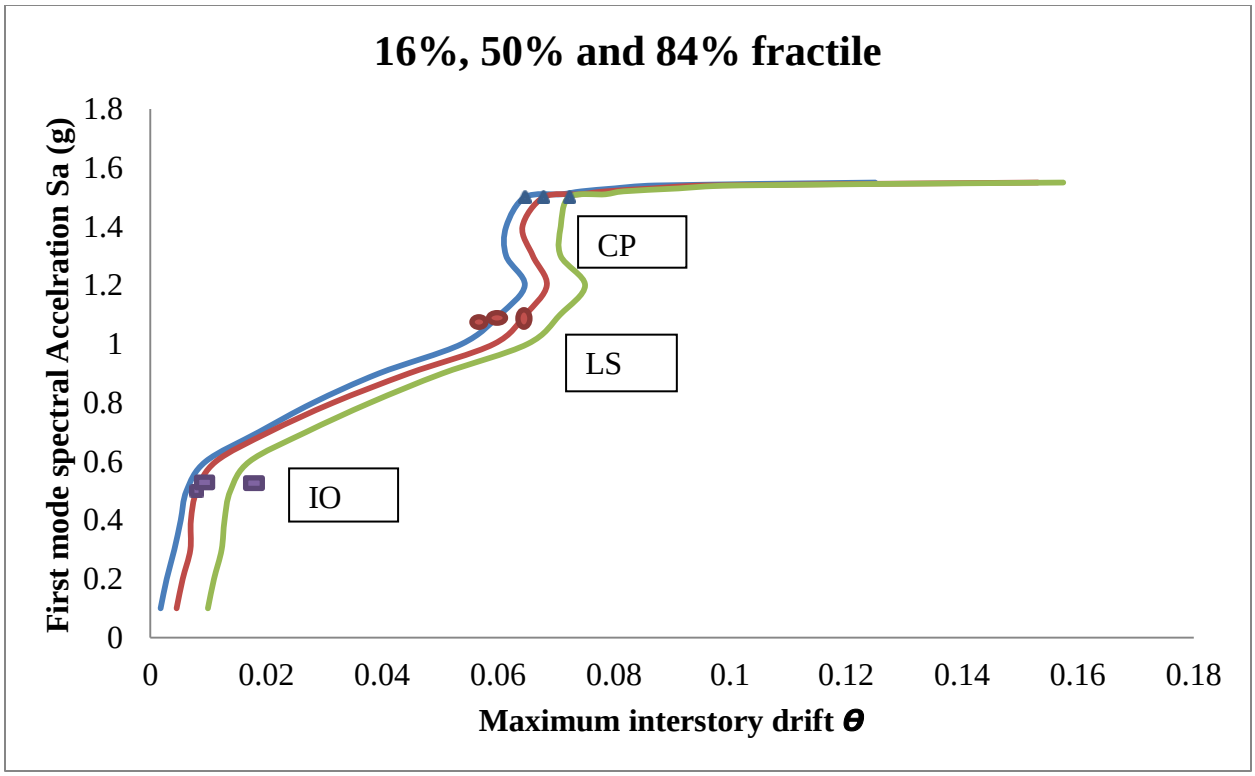


**Figure 5.4: 16%, 50% and 85% Fractile for IDA**

## 5.6. NEAR FIELD GROUND MOTIONS FOR SINGLE PERIOD

For the near field ground motions which are selected on the bases of single period scaling the IDA curves get scattered. The reason might be the spectrum of those ground motions are matched for one point to the target spectrum. And rest of the spectrum may exceed or decreased randomly. As all of the ground motion have matched the spectrum at one point means at one point record amplitude is according to target spectrum while rest of the time history varies drastically causing a large scatter in damage measure.

Some of the records show smooth transition with increase in intensity measure damage measure increases from elastic state to plastic and then show failure. Two records show drastic weaving behavior which is representative of reverse cycle may undo the damage accumulation. The reverse of cycles of a time history of smaller amplitude at first seconds may reverse the damage for instance cause the closing of joints and cracks which lead to instability. So at some points with the increase in intensity measure damage measure gets reversed, thus showing a changing behavior.

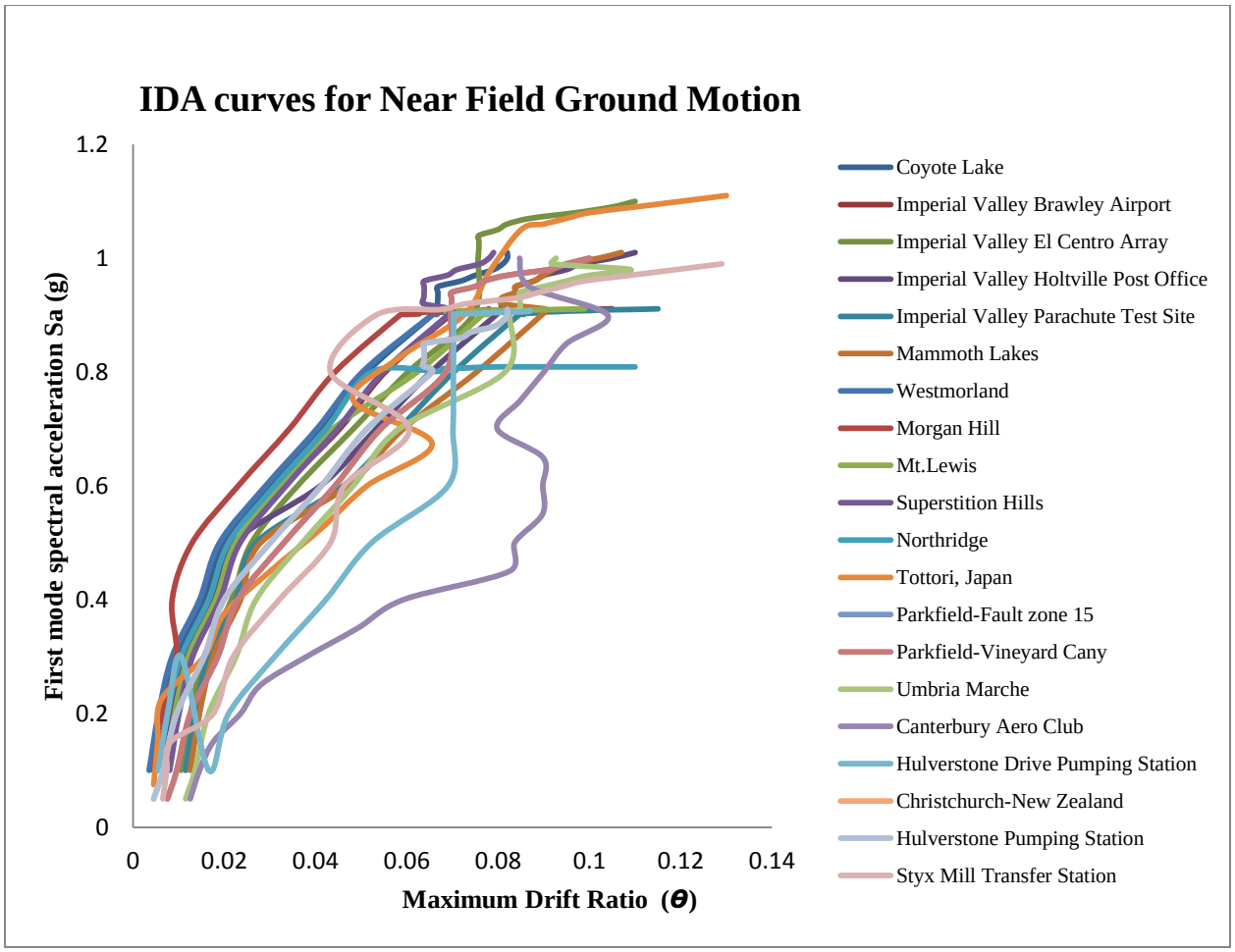


**Figure 5.5: IDA Curves for Near Field Ground Motion**

Unlike those records which are near field and are chosen on the basis of comparison of spectrum for a range of fundamental period of building, this method tends to give less confidence bound in the results due to its large scatter and not having very defined curves for fractile.

**Table 4.3:Performance Based Limits for Near Field Ground Motions**

| | $S_a$(g) | | | $\theta_{max}$(%) | | |
|---|---|---|---|---|---|---|
| | CP | LS | IO | CP | LS | IO |
| 84% | 0.95 | 0.75 | 0.39 | 0.081 | 0.061 | 0.015 |
| 50% | 0.9 | 0.75 | 0.3 | 0.07 | 0.0525 | 0.015 |
| 16% | 0.82 | 0.5 | 0.18 | 0.06 | 0.045 | 0.02 |

In this bin 84% of the earthquake records cause, to cross collapse prevention performance level to cross at 0.95g intensity with damage measure of 0.081% which is less than the values we got for the bin in which all the earthquakes are selected for the range of period. For this bin records are so random that there is no definite line between performance limit. For instance immediate occupancy limit for the 16% of the earthquake records increase damage measure percentage to 0.02% which is more than the 50 and 84%.

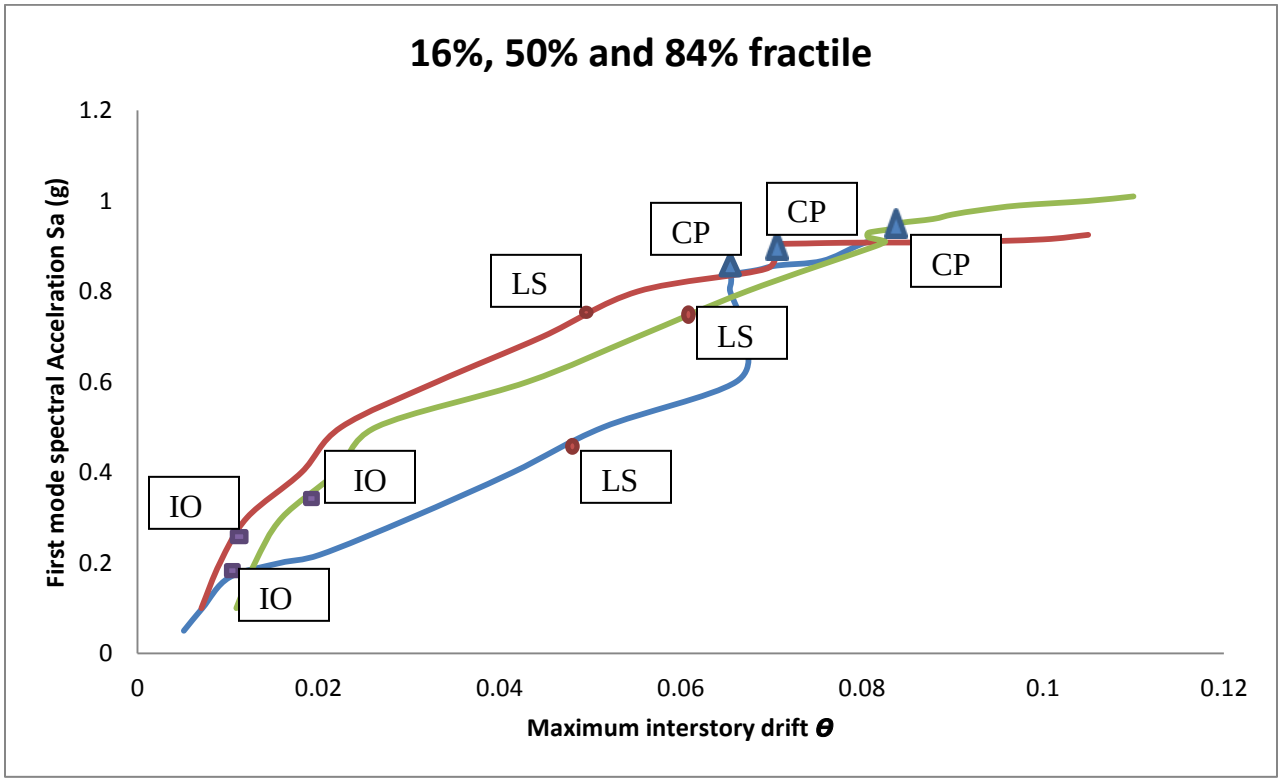


**Figure 5.6: 16%, 50% and 84% Fractile for IDA**

## 5.7. FAR FIELD GROUND MOTIONS FOR SINGLE PERIOD

Far field motions for this particular bin are selected on the basis of single period. The scatter in the result but far less than when it is compared to near field motions. As for this bin records are sorted out according to the single period matching of the entire selected spectrum with target spectrum. This scatter is not very pronounce because if a building is subjected to the earthquakes which are at far distance from the site, their amplitude whether high or low do not effect much on the structure.

As with the increase in scale factor of intensity, damage measure increases following the usual trend. Except three records which show weaving behavior after elastic state, this is due to the damage accumulation in the structure when the flexural cracks which are open get close with the reversal of the cycle and thus show the less damage measure with the increase in scale factor of spectral acceleration. One of the ground motions shows diverse behavior, a usual increase and then sudden drop in IM but damage continues, this is due to the peak displacements which occur at very few seconds of the time history and then decreased. Overall IDA curve due to this particular ground motion has relatively more DM at less IM than because of the damage which already has occurred due to the first sever cycles.

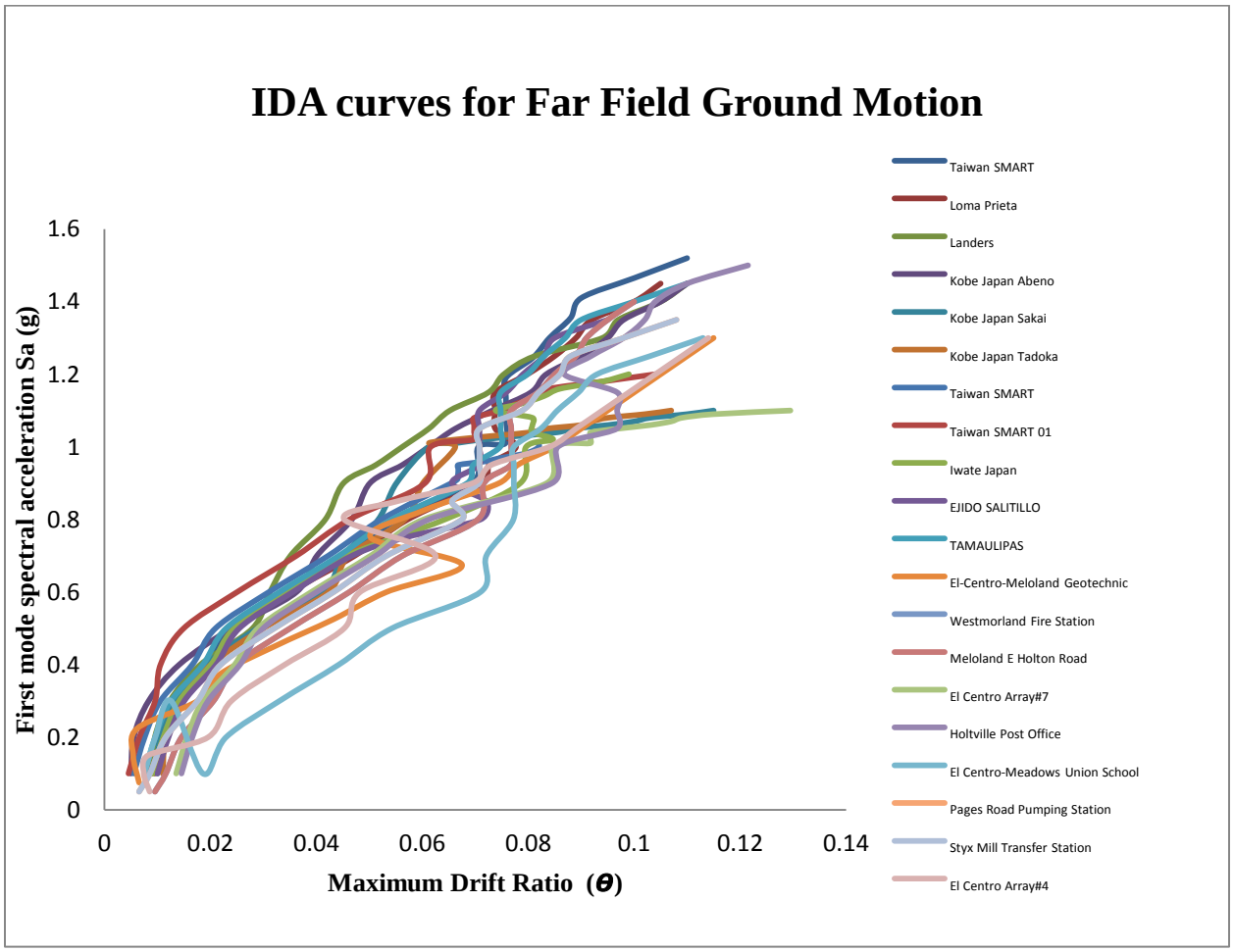


**Figure 5.7: IDA Curves for Far Field Ground Motion**

As far as the performance limits are concerned 84% of the earthquake records in this bin will cause the collapse prevention limit to hit at 1.4g with damage measure of 0.11%. For

the bin in which records are selected for far field site on the basis of spectrum range matching, CP limit for 84% of earthquakes was 1.5g with 0.07% of interstory drift.

**Table 4.4: Performance Based Limits for Far Field Ground Motions**

| | $S_a$(g) | | | $\theta_{max}$(%) | | |
|---|---|---|---|---|---|---|
| | CP | LS | IO | CP | LS | IO |
| 84% | 1.4 | 1.05 | 0.4 | 0.11 | 0.0825 | 0.010 |
| 50% | 1.2 | 0.9 | 0.3 | 0.1 | 0.075 | 0.015 |
| 16% | 0.9 | 0.7 | 0.2 | 0.07 | 0.06 | 0.01 |

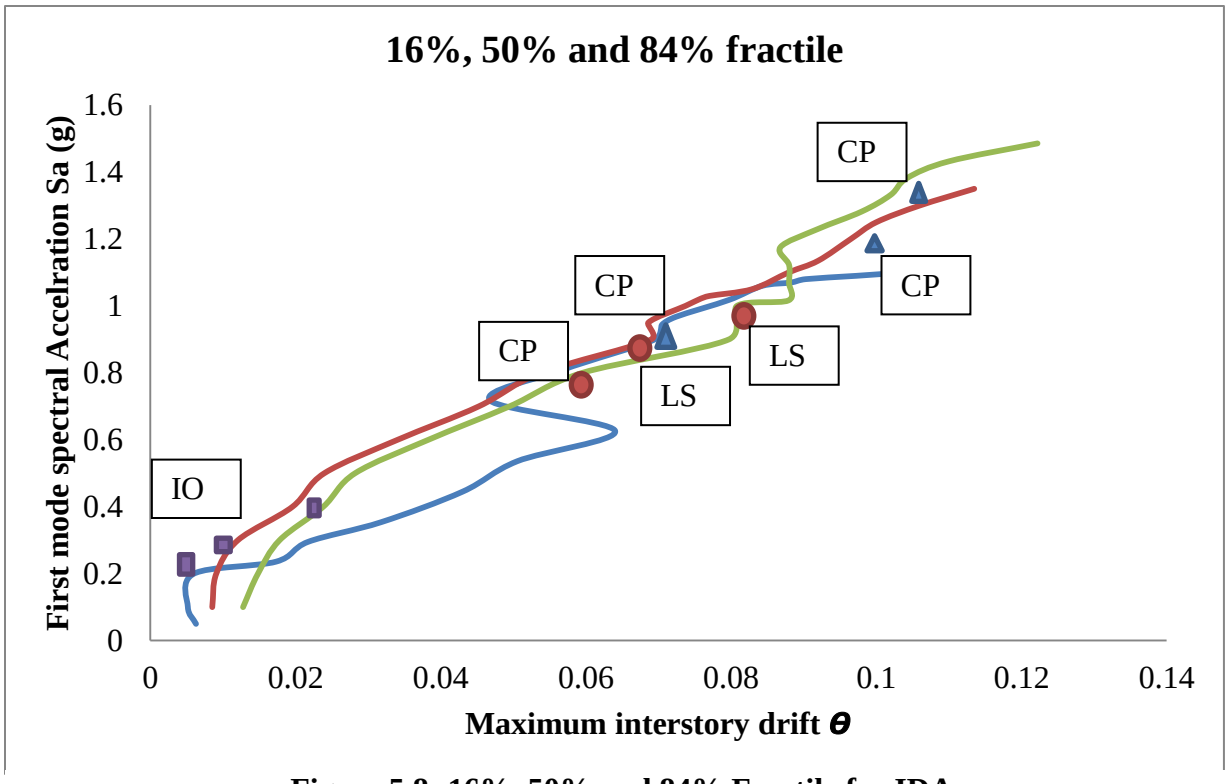


**Figure 5.8: 16%, 50% and 84% Fractile for IDA**

## 5.9. FRAGILITY CURVE

Following are the fragility curves which are derived for all the bins of earthquakes. The probability of exceedence of 100 percent for immediate occupancy (IO) limit occurs at 0.2g spectral acceleration. In other words the immediate occupancy is likely to touch the maximum probability of 100 at 0.2g spectral acceleration. Life safety tend to approach maximum probability of damage at 1.25g acceleration i-e the damage which is defined as life safety limit will tend to exceed at aforementioned spectral acceleration. Similarly the collapse prevention damage state will approach at spectral acceleration of 2g.

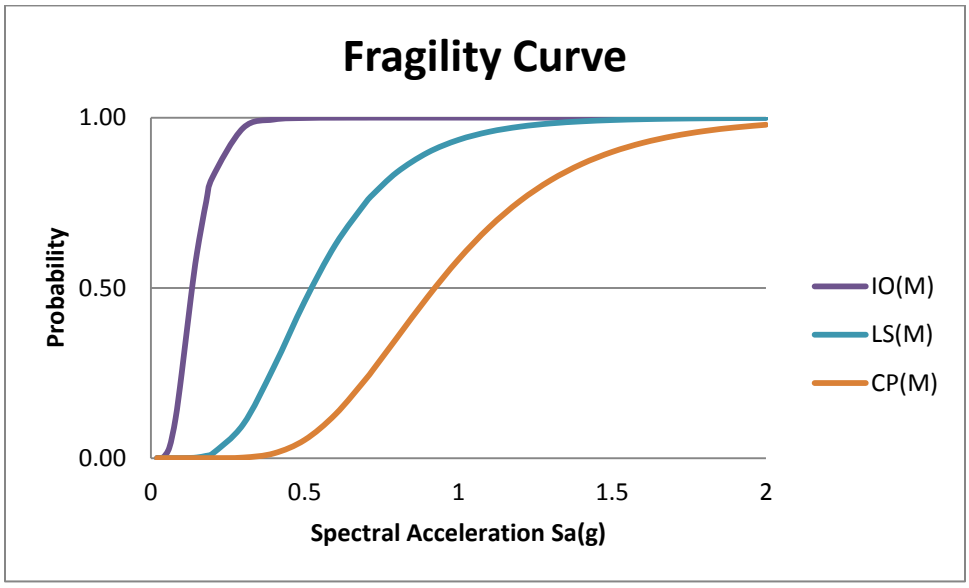

*Chapter 6*

# RECOMMENDATIONS

For the future studies which are intended to be carried out on IDA following improvements can be made;

- Only 2-D models were used in the present studies and stiffness in one direction is considered. 3D models are recommended for next studies and stiffness of the elements in both the directions is needed to be counted.
- As for the present studies only one regular building was considered, neither the geometric nor the mass irregularities are taken into account. For the future studies stiffness and mass irregularities should be considered to see the effects induced due to seismic torsion.
- Only bare frames are considered in the most of the studies carried out in Pakistan, frames with infilled non load bearing wall, shear walls and shear panels should also be considered.
- Synthetic ground motion records should be developed for the region which consist the same characteristic as the historical actual earthquake happened.
- More ground motion selection and scaling procedures can be used to determine the best suitor for IDA.
- Under reinforced and poorly constructed full scale models for Pakistani building representations are constructed and tested for the purpose of comparison with fragility curves which are drawn.
- More uncertain parameters should be accounted for

# REFERENCES


Tyagunov, S., Stempniewski, L., Grünthal, G., Wahlström, R., Zschau, J.: Vulnerability and risk assessment for earthquake prone cities. 13th World Conference on Earthquake Engineering (Vancouver/Canada 2004). Proceedings, paper 868, 2004.

Kyriakides N. (2007). PhD Thesis. "Vulnerability of RC buildings and risk assessment for Cyprus". Center for Cement and Concrete, Department of Civil & Structural Engineering, University of Sheffield.

Palacios, S. (2004). "State of the art in seismic vulnerability assessment". Institutional repository of Alicante University.

T. Rossetto, A. E. (2003). Derivation of vulnerability function for European-type RC structure based on observational data. *Engineering Structures, 25*(10), 1241-1263.

Orsini, G. (1999). A model for buildings' vulnerability assessment using the parameterless scale of seismic intensity (PSI). Earthquake Spectra, 15(3), 463-483.

Calvi, G. M., Pinho, R., Magenes, G., Bommer, J. J., Restrepo-Velez, L. F., & Crowley, H. (2006). Development of seismic vulnerability assessment methodologies over the past 30 years. *ISET Journal of Earthquake Technology, 43*(472).

Whitman, R.V., Reed, J.W. and Hong, S.T. (1973). "Earthquake Damage Probability Matrices", Proceedings of the Fifth World Conference on Earthquake Engineering, Rome, Italy, Vol. 2, pp. 2531-2540.

Scawthorn, C., & Chen, W.-F. (2002). Earthquake engineering handbook: CRC press.



Calvi, G. M., Pinho, R., Magenes, G., Bommer, J. J., Restrepo-Velez, L. F., & Crowley, H. (2006). Development of seismic vulnerability assessment methodologies over the past 30 years. *ISET Journal of Earthquake Technology, 43*(472).



Braga, F., Dolce, M., & Liberatore, D. 1982. A Statistical Study on Damaged Buildings and an Ensuing Review of the M.S.K.-76 Scale. Proc. 7th ECEE, Athens, September 1982.

Sabetta, F., et al. (1998). Empirical fragility curves from damage surveys and estimated strong ground motion. Proceedings of the 11th European conference on earthquake engineering, Paris, France.

Yamazaki, F. and O. Murao (2000). "7. Vulnerability Functions for Japanese." Implications of Recent Earthquakes on Seismic Risk.

Rota, M., Penna, A., & Strobbia, C. (2006). “Typological fragility curves from Italian earthquake damage data”. Paper presented at the Proceedings 1st European conference on earthquake engineering and seismology, Geneva, paper.

T. Rossetto, A. E. (2003). Derivation of vulnerability function for European-type RC structure based on observational data. Engineering Structures, 25(10), 1241-1263.

Scholl, R.E., O. Kustu, C. Perry, and J.M. Zanetti, 1982, Seismic Damage Assessment for High-Rise Buildings, JAB-8020, Final Technical Report to U.S. Geological Survey, URS/John A. Blume & Associates, Engineers, San Francisco

Singhal A, and Kiremidjan AS (1996).Method for Probabilistic Evaluation of Seismic Structural Damage.Journal of Structural Engineering, ASCE,Vol 122, No.12(December, 1996).pp 1459-1467.

Park YJ, and Ang AS (1985).Seismic Damage Analysis of Reinforced Concrete Buildings.Journal of Structural Engineering. ASCE, Vol. III, No. 4.pp740-757.

Scholl, R.E., O. Kustu, C. Perry, and J.M. Zanetti, 1982, Seismic Damage Assessment for High-Rise Buildings, JAB-8020, Final Technical Report to U.S. Geological Survey, URS/John A. Blume & Associates, Engineers, San Francisco

Singhal A, and Kiremidjan AS (1996).Method for Probabilistic Evaluation of Seismic Structural Damage.Journal of Structural Engineering, ASCE,Vol 122, No.12(December, 1996).pp 1459-1467.

Park YJ, and Ang AS (1985).Seismic Damage Analysis of Reinforced Concrete Buildings.Journal of Structural Engineering. ASCE, Vol. III, No. 4.pp740-757.

Calvi, G. M. (1999). A displacement-based approach for vulnerability evaluation of classes of building Journal of Earthquake Engineering, 3(03), 411-438.

Chen, W.-F., & Lui, E. M. (2005). Handbook of structural engineering: CRC press.

Wald, D. J., Quitoriano, V., Heaton, T. H., & Kanamori, H. (1999). Relationships between peak ground acceleration, peak ground velocity, and modified Mercalli intensity in California. Earthquake Spectra, 15(3), 557-564.

Vamvatsikos, D., & Cornell, C. A. (2002). Incremental dynamic analysis. Earthquake Engineering & Structural Dynamics, 31(3), 491-514.

Karbassi, A., & Nollet, M.-J. (2013). Performance-Based Seismic Vulnerability Evaluation of Masonry Buildings Using Applied Element Method in a Nonlinear Dynamic-Based Analytical Procedure. Earthquake Spectra, 29(2), 399-426.

Mander, J. B., Dhakal, R. P., Mashiko, N., & Solberg, K. M. (2007). Incremental dynamic analysis applied to seismic financial risk assessment of bridges. Engineering Structures, 29(10), 2662-2672.